**ΕΘΝΙΚΟ ΜΕΤΣΟΒΙΟ ΠΟΛΥΤΕΧΝΕΙΟ**
**Εργαστήριο Ατμοκινητήρων & Λεβήτων**
***Τομέας Θερμότητας της Σχολής Μηχανολόγων Μηχανικών***

***ΔΙΠΛΩΜΑΤΙΚΗ ΕΡΓΑΣΙΑ***

# *Αξιολόγηση εναλλακτικών ζευγών για εφαρμογή σε κύκλο ψύξης με απορρόφηση*

# *Investigation of alternative absorption cycle working pairs*

**Του Φοιτητή**
Σταυρόπουλος Λαζαρόπουλος Ιάσονας

**Επιβλέπων**

**Καρέλλας Σωτήριος, Καθηγητής**
Σχολή Μηχανολόγων Μηχανικών, ΕΜΠ

Αθήνα, Σεπτέμβριος 2019

# Abstract

Amidst the climate and ecological crisis that plagues the planet due primarily to human activity in the fields of energy, animal agriculture and transport, the need for lifestyle changes at both the government and individual level has emerged in recent years. Regarding energy, laws have been passed in favor of the adoption of renewable sources of energy to minimize carbon dioxide emissions and to avoid dependency on fossil fuels whose reserves are exhausted worldwide. Refrigeration applications are an important part of the energy sector and there is a lot of room for improvement in efficiency, especially with the use of low temperature waste heat from various systems. One of these applications is absorption refrigeration and the subject of this thesis was to evaluate alternative pairs.

The most common pairs in absorption refrigeration applications are water/lithium bromide ($H_2O$/LiBr) and ammonia/water ($NH_3/H_2O$). Firstly, the single-effect absorption refrigeration cycle for $H_2O$/LiBr was modeled in Aspen Plus, the model was validated in terms of mass and energy balance, results were presented for the state points of the cycle, including the coefficient of performance COP, and a sensitivity analysis was performed for the heat duty of the evaporator (cooling capacity) and the COP as a function of the temperature of the generator and the evaporator for various values of the mass concentration of the absorbent in the rich solution: 40%, 50%, 51.4%, 53%, 55%. The single-effect absorption refrigeration cycle was then modeled for the alternative pairs, in which the refrigerant was water and the absorbent was composed of lithium or sodium compounds, which were: $H_2O$/LiF, $H_2O$/LiCl, $H_2O$/NaOH and $H_2O$/HCOONa. Ternary mixtures were also examined which were: $H_2O$/LiBr+$LiNO_3$ (salt mole ratio 4:1), $H_2O$/LiBr+$ZnBr_2$ (2:1), $H_2O$/LiCl+$LiNO_3$ (2.8:1), $H_2O$/LiCl+$ZnCl_2$ (2:1) and $H_2O$/LiBr+LiI (4:1). Every alternative pair was validated in the same way and the results and sensitivity analysis were presented. The $NH_3/H_2O$ pair was also modeled for completeness of the comparisons, which required modifications due to some of the ammonia properties. In addition, a financial analysis was performed for every working pair (including ternary mixtures), calculating the various installation costs (ISBL, OSBL, Engineering costs, Contingency charges) as well as the total Fixed Capital Investment costs.

Based on the results, higher cooling capacity and COP were obtained for a mass concentration of the absorbent in the rich solution of 40% for all working pairs and the curves of the sensitivity analysis were similar to previous studies. The $H_2O$/HCOONa, $H_2O$/LiF, $H_2O$/LiCl+$ZnCl_2$, $H_2O$/LiCl+$LiNO_3$, and $H_2O$/LiBr+$ZnBr_2$ working pairs had the highest cooling capacity over the entire range of the generator and evaporator temperatures, while the conventional $NH_3/H_2O$ and $H_2O$/LiBr working pairs had the lowest values. Correspondingly, as far as COP is concerned, the $H_2O$/LiF, $H_2O$/HCOONa, $H_2O$/LiBr+$ZnBr_2$, $H_2O$/LiCl+$ZnCl_2$ and $H_2O$/LiBr+LiI working pairs had the highest values, whereas the $NH_3/H_2O$ and $H_2O$/NaOH working pairs had the lowest values. Based on the results of the economic evaluation, the $NH_3/H_2O$ working pair had the highest total Fixed Capital Investment cost due to the much higher pressures in the system, while the $H_2O$/NaOH, $H_2O$/LiBr, $H_2O$/LiCl, $H_2O$/LiCl+$ZnCl_2$ and $H_2O$/LiBr+$LiNO_3$ working pairs had the lowest total Fixed Capital Investment costs. Also, the total Fixed Capital Investment cost per kW of cooling capacity (€/kWevap) was calculated and $H_2O$/LiCl+$ZnCl_2$, $H_2O$/LiF and $H_2O$/LiBr+$ZnBr_2$ had the lowest values, while $NH_3/H_2O$ had

the highest value by a long margin. Therefore, it is clear that $NH_3/H_2O$, $H_2O$/LiBr and $H_2O$/NaOH are the worst working pairs as far as COP and total Fixed Capital Investment cost per kW of cooling capacity are concerned, while the most competitive working pairs are $H_2O$/LiF, $H_2O$/LiCl+$ZnCl_2$, $H_2O$/LiBr+$ZnBr_2$ and $H_2O$/HCOONa.

# Περίληψη

Εν μέσω της κλιματικής και οικολογικής κρίσης που μαστίζει τον πλανήτη εξαιτίας πρωτίστως της ανθρώπινης δραστηριότητας στους τομείς της ενέργειας, της κτηνοτροφίας και των μεταφορών, αναδύεται πιο έντονα τα τελευταία χρόνια η ανάγκη για αλλαγές στον τρόπο ζωής τόσο σε κυβερνητικό επίπεδο όσο και σε ατομικό. Όσον αφορά στην ενέργεια, έχουν θεσπιστεί νόμοι υπέρ της υιοθέτησης ανανεώσιμων πηγών ενέργειας, ώστε να ελαχιστοποιηθούν οι εκπομπές διοξειδίου του άνθρακα που συμβάλλουν στο φαινόμενο του θερμοκηπίου και να μην υπάρχει όσο είναι δυνατόν εξάρτηση από ορυκτά καύσιμα, τα αποθέματα των οποίων εξαντλούνται παγκοσμίως. Οι εφαρμογές ψύξης είναι σημαντικό κομμάτι του τομέα της ενέργειας και υπάρχουν πολλά περιθώρια βελτίωσης της απόδοσης, ιδιαίτερα με τη χρήση της απορριπτόμενης θερμότητας χαμηλής θερμοκρασίας από διάφορα συστήματα. Μία από αυτές τις εφαρμογές είναι η ψύξη με απορρόφηση και το αντικείμενο της παρούσας διπλωματικής εργασίας ήταν η αξιολόγηση εναλλακτικών ζευγών.

Τα πιο διαδεδομένα ζεύγη σε εφαρμογές ψύξης με απορρόφηση είναι τα νερό/βρωμιούχο λίθιο ($H_2O$/LiBr) και αμμωνία/νερό ($NH_3/H_2O$). Αρχικά, μοντελοποιήθηκε ο μονοβάθμιος κύκλος ψύξης με απορρόφηση για το $H_2O$/LiBr στο Aspen Plus, έγινε η επιβεβαίωση της εγκυρότητας του μοντέλου όσον αφορά στα ισοζύγια μάζας και ενέργειας, παρουσιάστηκαν τα αποτελέσματα για τα διάφορα σημεία του κύκλου, συμπεριλαμβανομένου και του συντελεστή συμπεριφοράς COP, και έγινε ανάλυση ευαισθησίας για τη ψυκτική ισχύ του ατμοποιητή και το COP συναρτήσει της θερμοκρασίας της ατμογεννήτριας και του ατμοποιητή για διάφορες τιμές της συγκέντρωσης μάζας του μέσου απορρόφησης στο πλούσιο διάλυμα: 40%, 50%, 51.4%, 53%, 55%. Στη συνέχεια, μοντελοποιήθηκε ο μονοβάθμιος κύκλος ψύξης με απορρόφηση για τα εναλλακτικά ζεύγη, στα οποία το ψυκτικό μέσο ήταν το νερό και το μέσο απορρόφησης αποτελείτο από ενώσεις λιθίου ή νατρίου, τα οποία ήταν: $H_2O$/LiF, $H_2O$/LiCl, $H_2O$/NaOH και $H_2O$/HCOONa. Εξετάστηκαν, επίσης, τριαδικά μείγματα τα οποία ήταν: $H_2O$/LiBr+$LiNO_3$ (μοριακή αναλογία αλάτων 4:1), $H_2O$/LiBr+$ZnBr_2$ (2:1), $H_2O$/LiCl+$LiNO_3$ (2.8:1), $H_2O$/LiCl+$ZnCl_2$ (2:1) and $H_2O$/LiBr+LiI (4:1). Για όλα τα εναλλακτικά ζεύγη έγινε με τον ίδιο τρόπο επιβεβαίωση της εγκυρότητας του μοντέλου και παρουσιάστηκαν τα αποτελέσματα και η ανάλυση ευαισθησίας. Για την πληρότητα των συγκρίσεων μοντελοποιήθηκε και το ζεύγος $NH_3/H_2O$, για το οποίο χρειάστηκαν τροποποιήσεις λόγω κάποιων ιδιοτήτων της αμμωνίας. Επιπροσθέτως, εκπονήθηκε οικονομική ανάλυση για όλα τα εργαζόμενα ζεύγη (συμπεριλαμβάνονται τα τριαδικά μείγματα), στην οποία υπολογίστηκαν τα διάφορα κόστη της εγκατάστασης (ISBL, OSBL, Κόστη μηχανικού, Επιπλέον ενδεχόμενα κόστη), καθώς και τα συνολικά κόστη Επενδύσεων Παγίου Κεφαλαίου.

Βάσει των αποτελεσμάτων, προέκυψε υψηλότερη ψυκτική ισχύς και απόδοση για συγκέντρωση μάζας του μέσου απορρόφησης στο πλούσιο διάλυμα 40% για όλα τα εργαζόμενα ζεύγη και οι καμπύλες των αναλύσεων ευαισθησίας ήταν οι αναμενόμενες βάσει προηγούμενων μελετών. Σε όλο το εύρος των θερμοκρασιών της ατμογεννήτριας και του ατμοποιητή την υψηλότερη ψυκτική ισχύ είχαν τα ζεύγη $H_2O$/HCOONa, $H_2O$/LiF, $H_2O$/LiCl+$ZnCl_2$, $H_2O$/LiCl+$LiNO_3$ και $H_2O$/LiBr+$ZnBr_2$, ενώ τη χαμηλότερη είχαν τα συμβατικά

ζεύγη $NH_3/H_2O$ και $H_2O/LiBr$. Αντίστοιχα, όσον αφορά στο συντελεστή συμπεριφοράς COP, τις υψηλότερες τιμές είχαν τα ζεύγη $H_2O/LiF$, $H_2O/HCOONa$, $H_2O/LiBr+ZnBr_2$, $H_2O/LiCl+ZnCl_2$ και $H_2O/LiBr+LiI$, ενώ τις χαμηλότερες είχαν τα $NH_3/H_2O$ και $H_2O/NaOH$. Από οικονομική άποψη, το ζεύγος $NH_3/H_2O$ είχε το υψηλότερο με διαφορά συνολικό κόστος λόγω των πολύ υψηλότερων πιέσεων που επικρατούν στο σύστημα, ενώ τα ζεύγη $H_2O/NaOH$, $H_2O/LiBr$, $H_2O/LiCl$, $H_2O/LiCl+ZnCl_2$ και $H_2O/LiBr+LiNO_3$ είχαν τα χαμηλότερα συνολικά κόστη. Επίσης, υπολογίστηκε το συνολικό κόστος Επενδύσεων Παγίου Κεφαλαίου ανά kW ψυκτικής ισχύος (€/kWevap) και βρέθηκε ότι τα $H_2O/LiCl+ZnCl_2$, $H_2O/LiF$ και $H_2O/LiBr+ZnBr_2$ είχαν τις χαμηλότερες τιμές, ενώ το ζέυγος $NH_3/H_2O$ είχε την υψηλότερη τιμή με τεράστια διαφορά από τα υπόλοιπα. Επομένως, γίνεται εύκολα αντιληπτό ότι τα ζεύγη $NH_3/H_2O$, $H_2O/LiBr$ και $H_2O/NaOH$ είναι τα λιγότερο συμφέροντα από άποψη COP και κόστους Επενδύσεων Παγίου Κεφαλαίου ανά kW ψυκτικής ισχύος, ενώ τα πιο ανταγωνιστικά ζεύγη είναι τα $H_2O/LiF$, $H_2O/LiCl+ZnCl_2$, $H_2O/LiBr+ZnBr_2$ και $H_2O/HCOONa$.

# Preface

Curiosity is an important part of my character and I always remember wondering about even the most seemingly trivial things. I feel lucky to be living in an age where science and technology have reached the point where they can shed light on most of my questions, except for the most existential ones of course.

However, the tremendous power that humanity has acquired is capable of changing people's way of life for the worse, even leading to their extinction over the next decades due to the anthropogenic climate crisis. The job of the engineer is to provide solutions to problems and perhaps through this thesis I will be able to make a tiny contribution to the viability of the energy sector, and in particular refrigeration, which is an important part of people's daily lives. This thesis taught me a lot, particularly how to exchange ideas and collaborate better, and it was a very important experience because I acquired a better understanding of what it means to be an engineer.

At this point, I would like to thank the Professor and supervisor of this thesis, Mr. Sotirios Karellas, for the assignment.

An important factor in the preparation of this thesis was Tryfonas Roubedakis, who answered to all of my questions and offered me his insight into various complex issues, and I thank him kindly. Also, I would like to thank Dimitrios Grimekis for his help with Aspen Plus.

Last but not least, I would like to thank my family and friends for their support throughout my studies.

# Contents

# List of Figures

# List of Tables

# Nomenclature

| | | | |
|---|---|---|---|
| $A$ | | *Area* | $[m^2]$ |
| $a$ | | *Cost constant* | [-] |
| $b$ | | *Cost constant* | [-] |
| $C_e$ | | *Purchased equipment cost* | [€] |
| $COP$ | | *Coefficient of performance* | [-] |
| $COP_{carnot}$ | | *Carnot coefficient of performance* | [-] |
| $D_c$ | | *Vessel diameter* | $[m]$ |
| $D_i$ | | *Vessel internal diameter* | $[m]$ |
| $E$ | | *Welded-joint efficiency* | [-] |
| $g$ | | *Solution circulation ratio* | [-] |
| $GWP$ | | *Global warming potential* | [-] |
| $h$ | | *Specific enthalpy* | $[kJ/kg]$ |
| $ISBL$ | | *Inside battery limits investment* | [€] |
| $L_c$ | | *Vessel length* | $[m]$ |
| $LMTD$ | | *Logarithmic mean temperature difference* | $[K]$ |
| $m$ | | *Mass flow* | $[kg/s]$ |
| $n$ | | *Exponent of the type of equipment* | [-] |
| $ODP$ | | *Ozone depletion potential* | [-] |
| $OSBL$ | | *Off-site cost investment* | [€] |
| $p$ | | *Pressure* | $[kPa]$ |
| $P_i$ | | *Internal pressure* | $[Pa]$ |
| $Q$ | | *Heat duty* | $[kW]$ |
| $S$ | | *Size parameter* | [-] |
| $S$ | | *Maximum allowable stress* | $[N/mm^2]$ |
| $T$ | | *Temperature* | $[°C\ (K)]$ |
| $t_w$ | | *Wall thickness* | $[m]$ |
| $U$ | | *Overall heat transfer coefficient* | $[W/m^2K]$ |
| $W$ | | *Power* | $[kW]$ |
| $X$ | | *Mass concentration/Mass fraction* | [-] |
| $x$ | | *Volume flow* | $[L/s]$ |
| *Greek symbols* | | | |
| $\Delta h$ | | *Specific enthalpy difference* | $[kJ/kg]$ |
| $\Delta T$ | | *Temperature difference* | $[K]$ |
| $\xi$ | | *Mass percent composition* | $[\%]$ |
| $\pi$ | | *Pi constant* | [-] |
| $\rho$ | | *Density* | $[kg/m^3]$ |
| *Subscripts and superscripts* | | | |

| | | | |
|---|---|---|---|
| abs (a) | | Absorber | |
| comp | | Compressor | |
| cond (c) | | Condenser | |
| d | | Vapor | |
| des (g) | | Desorber/Generator | |
| evap (e) | | Evaporator | |
| r | | Strong solution | |
| th | | Theoretical | |
| w | | Weak solution | |

# Chapter 1. Introduction

Of all the inventions made in the past centuries, refrigeration was among those that altered the course of humans' everyday lives in the most tasteful way. Industrial and commercial refrigeration and air-conditioning are some of the applications of refrigeration [1]. As far as industrial refrigeration is concerned, refrigeration and freezing of food products are vital parts of human civilization and are used to maintain the product quality and prolong their storage life [2].

*Figure 1.1. Iceman in Berlin, 1957 [3].*

The idea of preserving food dates back to at least the ancient Roman and Chinese empires. Long before there was refrigeration, cooks found ways to preserve what would otherwise be perishable by pickling, potting, drying or salting it (and later, canning) - all methods that changed the food's flavor and texture. As for the use of ice, that dates back to at least 1100 B.C., based on underground icehouses in China. Historical sources show that donkeys carted ice from the Alps to the Roman emperors and snow was shipped by boat to Istanbul in the 16th century. For the common people at home, depending on where they lived, they may have harvested ice from lakes and streams or frozen it in pans when the temperature dropped.

Mechanical refrigeration technology has rapidly evolved in the last century. Refrigeration has a large impact on industry, lifestyle, agriculture, and settlement patterns. In most developed countries, cities are heavily dependent on refrigeration in supermarkets, in order to obtain their food for daily consumption. The increase in food sources has led to a larger concentration of agricultural sales coming from a smaller percentage of existing farms. Farms today have a much larger output per person in comparison to the late 1800s. This has

resulted in new food sources available to entire populations, which has had a large impact on the nutrition of society [4].

Except from food, refrigeration unlocks a plethora of home and industrial applications, including, but not limited to: household refrigerators, industrial freezers, cryogenics, and air conditioning. Heat pumps may use the heat output of the refrigeration process, and also may be designed to be reversible, but are otherwise similar to air conditioning units.

In commerce and manufacturing, there are many uses for refrigeration. Refrigeration is used to liquify gases (e.g. oxygen, nitrogen, propane and methane). In compressed air purification, refrigeration is used to condense water vapor from compressed air to reduce its moisture content. In oil refineries, chemical plants, and petrochemical plants, refrigeration is used to maintain certain processes at the required low temperatures (e.g. in alkylation of butenes and butane to produce a high octane gasoline component). Metal workers use refrigeration to temper steel and cutlery.

Unfortunately, the increasing demand for energy consumption across the globe is hugely responsible for the rise of the average global temperature which accelerates climate change and has an immense impact on the environment. Therefore, it is needed to collectively find alternative and viable solutions to produce sustainable energy, which of course includes refrigeration. The International Institute of Refrigeration in Paris estimated that approximately 15% of all the electrical energy produced worldwide is employed for refrigeration processes and air-conditioning [5].

## 1.1. Refrigeration Technologies

Refrigeration is a process of removing heat from a low-temperature reservoir and transferring it to a high-temperature reservoir. Refrigeration can be defined as "The technology of providing and maintaining temperature below that of surrounding atmosphere". It means continuous extraction of heat from a body whose temperature is already below the temperature of its surroundings [4].

As it is mandated by the second law of thermodynamics, heat is naturally transferred from warmer bodies to colder bodies. The opposite may happen only if work is consumed.

The flow of energy in refrigeration machines, as well as heat engines and heat pumps, is shown in Figure 1.2:

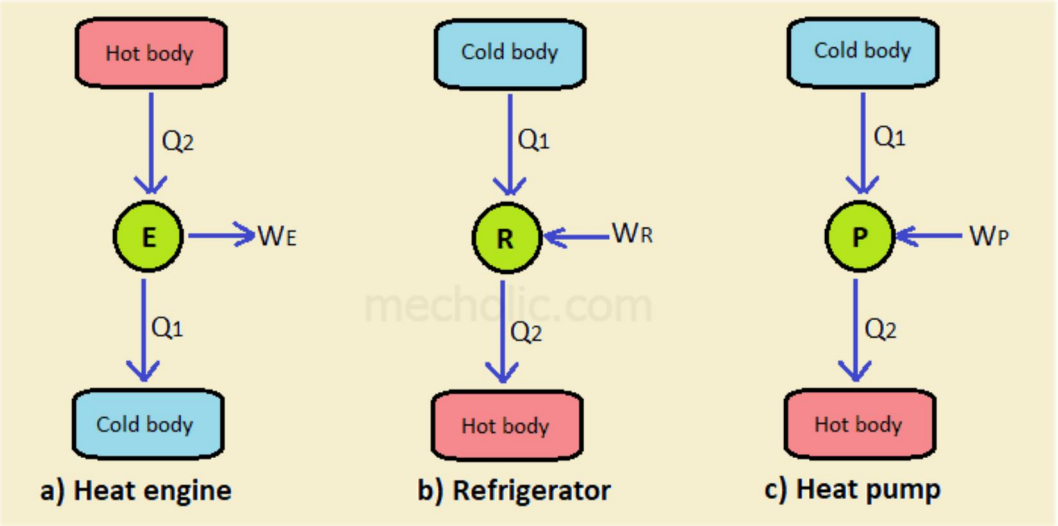


*Figure 1.2. Flow of energy in various machines.*

Heat machines are traditionally driven by mechanical means, but can also be driven by heat, magnetism, electricity, laser, or other sources. Methods of refrigeration can also be classified as non-cyclic and cyclic, depending on the existence of a thermodynamic cycle. The most common methods of refrigeration are:

- Vapor compression cooling
- Absorption cooling
- Adsorption cooling

## 1.2. Vapor compression cycle

Vapor compression cycles are quite easy to construct and have a low capital cost, therefore they are the most commonly used. As a matter of fact, conventional home refrigerators use this method of cooling to keep food and drinks chilled. A vapor compression cycle is also employed in air conditioning to cool the ambient air temperature in a room [6].

A working fluid, often called the refrigerant, is flowing through the system and undergoes state changes (from liquid to gas and back). The refrigerant's latent vaporizing heat is used to transfer large quantities of heat, and pressure changes are used to control when the refrigerant expels or absorbs heat.

However, for a refrigeration cycle that has a hot reservoir at around room temperature (or a bit higher) and a cold reservoir that is desired to be at around 2 °C, the boiling point of the refrigerant needs to be fairly low. Thus, various fluids have been identified as practical refrigerants. The most common include ammonia, Freon (and other chlorofluorocarbon refrigerants, also known as CFCs) and HFC-134a (a non-toxic hydrofluorocarbon). The refrigerant for a cycle needs to be selected carefully using as criteria the Global Warming Potential (GWP) index and the Ozone Depletion Potential (ODP) index, as a single leak of the refrigerant can be very harmful to the environment [7].

The key components of a simple vapor compression cycle are presented in Figure 1.3:

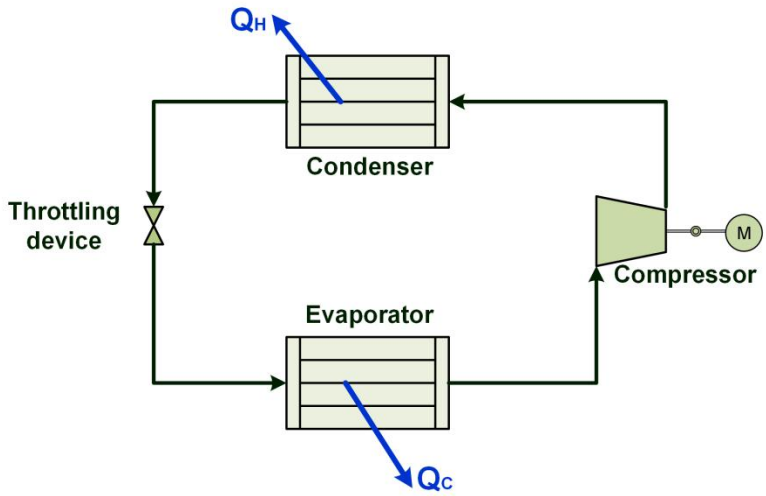


*Figure 1.3. Schematic of a conventional vapor compression cycle system*

Moreover, the processes taking place in an ideal vapor compression cycle in a pressure-enthalpy diagram can be depicted, as seen in Figure 1.4:

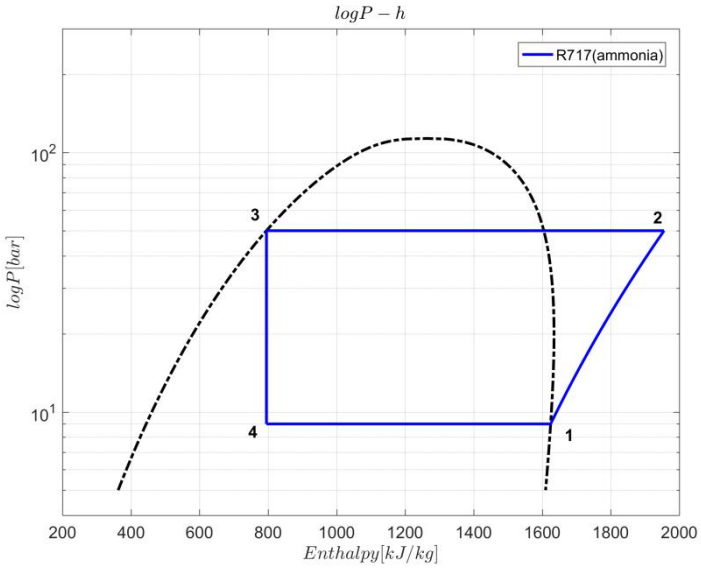


*Figure 1.4. Pressure-enthalpy diagram in an ideal vapor compression cycle*

As seen above, all such systems have four components:

- a compressor, process 1-2
- a condenser, process 2-3
- a thermal expansion valve (also called a throttle valve or metering device), process 3-4

- an evaporator, process 4-1

Circulating refrigerant enters the compressor in the thermodynamic state known as a saturated vapor (1) and is compressed to a higher pressure, resulting in a higher temperature as well. The hot, compressed vapor is then in the thermodynamic state known as superheated vapor (2) and is at a temperature and pressure at which it can be condensed with either cooling water or cooling air flowing across the coil/tubes of the condenser. This is where the circulating refrigerant rejects heat from the system and the rejected heat is carried away by either the water or the air (whichever may be the case). The condensed liquid refrigerant, in the thermodynamic state of saturated liquid (3), is next routed through an expansion valve where it undergoes an abrupt reduction in pressure. That pressure reduction results in the adiabatic flash evaporation of a part of the liquid refrigerant (4). The auto-refrigeration effect of the adiabatic flash evaporation lowers the temperature of the two-phase stream down to a level colder than the temperature of the enclosed space to be refrigerated. The cold mixture is then routed through the evaporator. A fan circulates the warm air in the enclosed space across the coil or tubes carrying the cold refrigerant liquid and vapor mixture. That warm air evaporates the liquid part of the cold refrigerant mixture. At the same time, the circulating air is cooled and thus lowers the temperature of the enclosed space to the desired temperature. The evaporator is where the circulating refrigerant absorbs and removes heat which is subsequently rejected in the condenser and transferred elsewhere by the water or air used in the condenser. To complete the refrigeration cycle, the refrigerant vapor from the evaporator is again a saturated vapor (1) and is routed back into the compressor.

The cooling load in a vapor compression cycle is equal to the cooling load of the evaporator:

$$\dot{Q}_e = \dot{m} \cdot (h_1 - h_4) \tag{1.1}$$

The power consumed by the compressor is equal to:

$$\dot{W}_{comp} = \dot{m} \cdot (h_2 - h_1) \tag{1.2}$$

The heat rejected by the condenser is equal to:

$$\dot{Q}_c = \dot{m} \cdot (h_2 - h_3) \tag{1.3}$$

The theoretical coefficient of performance of an ideal vapor compression cycle is given by the following equation:

$$COP_{th} = \frac{\dot{Q}_e}{\dot{W}_{comp}} \tag{1.4}$$

The actual coefficient of performance (COP) of a real vapor compression cycle is the ratio of the actual cooling load to the actual power consumed by the compressor. A non-ideal vapor compression cycle is slightly different than the ideal one due to irreversibilities related to the compressor, frictional pressure drop in the system or non-ideal gas behavior (if any).

Superheating and subcooling are two methods which enhance the performance of the cycle and ensure the proper operation of the throttling valve (no vapor bubbles) and the compressor (no liquid droplets).

Last but not least, it is worth mentioning that multiple compressors (multi-effect systems) can be used in order to achieve lower temperatures economically. Furthermore, systems with more than one evaporators or throttling valves exist, as well as with more than one refrigerants (cascade, seen in Figure 1.5).

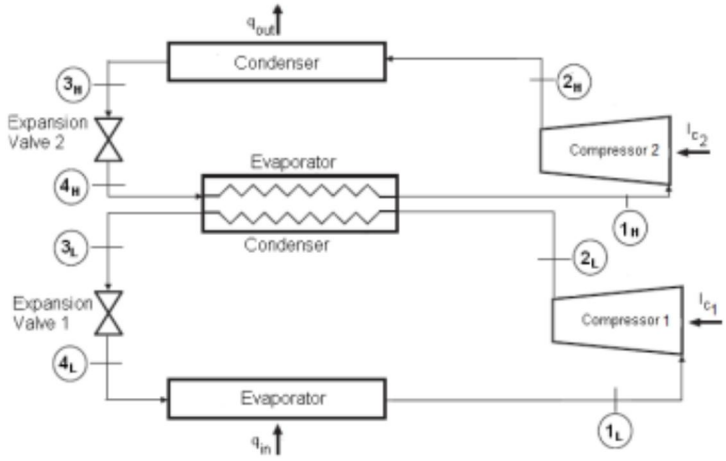


*Figure 1.5. Schematic of a cascade vapor compression refrigeration cycle*

## 1.3. Absorption cooling

One of the oldest refrigeration technologies is the absorption cycle. In the 1700s, the first study of an absorption system started. It was observed that ice can be made by evaporating pure $H_2O$ within an evacuated container in the presence of $H_2SO_4$ (sulfuric acid). Ferdinand Carre designed an installation in 1859 using an ammonia/water ($NH_3/H_2O$) working fluid pair. A new system with a water/lithium bromide ($H_2O$/LiBr) pairing for commercial purposes was implemented in 1950 [5].

The main benefits of absorption chillers are their long service life and efficient part-load operation [8]. In addition, both refrigerants with minimal ODP and GWP are their most ordinary working pairs, water-lithium bromide and ammonia-water, especially when compared to the less environmentally friendly refrigerants used in mechanical compression cycles. The relatively high initial cost of absorption chillers is considered unattractive for wider application in terms of cost considerations, yet the relatively low operating costs offer potential for broader use of such systems in the future. Their main disadvantages are the temperature limitations of their working pairs, their heavier weight compared to vapor compression cooling systems, their crystallization problems and their low COP (0.7-0.85 for single-effect systems and 1.1-1.3 for double-effect systems).

### 1.3.1 Operation of the absorption cycle

The refrigeration cycle of absorption technology is analogous to the cycle of vapor compression. An absorption refrigerator is a refrigerator that utilizes a heat source (e.g. solar energy, fossil-fueled flames, geothermal sources, biomass or natural gas combustion, waste heat from factories or district heating systems) instead of compressor mechanical work to provide the energy required to drive the cooling process, making it more environmentally sustainable. The evaporator, condenser and expansion device serve common purposes, but a heat-driven absorber and generator/desorber replace the compressor, as seen in Figure 1.6. In a single-effect system, one or two heat exchangers can be used to enhance the COP (in Figure 1.6 there is a Solution Heat Exchanger) [9].

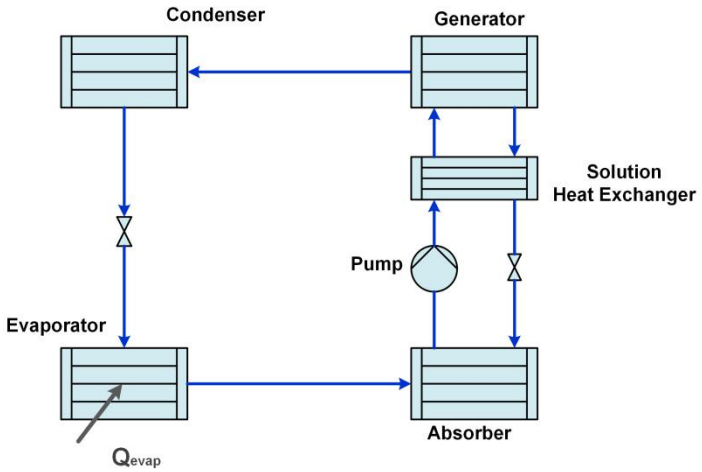


*Figure 1.6. Schematic of a single-effect absorption cooling cycle*

Both absorption chillers and conventional chillers use a very low boiling point refrigerant. When this refrigerant evaporates (boils) in both types, it takes away some heat, providing the cooling effect. The main difference between the two systems is how the refrigerant is transformed back into a liquid from a gas in order to repeat the cycle. An absorption refrigerator creates the pressure levels using a heat-only method and has no moving parts. Absorption cooling systems are driven by heat of a temperature from 70°C to 130°C. The single-effect absorption system gives best results with a heat supply temperature of 70-100 °C. Double- and triple-effect systems require higher supply temperatures.

The absorption cooling cycle can be described in three phases [10]:

- Evaporation: In a low partial pressure environment, a liquid refrigerant evaporates and thus extracts heat from its environment (e.g. the refrigerator compartment). The temperature required for evaporation is also low due to the low partial pressure.
- Absorption: Another liquid (e.g. a salt solution) absorbs the now gaseous refrigerant.
- Generation: The refrigerant-saturated liquid is heated, which causes evaporation of the refrigerant. The hot gaseous refrigerant transfers its heat outside of the system (such as surrounding ambient temperature air) through a heat exchanger and condenses. The condensed refrigerant (liquid) supplies the phase of evaporation.

The pressure in the solution is raised with the use of a pump, whose energy consumption is less than 1% of the cooling load in the evaporator and its impact from an energy point of view is considered in most cases negligible. The weak solution returning to the absorber is expanded by a throttling device and a heat recovery exchanger (Solution Heat Exchanger or SHX) is installed to recover heat from the hot solution exiting the generator to the cold solution exiting the absorber [7]. A 60% higher COP can be achieved by using the SHX. Given that the absorption is exothermic, the absorber is chilled by cooling water [11].

### 1.3.2 Working pairs

The refrigerant/absorbent working pair's thermodynamic properties are the most critical factors in analyzing and optimizing the absorption system performance. The most prevalently used refrigerant/absorbent working pairs in absorption systems are $NH_3/H_2O$ and $H_2O/LiBr$.

*Table 1.1. Advantages and disadvantages of $NH_3/H_2O$ and $H_2O/LiBr$ [5]*

| Working Pair | Advantages | Disadvantages |
|---|---|---|
| $NH_3/H_2O$ | Evaporative at temperatures below 0 °C | Toxic and dangerous for health ($NH_3$) |
| | | Column of rectifier required |
| | | Operation at high pressure |
| $H_2O/LiBr$ | High COP | Risk of congelation, therefore anticrystallization device required |
| | Low operation pressures | Relatively expensive (LiBr) |
| | Environmetally friendly and innoxious | |
| | Large latent heat of vaporisation | |

Most large-scale applications (>300 kW) use $H_2O$/LiBr and produce chilled water at about 6-7 °C, at a COP relatively higher than using $NH_3/H_2O$. However, LiBr systems must be water-cooled and thus usually require a cooling tower, whereas $NH_3$ systems can have an air-cooled condenser. $H_2O$/LiBr chillers usually have large physical dimensions due to the large water refrigerant vapor volume. A $NH_3/H_2O$ system is favoured for small cooling loads and applications where water-cooling cannot be used.

The refrigerant freezes at 0 °C in $H_2O$/LiBr systems, so proper measurements should be considered while the system is idle, particularly in winter. Another potential problem is crystallization of the LiBr solution at high concentrations, which may result from high generator temperatures or from inadequate temperature control at other parts of the system. Thus, it is necessary to adequately control the heat supply temperature from the heat storage. The temperature of the cooling-water, especially for the absorber, must also be monitored. Chiller capacity can be controlled by increasing the temperature of the heat supply or by decreasing the temperature of the cooling-water.

The most suitable refrigerant/absorbent working pair alternative to $H_2O$/LiBr and $NH_3/H_2O$ can be water/lithium fluoride ($H_2O$/LiF), water/lithium chloride ($H_2O$/LiCl), water/sodium hydroxide ($H_2O$/NaOH) and water/sodium formate ($H_2O$/HCOONa). Moreover, there are ternary mixtures suitable for the absorption cycle such as water/lithium bromide+lithium nitrate ($H_2O$/LiBr+$LiNO_3$) and water/lithium chloride+zinc chloride ($H_2O$/LiCl+$ZnCl_2$).

Multi-stage absorption chillers were introduced to more efficiently exploit medium temperature heat sources and enhance the COP of the absorption chiller. The number of stages is equivalent to the number of generator heat exchangers installed at various temperature levels in the chiller. However, only double-stage absorption chillers, as seen in Figure 1.7, have reached commercialization mainly due to their complexity and the increased cost of such systems. Double-stage absorption chillers generate almost twice the refrigerant vapor generated in the respective single-stage unit, and thus a significant increase in the COP is reported, allowing double-stage chillers to more efficiently exploit higher temperature heat sources [12]. Apart from enhancing the COP, multi-stage configurations also allow for a higher temperature lift (the temperature difference between the condenser and the evaporator) [8, 13].

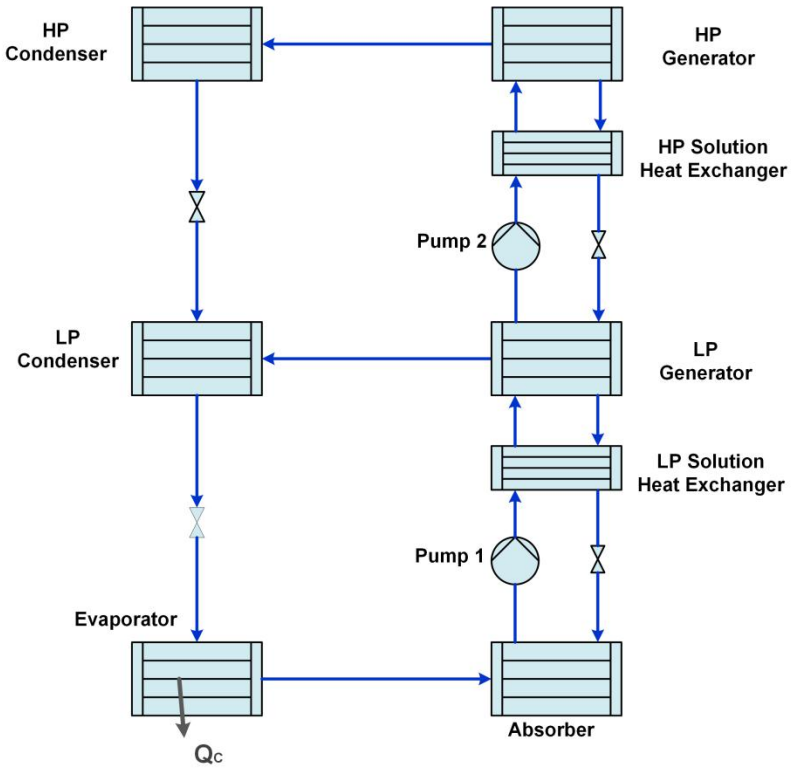


*Figure 1.7. Schematic of a double-effect absorption cooling cycle[8]*

### 1.3.3 Energy analysis

The energy analysis presented below is based in the schematic in Figure 1.6 (state points 1, 2, 3, 4 beginning from the generator up to the absorber and passing through the condenser, the refrigerant valve and the evaporator, state points 8, 9, 10 beginning from the absorber up to the generator and passing through the pump and the SHX and state points 5, 6 ,7 beginning from the generator up to the absorber and passing through the SHX and the solution valve):

Mass balance

$$\dot{m}_1 = \dot{m}_2 = \dot{m}_3 = \dot{m}_4 \quad (1.5)$$

$$\dot{m}_5 = \dot{m}_6 = \dot{m}_7 \quad (1.6)$$

$$\dot{m}_8 = \dot{m}_9 = \dot{m}_{10} \quad (1.7)$$

$$\dot{m}_8 = \dot{m}_1 + \dot{m}_7 \quad (1.8)$$

Energy balance

Condenser: Heat rejection to the environment, in intermediate temperature level.

$$\dot{Q}_c = \dot{m}_1 \cdot (h_1 - h_2) \quad (1.9)$$

Evaporator: Heat gain in the refrigerant from the chilled space.

$$\dot{Q}_e = \dot{m}_1 \cdot (h_4 - h_3) \quad (1.10)$$

Absorber: Heat rejection to the environment, in intermediate temperature level.

$$\dot{Q}_a = \dot{m}_4 \cdot h_4 + \dot{m}_7 \cdot h_7 - \dot{m}_8 \cdot h_8 \quad (1.11)$$

Generator/desorber: Heat input to generator in high temperature level from external heat source.

$$\dot{Q}_g = \dot{m}_1 \cdot h_1 + \dot{m}_5 \cdot h_5 - \dot{m}_{10} \cdot h_{10} \quad (1.12)$$

Solution heat exchanger:

$$\dot{m}_7 \cdot (h_5 - h_6) = \dot{m}_8 \cdot (h_{10} - h_9) \quad (1.13)$$

Pump:

$$\dot{W}_{pump} = \dot{m}_8 \cdot (h_9 - h_8) \quad (1.14)$$

Throttling valves:

$$\Delta h = 0 \quad (1.15)$$

The whole system's energy analysis gives:

$$\dot{Q}_g + \dot{Q}_e = \dot{Q}_a + \dot{Q}_c \quad (1.16)$$

The coefficient of performance COP for the absorption cooling cycle is:

$$COP = \frac{\dot{Q}_e}{\dot{Q}_g + \dot{W}_{pump}} \quad (1.17)$$

It is worth mentioning that the work of the pump is negligible compared to the heat gain in the evaporator.

The highest value of the COP in absorption cooling is $COP_{carnot}$ and serves as a benchmark:

$$COP_{carnot} = (1 - \frac{T_a}{T_g}) \cdot (\frac{T_e}{T_c - T_e}) \quad (1.18)$$

In order to carry out an energetic analysis of the absorption process, an enthalpy-concentration diagram for the working binary mixture must be used, as shown in Figure 1.8:

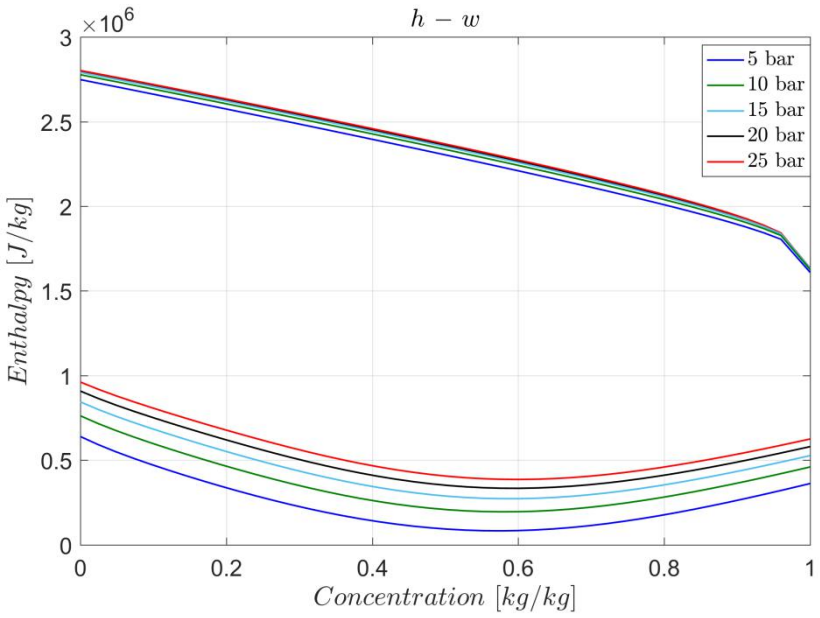


*Figure 1.8. The enthalpy-concentration diagram for $NH_3/H_2O$ [8]*

The solution circulation ratio g is defined as:

$$g = \frac{\xi_d - \xi_r}{\xi_r - \xi_w} = \frac{\dot{m}_5}{\dot{m}_1} \tag{1.19}$$

The values $\xi_d$, $\xi_r$, $\xi_w$ [kg of refrigerant/kg of solution] are the mass percent compositions of $\dot{m}_1, \dot{m}_{10}, \dot{m}_5$ .

Compared to the aforementioned theoretical case, there are some deviations in the cycle in actual applications due to irreversibilities. The main problems include the losses in the processes of internal and external heat transfer, the non-ideal processes of absorption and desorption, the pressure drops and the non-condensable gases.

## 1.4. Adsorption cooling

Adsorption entails molecules being distributed between two phases, one being a solid while the other either a liquid or a gas. Adsorption is a well-known and documented technology for water treatment, liquid purification, and gas cleaning. Only in the 1990s, however, did researchers begin to investigate the potential use of adsorption as a cycle of refrigeration [8, 14-16].

The adsorption cycle consists of two main phases: desorption and adsorption. Initially, the system is at low pressure and temperature: refrigerant saturates the adsorbent in the adsorber. The desorption phase is initiated to regenerate it. An external heat source heats the adsorbent, driving the coolant out of the adsorbent and increasing the pressure of the system. In the condenser, the desorbed refrigerant condenses, producing heat. Adsorption is the next phase. The adsorber is cooled back to ambient temperature and connected to the evaporator, resulting in the adsorption of the refrigerant.

Figure 1.9 presents the basic layout of a two-bed adsorption cycle, as described previously.

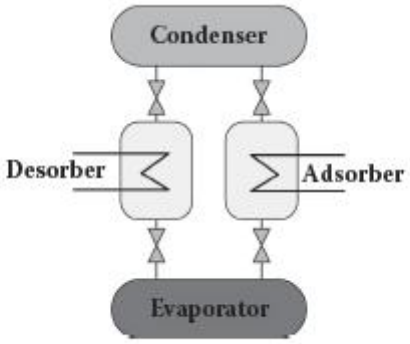


*Figure 1.9. Schematic of a double-bed adsorption system* [8]

Adsorption allows extremely low temperature heat sources to be exploited while using rather simple, compared to absorption, equipment. In addition, the absence of moving parts and vibrations, low operating costs and the potential use of waste heat and solar energy make adsorption a highly competitive alternative to conventional VCC systems [17, 18]. The main constraint of adsorption technology is the relatively low COP resulting from the limited adsorptive capacity of commercially used adsorbents [19].

Two working pairs are mainly used in commercial applications as far as working pairs are concerned: silica gel-water and zeolite-water. For a single stage adsorption cycle with partial vacuum pressure and 6.7 °C evaporation temperature, 29.4 °C condensation temperature and 80 °C regeneration temperature, the theoretical refrigeration COP may be as high as 0.68, with 217.3 kJ/kg corresponding specific cooling effect [20]. Standard working COP for a zeolite-based domestic adsorption chiller is within the range of 0.5-0.55 - 15 °C evaporation, 30 °C condensation and 90 °C regeneration temperature [7, 21].

## 1.5. Literature review

Direct-fired machines with capacities greater than 35 kW take over the largest portion of the current absorption chiller market. Recent R&D efforts in the field of direct-fired machines focus primarily on the development of high-efficiency machines by raising the working temperatures or hybridization of absorption cycles.

On the other hand, there is a relatively small market for indirect-fired chillers, i.e. water or steam-fired machines and the development of absorption chillers for small-scale residential and commercial applications is the focus of many recent R&D activities. Table 1.2 lists some small absorption chillers available in the market.

*Table 1.2. Small-capacity absorption chillers (cooling capacity smaller than 35 kW) [22].*

| Cycle type | Working pair | Manufacturer | Country | Qe (kW) | Cooling medium | Heating medium | Min. driving T (°C) | Cooling COP |
|---|---|---|---|---|---|---|---|---|
| SE | $H_2O$/LiBr | Phoenix | Germany | 10 | water | Hot water | 90-100 | 0.74 |
| | $H_2O$/LiCl | EAW | Germany | 15 | water | Gas-fired | 150-170 | 0.74 |
| | $NH_3/H_2O$ | Yazaki | Japan | 35 | air | | 160-180 | 0.71 |
| DE | $H_2O$/LiBr | Rotartica | Spain | 11 | | | | 0.67 |
| GAX | $NH_3/H_2O$ | ClimateWell AB | Sweden | 7 | | | | 0.7 |
| | | Pink | Austria | 10 | | | | 0.6 |
| | | Rinnal | Japan | 5 | | | | 1.2-1.3 |
| | | Robur | Italy | 18 | | | | 0.8-0.9 |
| | | Cooling Technologies | USA | 17 | | | | |

Only the single-effect chillers are suitable for solar cooling among the chillers in Table 1.2. The particular double-effect and GAX chillers are all direct-fired.

All single-effect absorption chillers on the market are currently water-cooled and they require a driving temperature in the range between 90 and 100 °C for a COP between 0.6 and 0.74.

The particular double-effect chiller in the table is a water-cooled, city gas-fired machine and yields a cooling COP of about 1.2. It would require approximately 160 °C steam or pressurized hot water to drive an equivalent indirect-fired machine.

*Table 1.3. Listing of studies on absorption chillers [5, 8, 22]*

| Reference | Cycle type | Working pair | COP (-) | $Q_e$ (kW) | Hot water provided (heat source) (°C) | Chilled water produced (°C) | Cooling water (°C) | $T_g$ (°C) | $T_e$ (°C) | $T_c$ (°C) | $T_a$ (°C) | $Q_g$ (kW) |
|---|---|---|---|---|---|---|---|---|---|---|---|---|
| Hattem and Dato (1981) | SE | $H_2O$-LiBr | 0.54 | - | - | - | - | - | - | - | - | - |
| Al-Karaghouli et al (1991) | SE | $H_2O$-LiBr | 0.62 | - | - | - | - | - | - | - | - | - |
| Best and Ortega (1983-1986) | SE | $H_2O$-LiBr | 0.53 - 0.73 | - | 75-95 | - | - | - | - | - | - | - |
| Izquierdo et al (2005) | SE | $H_2O$-LiBr | 0.34 | 7.5 | - | - | - | - | - | - | - | - |
| Storkenmaier et al (2003) | SE | $H_2O$-LiBr | 0.74 | 10 | 85 | 15 | 27 | - | - | - | - | - |
| Safarik et al (2005) | SE | $H_2O$-LiBr | 0.75 | 16 | 90 | 15 | 32 | - | - | - | - | - |
| Safarik et al (2005) | SE | $H_2O$-LiBr | 0.8 | 16 | 80 | 15 | 27 | - | - | - | - | - |
| Richter and Safarik (2005) | SE | $NH_3$-$H_2O$ | 0.54 | 15 | 95 | 3 | - | - | - | - | - | - |
| Richter and Safarik | SE | $NH_3$-$H_2O$ | 0.54 | 20 | 100 | -6 | - | - | - | - | - | - |

| | | | | | | | | | | | | |
|---|---|---|---|---|---|---|---|---|---|---|---|---|
| (2005) | | | | | | | | | | | | |
| Erhard and Hahne (1994) | - | $NH_3$-$SrCl_2$ | 0.49 | - | - | - | - | - | - | - | - | - |
| Erhard and Hahne (1995) | - | $NH_3$-$SrCl_2$ | 0.45 - 0.82 | - | - | - | - | - | - | - | - | - |
| Medrano et al (-) | - | TFE-TEGDME | 0.45 | - | - | - | - | - | - | - | - | - |
| Medrano et al (-) | - | methanol-TEGDME | 0.45 | - | - | - | - | - | - | - | | - |
| Pilatowsky et al (-) | - | monomethyl amine-$H_2O$ | 0.72 | - | - | 10 | - | 60 | - | - | - | - |
| Rivera and Rivera (-) | - | $H_2O$-LiBr | 0.15 - 0.40 | - | - | - | - | 120 | - | 40-44 | - | - |
| Nakahara et al (-) | SE | $H_2O$-LiBr | 0.4-0.8 | 6.5 | - | - | - | 70-100 | - | - | - | - |
| Darkwa et al (-) | - | $H_2O$-LiBr | 0.69 | - | 96.3 | - | - | - | - | - | - | - |
| Brendel et al (-) | - | $NH_3$-$H_2O$ | 0.58 - 0.74 | 10 | - | - | - | 80-120 | - | - | - | - |
| Bermejo et al (-) | DE | $H_2O$-LiBr | 1.10 - 1.25 | - | - | - | - | - | 8 | - | - | - |
| Balamure et al (2000) | - | $NH_3$-($H_2O$-NaOH) | 0.58 | 4.0-10.0 | - | - | - | 60-160 | - | - | - | - |

| | | | | | | | | | | | | |
|---|---|---|---|---|---|---|---|---|---|---|---|---|
| De Lucas et al (-) | - | $H_2O$-LiBr | 0.75 | 1580 | - | - | - | 101.7 | 5.5 | 46.1 | 40 | 2084.67 |
| De Lucas et al (-) | - | $H_2O$-(LiBr:$CHO_2K$= 2:1) | 0.85 | 1580 | - | - | - | 66 | 5.5 | 46.1 | 15 | 1850.21 |
| Kaushik and Arora (2009) | SE | $H_2O$-LiBr | 0.6-0.75 | - | - | - | - | 91 | - | - | - | - |
| Kaushik and Arora (2009) | DE (series flow) | $H_2O$-LiBr | 1-1.28 | - | - | - | - | 150 | - | - | - | - |
| Gomri (2010) | TE (triple-effect) | $H_2O$-LiBr | 1.85 | 300 | - | - | - | >125 | - | 33 | - | - |
| Gomri (2010) | DE | $H_2O$-LiBr | 1.3 | 300 | - | - | - | 95-125 | - | 33 | - | - |
| Gomri (2010) | SE | $H_2O$-LiBr | 0.8 | 300 | - | - | - | 60 | - | 33 | - | - |
| Somers et al (2011) | SE | $H_2O$-LiBr | 0.738 | 10.77 | - | - | - | 89.9 | 1.3 | 40.2 | - | - |
| Somers et al (2011) | DE | $H_2O$-LiBr | 1.387 | 354.4 | - | - | - | 89.9 | 1.3 | 40.2 | - | - |
| Aman et al (2014) | SE | $NH_3$-$H_2O$ | 0.6 | 10 | - | - | - | 80 | 2 | 30 | - | 16.77 |
| Sochard et al (2017) | SE (GAX) | $NH_3$-$H_2O$ | 0.6 | 8 | - | - | - | - | - | - | - | - |
| Asdrubali and Grignaffini | SE | $H_2O$-LiBr | 0.42 | 17 | - | 6 | - | 70 | - | - | - | - |

| | | | | | | | | | | | | |
|---|---|---|---|---|---|---|---|---|---|---|---|---|
| (2005) | | | | | | | | | | | | |
| Arivazhagan et al (2006) | HE (double-stage) | R134a-DMAC | 0.36 | 1 | - | - | - | 70 | - | 20-25 | 20-35 | - |
| Zetzsche et al (2009) | - | $NH_3$-$H_2O$ | 0.72 | 10 | - | 14 | 27-32 | 100 | - | - | - | - |
| Le Costel et al (2013) | - | $NH_3$-$H_2O$ | 0.6 | 10 | - | - | - | 86 | 19 | 34 | 31 | - |
| Lamine and Said (2014) | - | $H_2O$-LiBr | 0.75 | - | - | - | - | 85-100 | 5 | 30 | 38 | - |
| Beausoleil-Morisson et al (2015) | SE | $H_2O$-LiBr | 0.56 - 0.83 | 6.9-40.5 | 70-93 | 15-19 (inlet) | - | - | - | - | - | 65 |
| Zamora et al (2015) | - | $NH_3$-$LiNO_3$ | 0.61 | 10.1 | - | - | - | 90 | 15.5 | 35 | - | - |
| Xu et al (2015) | variable effect | $H_2O$-LiBr | 0.69 - 1.08 | 50 (51.9) | - | 13.5 (inlet) | 27.6 (inlet) | 125 (120) | 5 | 40 | 35 | - |
| Franchini et al (2015) | - | $H_2O$-LiBr | 0.358 | 5 (3.25) | 88.2 | 19.8/16.6 (inlet/outlet) | - | - | 8.5 | 34.9 | - | - |
| Oh et al (1994) | DE | $H_2O$-LiBr | 1.27 | 7 | - | - | - | - | - | - | - | - |
| Mazloumi et al (2008) | SE | $H_2O$-LiBr | 0.67 - 0.76 | 17.5 | - | - | - | - | - | - | - | - |
| Ortega et al (2008) | - | $NH_3$-$H_2O$ | 0.458 | 4.8 | - | - | - | - | -10 | - | - | - |
| Kim and | HE | $H_2O$-LiBr | 0.38 | 10 | - | 5.7 | - | 90 | - | - | - | - |

| | | | | | | | | | | | | |
|---|---|---|---|---|---|---|---|---|---|---|---|---|
| Infante Ferreira (2009) | | | | (12.8) | | | | | | | | |
| Caciula et al (2013) | - | $NH_3$-$H_2O$ | 0.73 | - | - | - | - | 74 | 6 | - | - | - |
| Ssembatya et al (2014) | SE | vapor | 0.4-0.7 | 35.2 | - | - | - | - | - | - | - | - |
| Ketfi et al (2015) | SE | $H_2O$-LiBr | 0.78 | 70 | - | - | - | 92 | 7 | 30 | 30 | 90 |
| Lubis et al (2016) | single-double effect | - | 1.93 | - | 90 | - | 34 | - | - | - | - | - |
| Porumb et al (2017) | single-stage | $H_2O$-LiBr | 0.81 | - | 100 | 18 (inlet) | 27 (inlet) | - | - | - | - | - |
| Matsushima et al (2010) | TE | - | 1.6 | - | - | - | - | - | - | - | - | - |
| Yin et al (2013) | - | $H_2O$-LiBr | 0.31 | 8 (4.6) | 70-95 | 9 | - | - | - | - | - | - |
| Winston et al (2014) | DE | $H_2O$-LiBr | 0.99 | 23 | - | - | - | - | - | - | - | - |
| Albers (2014) | - | - | 0.76 | - | - | - | - | - | - | - | - | - |

*Table 1.4. Typical performance of absorption cycles [5].*

| Absorption system | COP (-) | Heat-source temperature (°C) | Type of solar collectors matched |
|---|---|---|---|
| Single-effect | 0.7 | 85 | Flat-plate |
| Double-effect | 1.2 | 130 | Flat-plate/Compound parabolic concentrator |
| Triple-effect | 1.7 | 220 | Evacuated-tube/Concentrating collector |

Table 1.4 may be used as an indicator of the typical performance values and the most preferable type of solar collectors of each absorption system. As the systems become more complex and efficient, the type of solar collectors required is also more complex (and expensive) in order to capture greater temperatures.

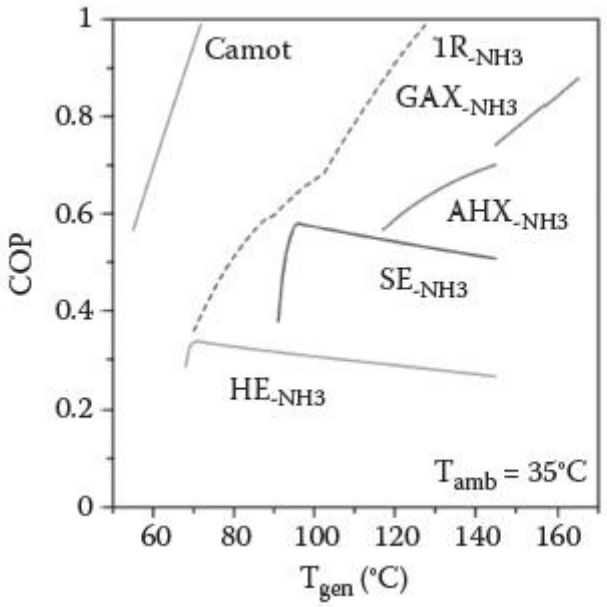


*Figure 1.10. COP performance of several $NH_3$-$H_2O$ absorption cycles (SE: single-effect, HE: half-effect) [8].*

This diagram is a comprehensive depiction of the various absorption systems used. In the single-effect (SE) system there is a steep rise of the COP for low generator temperatures until approximately 95 °C and a mild decrease for higher temperatures.

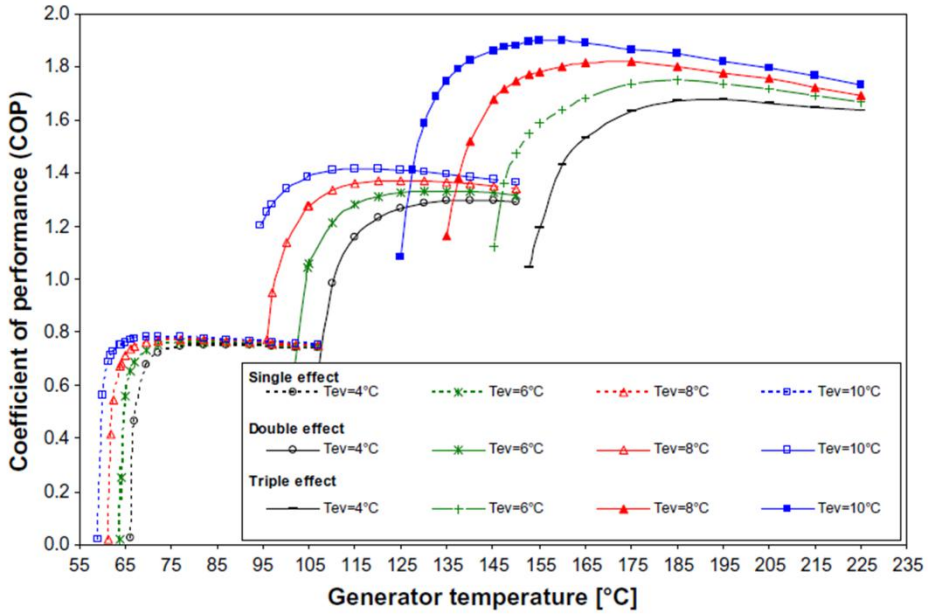


*Figure 1.11. Behavior of the COP for the single-, double- and triple-effect absorption chiller for several generator and evaporation temperatures. [8].*

The behavior of the COP of these systems as the generator temperature in Figure 1.11 rises is the same as in Figure 1.10. Moreover, there is an enhancement of the COP as the evaporator temperature increases.

*Table 1.5. Three $NH_3$-$H_2O$ prototype chillers [8, 23].*

| Parameter | 1st chiller | 2nd chiller | 3rd chiller |
|---|---|---|---|
| Capacity (kW) | 5 | 5 | 100 |
| Evaporator working range (°C) | -10/18 | 9/18 | -10/18 |
| Condenser working range (°C) | 15/45 | 23/33 | 18/45 |
| Generator working range (°C) | 60/130 | 60/95 | 70/180 |
| Experimental max reported COP (-) | 0.71 | 0.67 | 0.58 |

As it is expected, the COP values of the experimental systems are generally lower than those of a theoretical or simulated system (usually 0.73) because energy losses are more prevalent.

*Table 1.6. Overview of the Absorption Chiller Market [8, 23, 24]*

| Manufacturer (Country) | Model | Working pair | Capacity (kW) | COP (-) |
|---|---|---|---|---|
| AGO (Germany) | Congelo | $NH_3$-$H_2O$ | 50-150 | 0.51 |
| Baelz | Bee/Bumblebee | $H_2O$-LiBr | 50/160 | 0.8 |
| Broad Air Conditioning Co. (China) | BCT | $H_2O$-LiBr | 16-500 | 1.1 |
| Carrier Corporation (USA) | 16LJ | $H_2O$-LiBr | 90-4,000 | n/a |
| | 16TJ | $H_2O$-LiBr | 350-2,500 | n/a |
| | 16NK | $H_2O$-LiBr | 352-4,652 | n/a |
| CENTURY Corporation (South Korea) | AR-D | $H_2O$-LiBr | 98-193 | n/a |
| ClimateWell AB (Sweden) | ClimateWell Solar Chiller | LiCl-$H_2O$ | 7 | 0.7 |
| Colibri B.V. / Stork B.V. (Netherlands) | ARP | $NH_3$-$H_2O$ | 100 - >2,500 | Up to 0.8 |
| EAW (Germany) | Wecagral SE | $H_2O$-LiBr | 15-200 | 0.71-0.75 |
| En-Save (Germany) | En-Save Cold | $NH_3$-$H_2O$ | 30-100 | n/a |
| Heinen & Hopman (Netherlands) | SWM60-SWM1200 | $H_2O$-LiBr | 150-5,000 | Up to 0.8 |
| Helioclim (France) | (pilot plant) | $NH_3$-$H_2O$ | 10 | n/a |

| | | | | |
|---|---|---|---|---|
| JIANGSU HUINENG (China) | RXZ | $H_2O$-LiBr | 10-175 | 0.70 |
| Krloskar Pneumatic Company (India) | KVAC-SA/DA | $H_2O$-LiBr | 211-2400 | n/a |
| LG A/C (South Korea) | WCDH | $H_2O$-LiBr | 350-5,275 | 1.51 |
| | WCMH | $H_2O$-LiBr | 98.4-3,587 | 0.80 |
| Meibes System-Technik (Germany) | n/a | $H_2O$-LiBr | 5 | n/a |
| Phoenix (Germany) | n/a | $H_2O$-LiBr | 10 | 0.74 |
| PINK (Austria) | PC19 | $NH_3$-$H_2O$ | 19 | 0.63 |
| Robur (Italy) | GA ACF | $NH_3$-$H_2O$ | 17.7 | Up to 0.9 |
| Rotartica (Spain) | Solar 045 | $H_2O$-LiBr | 11 | 0.67 |
| SAKURA (Japan) | SHL | $H_2O$-LiBr | 10.5-176 | 0.71-0.80 |
| SOLARICE GmbH (Germany) | n/a | $NH_3$-$H_2O$ | 25 - several MWs | n/a |
| THERMAX (India) | LT 1/2/3/5 | $H_2O$-LiBr | 35-171 | 0.78 |

As seen in the table above, the most used working pair in the market is $H_2O$/LiBr followed by $NH_3$/$H_2O$ and $H_2O$/LiCl. It is also clear that Europe is a leader in the absorption chiller market.

## 1.6. Thesis scope

There are already some studies of the absorption refrigeration cycle using Aspen Plus, however there is not an extensive study of alternative working pairs, therefore there is room for improvement. Main goal of this study is to investigate the performance of various pairs

(and ternary mixtures) in a range of temperatures and calculate their cost in order to identify which pairs outcompete the conventional ones.

In the next chapters the main scientific questions to be addressed are the following:

- How will absorption refrigeration cycle modeling be performed on Aspen Plus?
- What are the appropriate inputs to be entered for the model to work without errors/warnings?
- How will the model be validated?
- What is the COP of the installation?
- How will the sensitivity analysis be performed?
- How do the various alternative pairs (including ternary mixtures) compare with conventional pairs?
- What is the total cost of installation for each pair?
- Considering performance and cost, which pairs stand out as the most advantageous?

In order to give an answer to the above, the $H_2O$/LiBr cycle has to be modeled in Aspen Plus and the results of the model along with the corresponding sensitivity analysis will be compared with the alternative pairs. The modeling of the unique $NH_3/H_2O$ cycle model is also necessary, as well as the calculation of the cost of the cycles.

# Chapter 2. Water/LiBr Cycle Modeling with Aspen Plus

This thesis' objective is to compare various absorption chiller working pairs as far as cooling capacity and COP is concerned. One of the most common pairs is $H_2O$/LiBr and it will be used as reference for the following cases. In order to model the $H_2O$/LiBr absorption cycle Aspen Plus was used [25]. It was selected over other programs, like EES, because it is easier and quicker to design chemical processes and vary operating conditions to understand the behavior of a system. ASPEN is a process modeling software suite and Aspen Plus is one of its programs useful for steady-state process modeling. The user interface is based on a library of ready-made, user-editable Fortran-based component models. By connecting these components with material, heat and work streams and providing values of predefined inputs, the user is able to model complex processes. Moreover, its user interface is elegant and easy to use. The integration of chiller models created in ASPEN into other processes modeled in ASPEN is feasible and helps when there is a waste heat source available.

## 2.1. Property method

The property method used for the $H_2O$/LiBr solution was the ELECNRTL property method because it is more appropriate compared to the Peng-Robinson method as it is precisely designed for electrolyte solutions [25]. States 7-10 are pure water, hence steamNBS property method was used in Aspen Plus, which includes look-up tables for pure steam. The property method selection is presented in Figure 2.1.

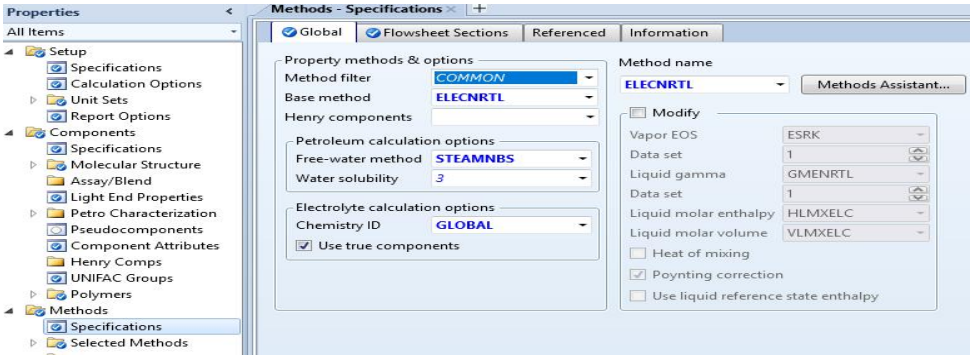


*Figure 2.1. Property method selection in Aspen Plus*

## 2.2. State Points

The schematic of the modeled cycle corresponds to Figure 1.6, but the state points are represented differently in order to resemble other studies. This will enable comparisons and verifications to be made more easily.

The state points will be defined in the following way and will be referred as such throughout this thesis to avoid confusion. For the single effect cycle of $H_2O$/LiBr, the absorber exit is state 1, the pump exit is state 2, the solution heat exchanger exit leading to the desorber is state 3, the liquid exit of the desorber is state 4, the solution heat exchanger exit leading to the solution valve is state 5, the solution valve exit is state 6, the gas exit of the desorber is

state 7, the condenser exit is state 8, the refrigerant valve exit is state 9, and the evaporator exit is state 10.

Some assumptions need to be made for the cycle in order to help the modeling process. States 1, 4 and 8 are saturated liquid, states 7 and 10 are saturated vapor, state 2 is calculated by the solution pump model, states 3 and 5 are calculated by the SHX model, state 6 is calculated by the solution valve model and state 9 is calculated by the refrigerant valve model.

## 2.3. Components modeling

At this point, it will be shown how the various parts of the cycle in Aspen Plus are modeled. Some parts are very simple and consist of a single block. Many basic components (pumps, valves etc) might be modeled simply by selecting the equivalent block in Aspen Plus. Other components, like the desorber, are more complex and need a number of blocks to be adequately represented. The complexity depends on the process and how it is programmed in Aspen Plus.

### 2.3.1 State Point 1

Since Aspen Plus uses a sequential solver, a “break” in closed cycles is needed to give the model inputs, inserted in this case at state point 1. Therefore, the exit of the absorber (stream 1A) and the inlet of the pump (stream 1) are not connected and if the two streams conclude giving the same results, it is an indication that the model is well designed and has converged. The inputs for state 1 are the temperature, a vapor quality of zero, the mass flow rate, and the concentration of water and lithium bromide. The “break” is presented in Figure 2.2.

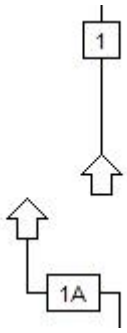


*Figure 2.2. The “break” between stream 1 and stream 1A*

### 2.3.2 Valves

The valves are modeled simply by selecting VALVE2 in valve/pressure changers in the simulation window. For the single effect cycle there are two valves that need to be modeled, one solution valve and one refrigerant valve. The only input needed for both valves is the outlet pressure. In “Calculation type”, “Adiabatic flash for specified outlet pressure (pressure changer)” is selected. To increase the possibility of convergence, the number of iterations is increased. The valve model is presented in Figure 2.3.

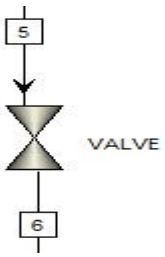


*Figure 2.3. H2O/LiBr valve model in Aspen Plus*

### 2.3.3 Pump

A pump is used after state point 1 and increases its pressure to a value determined as an input in discharge pressure. ICON1 is selected in pump/pressure changers in the simulation window. The efficiency in both pump and driver is considered 1, as the effect of the pump on the total energy balance is negligible (the pump work is less than 0.1% of the heat duties of the other components). The pump model is presented in Figure 2.4.

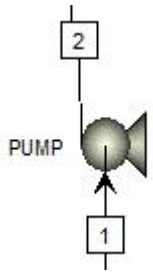


*Figure 2.4. H2O/LiBr pump model in Aspen Plus*

### 2.3.4 Solution Heat Exchanger

A solution heat exchanger is used in the cycle to enhance the overall performance. Heat is transferred from state 4 (the hot side inlet) to state 2 (the cold side inlet), resulting in states 5 (the hot side exit) and 3 (the cold side exit). Two heater blocks were used to model the solution heat exchanger and a heat stream (QSHX) connects them as an indication that the heat rejected on the hot side is to be transferred to the cold side. HEATER is selected twice in heater/exchangers in the simulation window. In both heaters pressure drop is assumed zero and heat duty is also an input in one of the two. The solution heat exchanger model is presented in Figure 2.5.

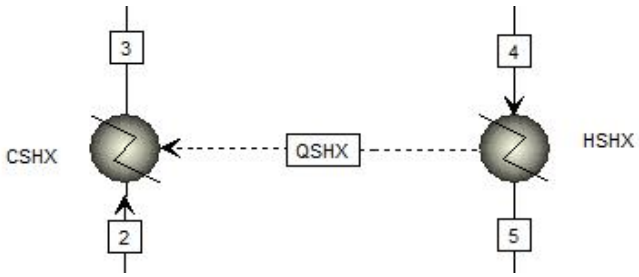


*Figure 2.5. $H_2O$/LiBr solution heat exchanger model in Aspen Plus*

### 2.3.5 Evaporator

The evaporator is modeled as a heater. Modeling the evaporator, or the succeeding components, as heat exchangers with two heaters was unnecessary as it only complicated

the cycle and led to warnings and errors in Aspen Plus. The refrigerant passing through the evaporator is pure water, therefore the steamNBS property method was used for this component, as well as in all refrigerant-only components. The inputs for the evaporator were zero pressure drop and zero degrees of superheating, as the refrigerant exits as saturated vapor. Heat is added in the evaporator. The evaporator model is presented in Figure 2.6.

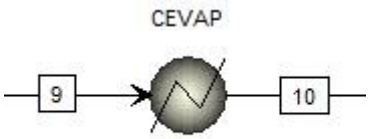


*Figure 2.6. $H_2O$/LiBr evaporator model in Aspen Plus*

### 2.3.6 Condenser

The condenser is also modeled as a heater and the steamNBS property method is used likewise. The inputs for the condenser were zero pressure drop and zero vapor fraction, as the water exits the condenser as saturated liquid. Heat is rejected from the condenser. The condenser model is presented in Figure 2.7.

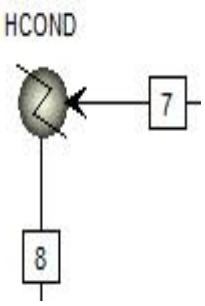


*Figure 2.7. $H_2O$/LiBr condenser model in Aspen Plus*

### 2.3.7 Absorber

The absorber is modeled as a heater with a solution inlet (stream 6), a refrigerant inlet (stream 10) and a solution exit (stream 1A). The inputs are zero pressure drop and the outlet temperature. Heat is rejected from the absorber. The absorber model is presented in Figure 2.8.

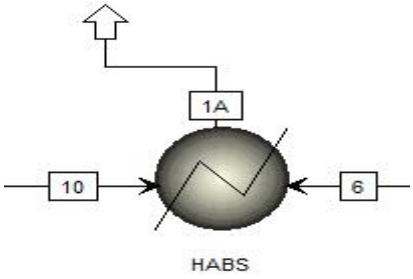


*Figure 2.8. $H_2O$/LiBr absorber model in Aspen Plus*

### 2.3.8 Desorber

The modeling of the desorber is more complicated and difficult as it involves separating components, while all the previous components dealt with mixing, pressure changes and heat addition or rejection. The desorber has a solution inlet (stream 3), a solution outlet which is saturated liquid (stream 4) and a pure water (refrigerant) outlet which is saturated vapor (stream 7). Heat is added in the desorber. To separate the vapor and the liquid a flash separator is used. V-DRUM1 is selected in Flash2/Separators in the simulation window. The inputs of the flash separator (block B5) are zero pressure drop and the outlet temperature. To define the state of the vapor outlet stream, its temperature needs to be assumed equal to the saturation temperature of the liquid solution at state 3. Therefore, a heater must be added after the flash to reduce the temperature and another heater before the flash to raise the temperature. The inputs are zero pressure drop and the heat duty (QS). The desorber model is presented in Figure 2.9.

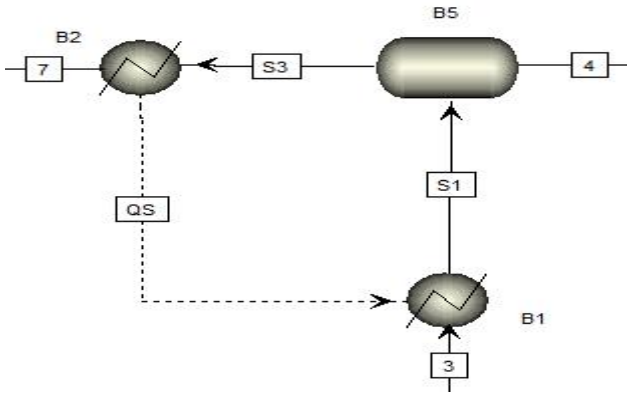


*Figure 2.9. $H_2O$/LiBr desorber model in Aspen Plus*

## 2.4. Complete model

The complete model of the $H_2O$/LiBr absorption cycle is shown in Figure 2.10.

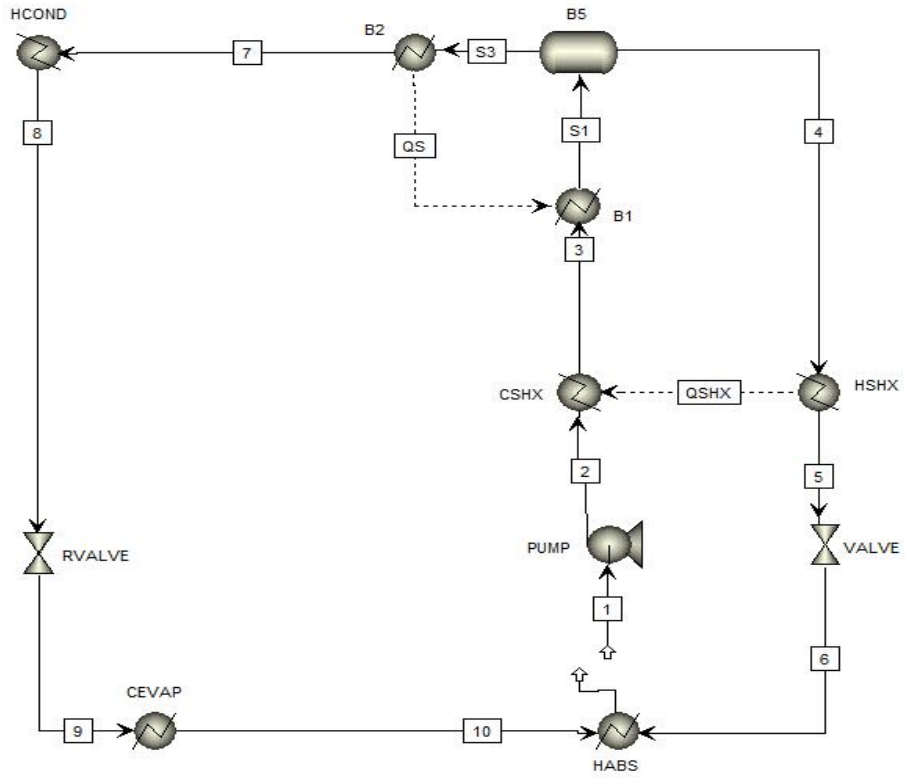


*Figure 2.10. Complete model of the single effect $H_2O$/LiBr cycle in Aspen Plus*

# Chapter 3. Water/LiBr model validation

In order to assess the validity of the model, the results must be checked in three ways. Firstly, a mass balance verification has to be performed to ensure that the system is correctly modeled. Then, an energy conservation verification is necessary to check for inconsistencies in the various blocks which add or reject heat. Last but not least, a comparison with the results of another study will be performed for further confirmation of the model.

## 3.1. Mass balance verification

After the absorber exit and before the pump inlet a "break" was modeled to provide inputs. The purpose of this "break" is to demonstrate if the model is well formulated by means of identical results, especially component and mass flow rates, between the streams before and after it.

As seen in Table 3.1 below, the streams 1 and 1A have equal mass flow rates. This demonstrates that the mass flow is conserved in the model.

*Table 3.1. Single effect $H_2O$/LiBr mass balance verification*

| Mass Flow (kg/s) | Stream 1 | Stream 1A |
|---|---|---|
| Total | 0.7839 | 0.7839 |
| $H_2O$ | 0.3810 | 0.3810 |
| LiBr | 0.4029 | 0.4029 |

## 3.2. Energy conservation verification

Moreover, an energy conservation verification is achieved in this model as the net amount of energy into and out of the cycle equals to zero. There are five components exchanging energy in the form of heat, while four are taken into consideration as the pump's contribution is negligible. The absorber and the condenser reject heat from the cycle, while the evaporator and the desorber add heat. Internal energy transfer, such as in the solution heat exchanger, is not regarded in the energy conservation verification. The energy equilibrium is presented in the following equation:

$$\left|Q_{des}+Q_{evap}\right|-\left|Q_{abs}+Q_{cond}\right|=363.941+307.455-352.207-319.138=0 \qquad (2.1)$$

As a result, the model is successful as far as energy conservation is concerned.

## 3.3. State point results and comparison with another study

After running the model of the single effect $H_2O$/LiBr cycle in Aspen Plus the following results were provided. They are presented in Table 3.2.

*Table 3.2. State point results for the single effect $H_2O$/LiBr cycle*

| State Point | $XH_2O$ (-) | XLiBr (-) | Temperature (°C) | Pressure (kPa) | Mass Flow (kg/s) | Vapor Fraction (-) |
|---|---|---|---|---|---|---|
| 1 | 0.486 | 0.514 | 33 | 1.228 | 0.7839 | 0 |
| 2 | 0.486 | 0.514 | 33 | 5.033 | 0.7839 | 0 |
| 3 | 0.486 | 0.514 | 56.49 | 5.033 | 0.7839 | 0 |
| 4 | 0.385 | 0.615 | 78.7 | 5.033 | 0.6547 | 0 |
| 5 | 0.385 | 0.615 | 47.63 | 5.033 | 0.6547 | 0 |
| 6 | 0.385 | 0.615 | 47.63 | 1.228 | 0.6547 | 0 |
| 7 | 1 | 0 | 58.68 | 5.033 | 0.1291 | 1 |
| 8 | 1 | 0 | 33 | 5.033 | 0.1291 | 0 |
| 9 | 1 | 0 | 10 | 1.228 | 0.1291 | 0.039 |
| 10 | 1 | 0 | 10 | 1.228 | 0.1291 | 1 |

Comparing these results to the results of another study [26] a number of small discrepancies in some streams can be spotted. These discrepancies are minute, and therefore negligible.

As shown by the results above, the low pressure is 1.228 kPa and the high pressure is 5.033 kPa. The concentration of LiBr in the strong solution side is 51.4% and in the weak solution side is 61.5%. The vapor fraction is either 0 or 1, namely saturated liquid and saturated vapor, except for state point 9 where it equals to 0.039, which is an acceptable value. As far as the mass flow rates are concerned, 83.5% of the total mass flow is led to the weak solution side, which is a typical value. Finally, the evaporation temperature is 10 °C, the desorber temperature is 78.7 °C and the condenser and absorber temperatures are 33 °C. Overall, the results are normal for a typical single-effect $H_2O$/LiBr cycle.

The heat duties and the COP of the cycle are presented in Table 3.3. The COP value is very satisfying as it is a bit above the typical COP value of a standard single-effect $H_2O$/LiBr cycle.

*Table 3.3. Heat duties and COP of the single-effect $H_2O$/LiBr cycle*

| | |
|---|---|
| Qcondenser (kW) | 319.138 |
| Qabsorber (kW) | 352.207 |
| Qevaporator (kW) | 307.455 |
| Qdesorber (kW) | 363.941 |
| COP (-) | 0.8448 |

## 3.4. Sensitivity analysis

The next step in this study is to run a sensitivity analysis in order to examine the model's behaviour to the changing variables. More specifically, the change of the value of Qevap (kW) and COP for different temperatures of the generator and the evaporator and for different strong solution LiBr concentrations will be examined.

Firstly, the generator temperature Tg is varied from 70 °C to 125 °C with an increment of 1°C. Then, the heat duties of the evaporator and the generator are defined and tabulated. The COP is also tabulated and its mathematical formula is written in the Fortran window. This sensitivity analysis is run for a number of LiBr concentrations.

Following the same idea, the evaporator temperature is varied by varying the low pressure in streams 6 and 9 from 0.7 kPa to 1.8 kPa with an increment of 0.1 kPa, which allows for temperatures between 1.9 °C and 15.8 °C. Then, the heat duties of the evaporator and the generator as well as the evaporator temperature are defined and tabulated. The COP is also tabulated and its mathematical formula is written in the Fortran window. This sensitivity analysis is also run for a number of LiBr concentrations.

The LiBr concentrations examined are 40%, 50%, 51.4%, 53% and 55%. Between 40% and 50% Aspen Plus bugged, therefore these values (e.g. 43%, 47%) are not taken into consideration.

The results of the sensitivity analysis while varying the generator temperature are presented below.

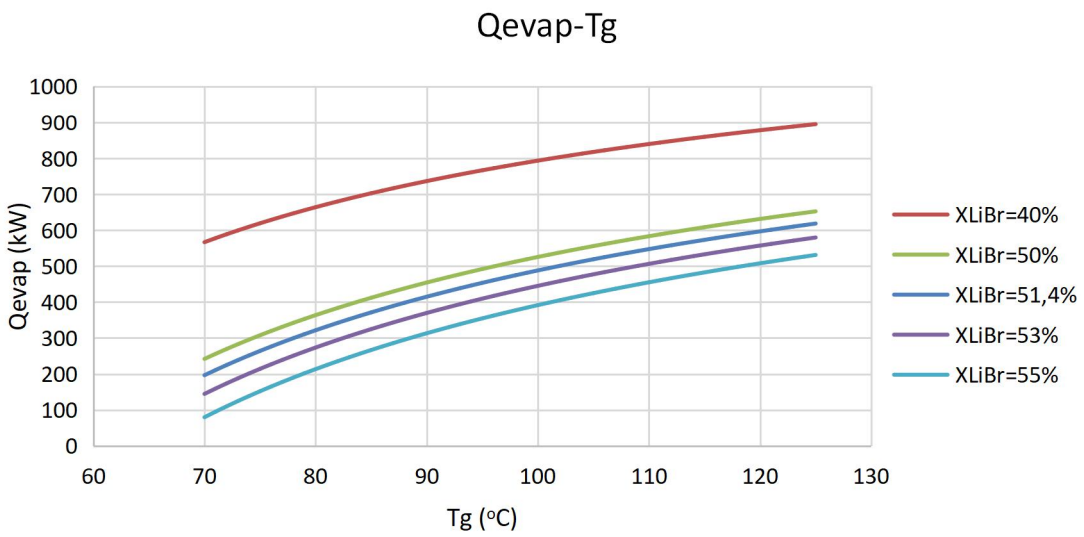


*Figure 3.1. Qevap-Tg diagram for various XLiBr values (Ta=33 °C, Tc=33 °C, Te=10 °C)*

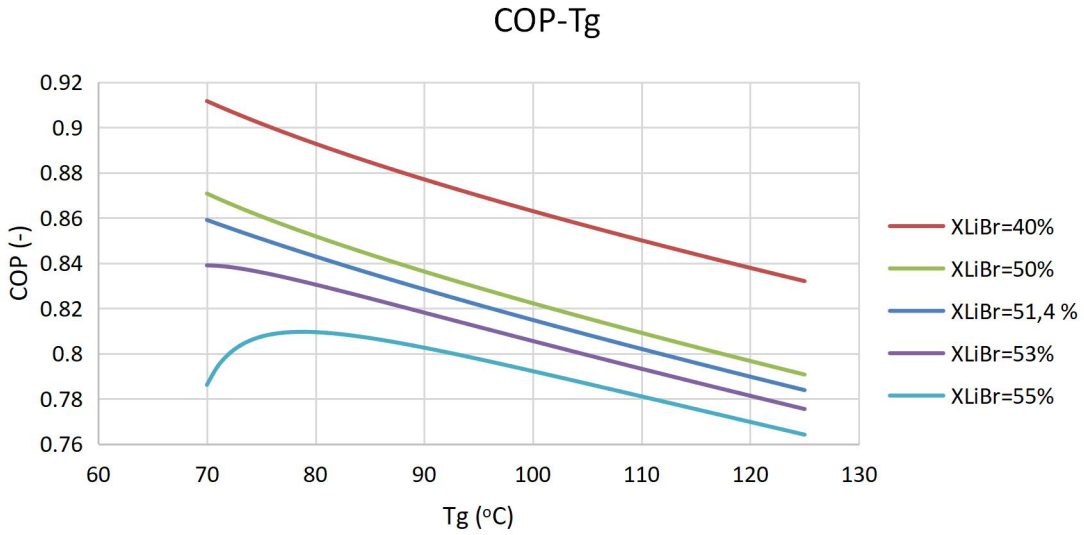


*Figure 3.2. COP-Tg diagram for various XLiBr values (Ta=33 °C, Tc=33 °C, Te=10 °C)*

As the generator temperature Tg increases, the heat duty of the evaporator Qevap also increases. However, the heat duty of the desorber increases in a higher rate, therefore the COP decreases. For the lowest concentrations of LiBr (XLiBr), in this case for XLiBr=55%, the COP curve has a different form, as for the lowest temperatures until approximately 78 °C there is a rise of the value of the COP and then a decrease. This form is also slightly visible in the XLiBr=53% curve, which suggests that the curves of higher XLiBr have the same form for lower temperatures.

Moreover, it is clear that the lower the value of XLiBr the higher the values of Qevap and COP. The reason for this is that as XLiBr decreases, $XH_2O$ increases in state point 1. This leads

to a higher mass flow of water after the separation in the desorber, which is directed towards the evaporator. The heat duty is proportional to the mass flow, hence its increase.

The range of Qevap for each curve is approximately 400 kW and that of COP is 0.1 for the examined temperatures.

The results of the sensitivity analysis while varying the evaporator temperature are presented below.

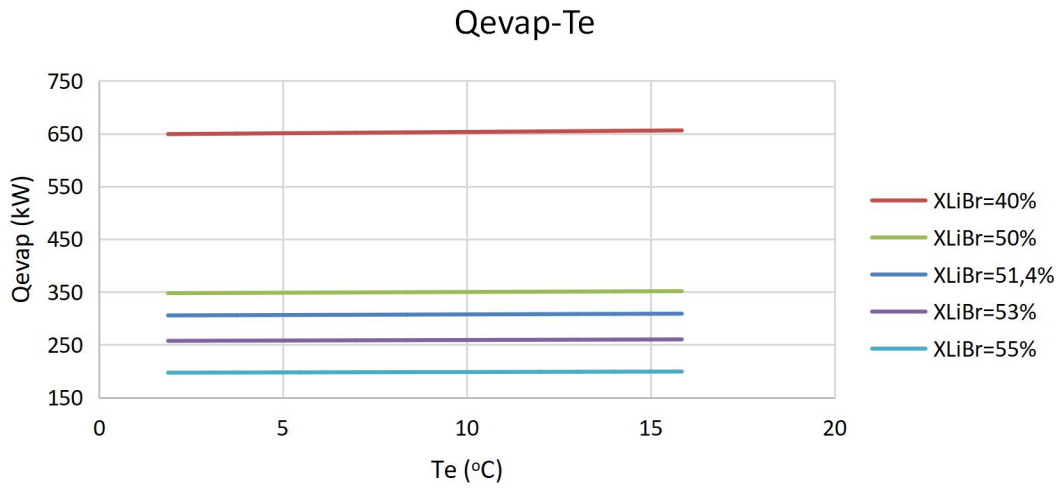


*Figure 3.3. Qevap-Te diagram for various XLiBr values (Ta=33 °C, Tc=33 °C, Tg=78.7 °C)*

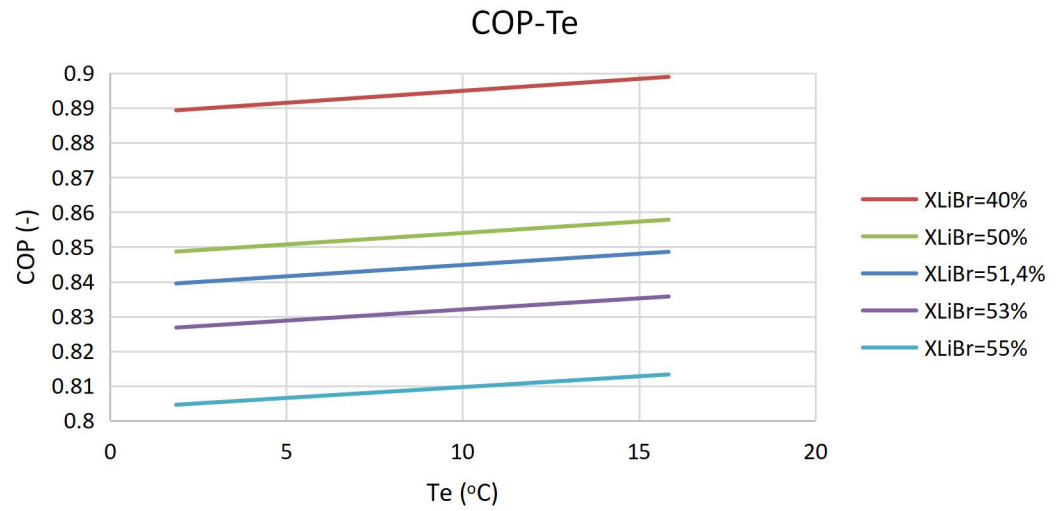


*Figure 3.4. COP-Te diagram for various XLiBr values (Ta=33 °C, Tc=33 °C, Tg=78.7 °C)*

In this case, it is clear that the heat duty of the evaporator has a small increase of 3-5 kW as the evaporator temperature rises and this affects the COP which has a very slight increase. The heat duty of the evaporator remains almost stable because of the shape of the curve in the p-h diagram, which allows for small changes of the latent heat duty for small changes of pressure or temperature (ranges: 1.1 kPa or 13.9 °C).

As in the previous sensitivity analysis, the lower the value of XLiBr the higher the values of Qevap and COP.

# Chapter 4. Lithium-based working pairs

The subject of this study is to analyze the behavior of different refrigerant-absorbent pairs as working fluids in an absorption cooling cycle and evaluate their energy efficiency. Even though the existing requirements of common applications are met adequately by the prevalent working pairs such as $H_2O$/LiBr, as these applications advance, additional requirements need to be discussed and research activities on new working pairs need to be resumed in order to overcome the disadvantages of the prevailing working pairs. New refrigerant-absorbent working pairs have been proposed and investigated by only a few research groups. As a matter of fact, the literature on other refrigerant-absorbent pairs and their mixtures for absorption chillers is limited, mainly due to the lack or inadequate number of pilot facilities, and mostly constrained by the operating and utility costs caused by exploring one by one each working pair.

Selection of the working fluids for the absorption cycles is depended on acceptability range for certain thermophysical and thermodynamic properties of the fluids and their chemical and physical properties.

The most common worthy characteristics of a refrigerant-absorbent mixture are:

- good chemical thermal stability,
- a large difference in boiling points of the absorbent and the refrigerant,
- non-corrosive, non-toxic, and non-flammable,
- freezing points of the liquid should be below the lowest temperature in the cycle,
- low viscosity of the solution under the desired operating conditions: this reduces the pump work,
- high equilibrium and solubility of the refrigerant in the absorbent, and
- high degree of negative deviation from Raoult's law.

The refrigerant should also possess the following characteristics:

- high critical temperature and pressure,
- high affinity for the absorbent at low temperatures, while less at high temperatures,
- low specific heat,
- high enthalpy of vaporization for better coefficients of performance, and
- low molecular weight.

Based on the already designed $H_2O$/LiBr model the following aqueous lithium-based working pairs were also simulated and their results compared: $H_2O$/LiF, $H_2O$/LiCl. The same assumptions were made in simulating all of the components in the model to allow for a meaningful comparison and inputs such as high and low pressures and temperatures were equal.

## 4.1. Mass balance verification of lithium-based working pairs

Firstly, the mass balance verification is examined. As seen in Table 4.1 below, the streams 1 and 1A have equal mass flow rates for all the lithium-based working pairs. This demonstrates that the mass flow is conserved in the model for these working pairs.

*Table 4.1. Single effect lithium-based working pairs mass balance verification*

| Mass Flow (kg/s) | Stream 1 | Stream 1A |
|---|---|---|
| Total | 0.7839 | 0.7839 |
| $H_2O$ | 0.3810 | 0.3810 |
| LiBr | 0.4029 | 0.4029 |
| LiF | 0.4029 | 0.4029 |
| LiCl | 0.4029 | 0.4029 |

## 4.2. Energy conservation verification of lithium-based working pairs

In addition, the energy conservation verification is examined. As stated in a previous chapter, the absorber and the condenser reject heat from the cycle, while the evaporator and the desorber add heat. Also, internal energy transfer, such as in the solution heat exchanger, is not regarded in the energy conservation verification. As seen in Table 4.2 below, the sums of the four heat streams equal zero for all working pairs, therefore the models are successful.

*Table 4.2. Single effect lithium-based working pairs energy conservation verification*

| | $H_2O$/LiBr | $H_2O$/LiF | $H_2O$/LiCl |
|---|---|---|---|
| Qcondenser (kW) | 319.138 | 657.457 | 442.539 |
| Qabsorber (kW) | 352.207 | 634.689 | 478.038 |
| Qevaporator (kW) | 307.455 | 628.36 | 424.503 |
| Qdesorber (kW) | 363.941 | 663.438 | 496.574 |
| Sum | 0 | 0 | 0 |

## 4.3. Parameter results comparison of lithium-based working pairs

A set of important and easy to compare results for the single-effect cycle for the selected working fluids is presented below. The results showed that among the four working fluids being assessed, $H_2O$/LiF has the highest COP value of 0.9471, followed by $H_2O$/LiCl, and $H_2O$/LiBr with COP values of 0.8549 and 0.8448 respectively. It is also clear that the concentration of the weak solution follows the same pattern, with $H_2O$/LiI having the highest value and $H_2O$/LiBr having the lowest. Table 4.3 shows the cycle parameter results for $H_2O$/LiBr, $H_2O$/LiF and $H_2O$/LiCl.

*Table 4.3. Single-effect lithium-based working pairs parameter results*

| Parameter | $H_2O$/LiBr | $H_2O$/LiF | $H_2O$/LiCl |
|---|---|---|---|
| P low (kPa) | 1.228 | 1.228 | 1.228 |
| P high (kPa) | 5.033 | 5.033 | 5.033 |
| Conc. strong sol. (-) | 0.514 | 0.514 | 0.514 |
| Conc. weak sol. (-) | 0.61538 | 0.77492 | 0.66534 |
| COP (-) | 0.84479 | 0.94712 | 0.85486 |

## 4.4. State point results of lithium-based working pairs

After running the same model of single-effect absorption cycle in Aspen Plus for different lithium-based working pairs, the following state point results occured for each one of them. These results are shown in Table 4.4, Table 4.5 and Table 4.6.

*Table 4.4. State point results for the single effect $H_2O$/LiF cycle*

| State Point | $XH_2O$ (-) | XLiF (-) | Temperature (°C) | Pressure (kPa) | Mass Flow (kg/s) | Vapor Fraction (-) |
|---|---|---|---|---|---|---|
| 1 | 0.486 | 0.514 | 33 | 1.228 | 0.7839 | 0 |
| 2 | 0.486 | 0.514 | 33 | 5.033 | 0.7839 | 0 |
| 3 | 0.486 | 0.514 | 50.64 | 5.033 | 0.7839 | 0 |
| 4 | 0.225 | 0.775 | 78.7 | 5.033 | 0.52 | 0 |
| 5 | 0.225 | 0.775 | 38.45 | 5.033 | 0.52 | 0 |

| | | | | | | |
|---|---|---|---|---|---|---|
| 6 | 0.225 | 0.775 | 39 | 1.228 | 0.52 | 0 |
| 7 | 1 | 0 | 69.14 | 5.033 | 0.264 | 1 |
| 8 | 1 | 0 | 33 | 5.033 | 0.264 | 0 |
| 9 | 1 | 0 | 10 | 1.228 | 0.264 | 0.039 |
| 10 | 1 | 0 | 10 | 1.228 | 0.264 | 1 |

*Table 4.5. State point results for the single effect $H_2O$/LiCl cycle*

| State Point | $XH_2O$ (-) | XLiCl (-) | Temperature (°C) | Pressure (kPa) | Mass Flow (kg/s) | Vapor Fraction (-) |
|---|---|---|---|---|---|---|
| 1 | 0.486 | 0.514 | 33 | 1.228 | 0.7839 | 0 |
| 2 | 0.486 | 0.514 | 33 | 5.033 | 0.7839 | 0 |
| 3 | 0.486 | 0.514 | 51.13 | 5.033 | 0.7839 | 0 |
| 4 | 0.3347 | 0.6653 | 78.7 | 5.033 | 0.6055 | 0 |
| 5 | 0.3347 | 0.6653 | 53.86 | 5.033 | 0.6055 | 0 |
| 6 | 0.3347 | 0.6653 | 49.73 | 1.228 | 0.6055 | 0 |
| 7 | 1 | 0 | 64.33 | 5.033 | 0.1783 | 1 |
| 8 | 1 | 0 | 33 | 5.033 | 0.1783 | 0 |
| 9 | 1 | 0 | 10 | 1.228 | 0.1783 | 0.039 |
| 10 | 1 | 0 | 10 | 1.228 | 0.1783 | 1 |

## 4.5. Sensitivity analysis for lithium-based working pairs

In order to have a deeper comprehension of the behavior of the lithium-based working pairs in the single-effect absorption cycle model a sensitivity analysis needs to be run for each working pair. Once again, we will examine the change of the value of Qevap (kW) and COP for various temperatures of the generator and the evaporator and for different strong solution concentrations.

The sensitivity analysis will be run for the same values of the concentrations of the strong solution and for the same values of generator and evaporator temperatures as in the sensitivity analysis of $H_2O$/LiBr.

The results of the sensitivity analysis while varying the generator temperature for the lithium-based working pairs are presented below.

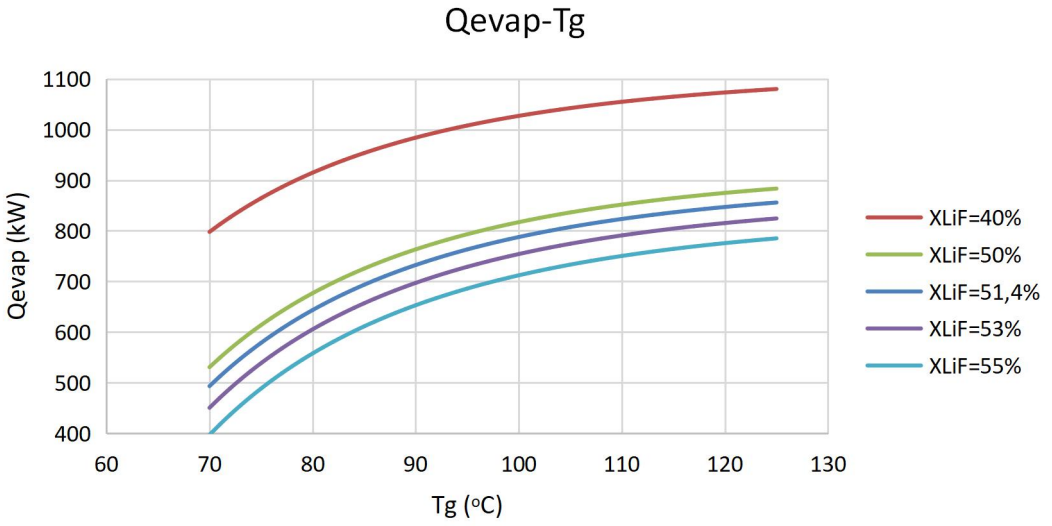


*Figure 4.1. Qevap-Tg diagram for various XLiF values (Ta=33 °C, Tc=33 °C, Te=10 °C)*

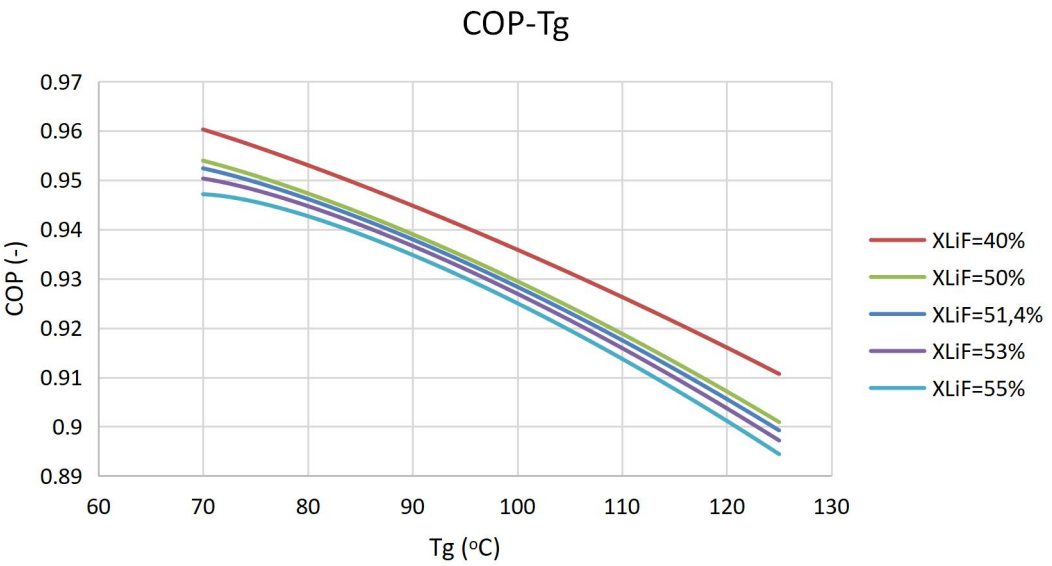


*Figure 4.2. COP-Tg diagram for various XLiF values (Ta=33 °C, Tc=33 °C, Te=10 °C)*

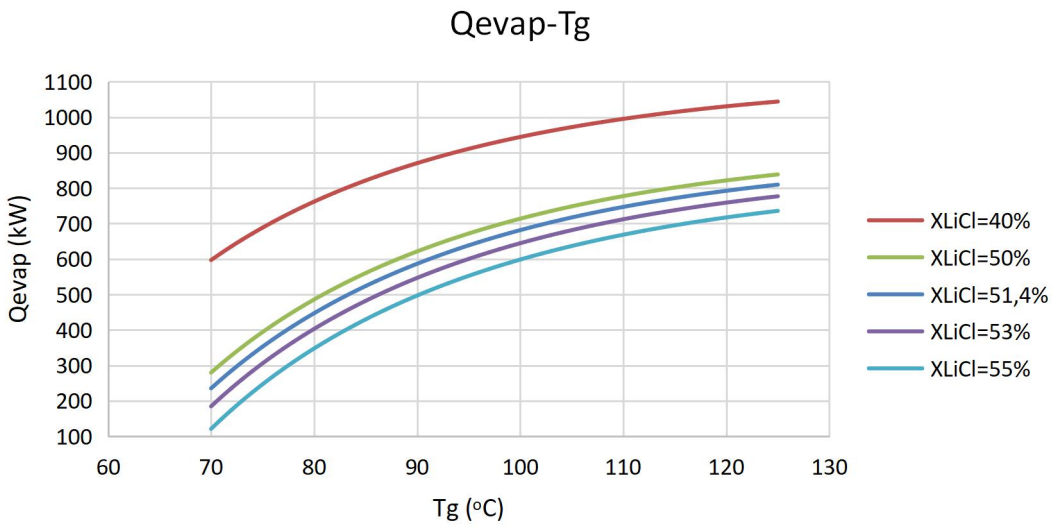


*Figure 4.3. Qevap-Tg diagram for various XLiCl values (Ta=33 °C, Tc=33 °C, Te=10 °C)*

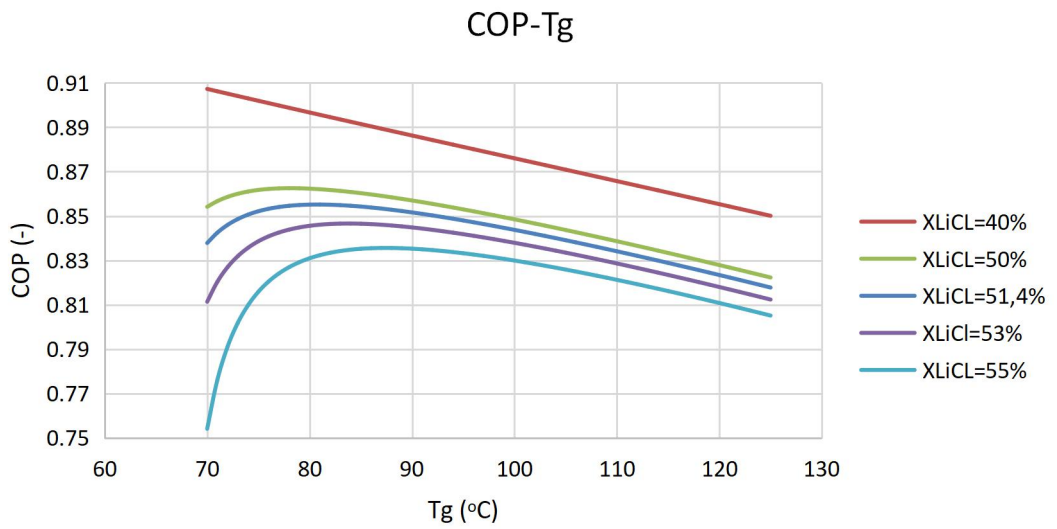


*Figure 4.4. COP-Tg diagram for various XLiCl values (Ta=33 °C, Tc=33 °C, Te=10 °C)*

The heat duty of the evaporator increases for both working pairs as the generator temperature rises. The COP for the $H_2O$/LiF cycle decreases and for the $H_2O$/LiCl increases until 77-87 °C, depending on the concentration, and then decreases as the generator temperature rises. The curves of the COP for the $H_2O$/LiF cycle have a straight form, while the curves of the COP for the $H_2O$/LiF cycle have a curvy form.

The results of the sensitivity analysis while varying the evaporator temperature for the lithium-based working pairs are presented below.

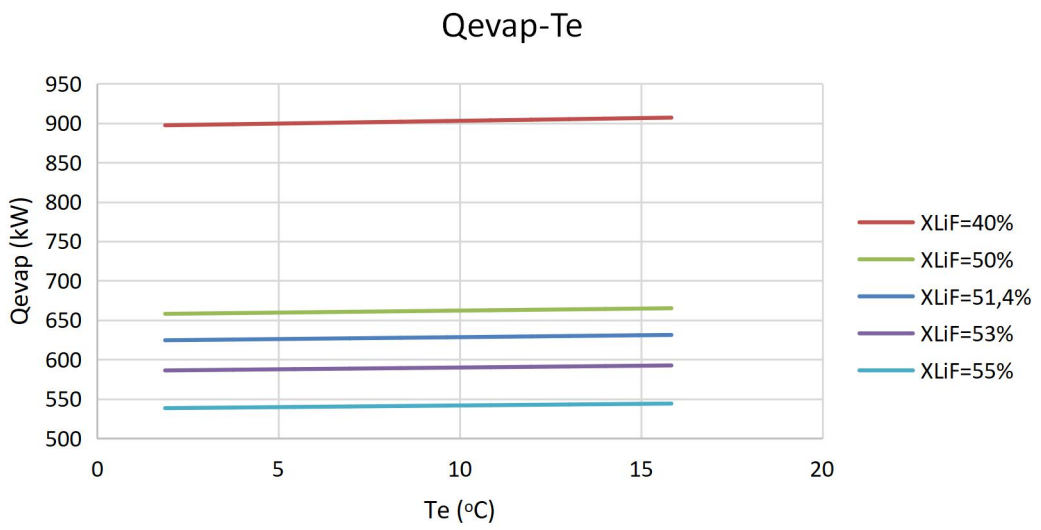


*Figure 4.5. Qevap-Te diagram for various XLiF values (Ta=33 °C, Tc=33 °C, Tg=78.7 °C)*

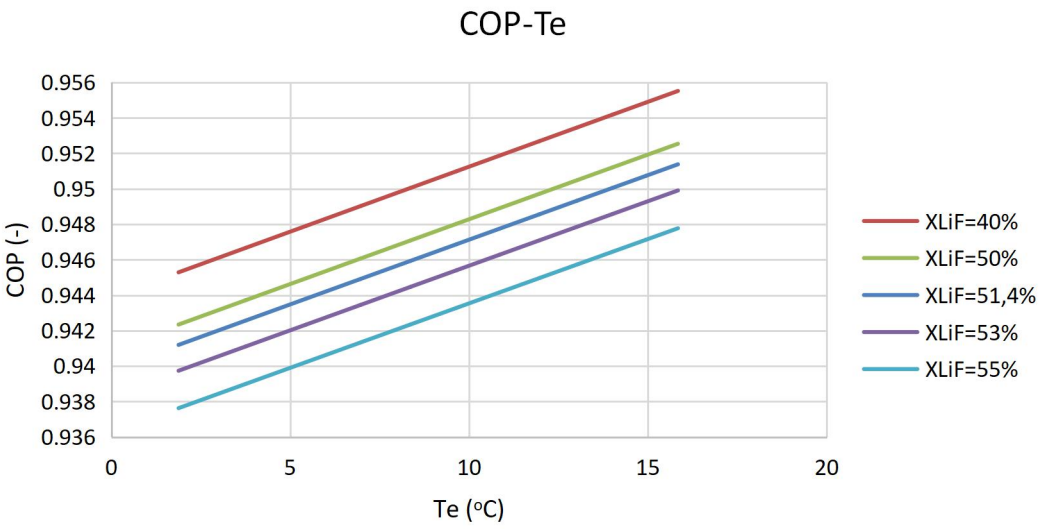


*Figure 4.6. COP-Te diagram for various XLiF values (Ta=33 °C, Tc=33 °C, Tg=78.7 °C)*

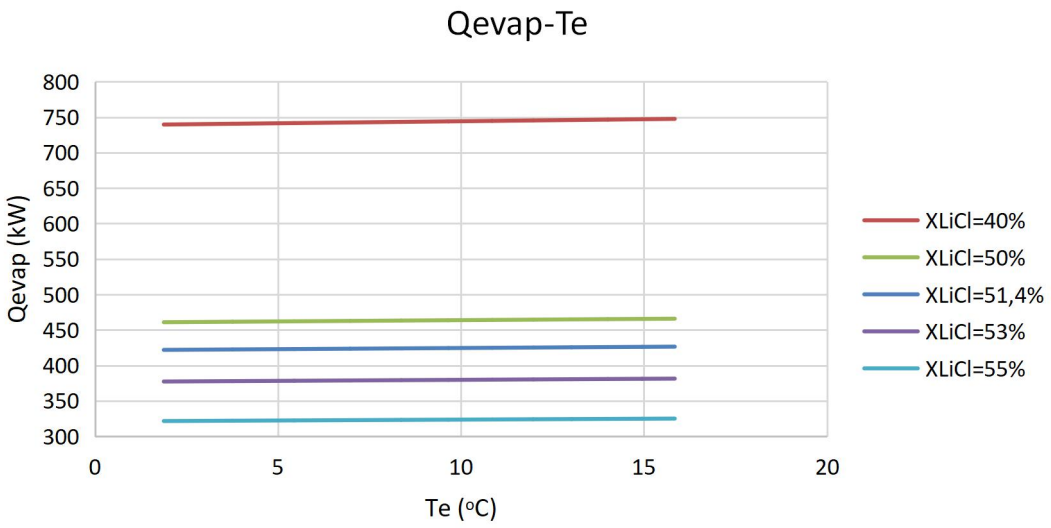


*Figure 4.7. Qevap-Te diagram for various XLiCl values (Ta=33 °C, Tc=33 °C, Tg=78.7 °C)*

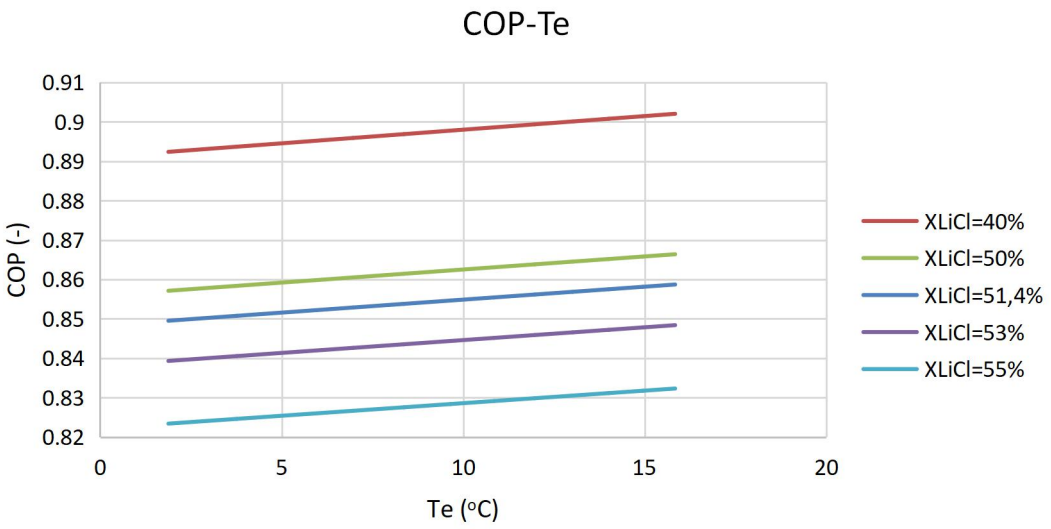


*Figure 4.8. COP-Te diagram for various XLiCl values (Ta=33 °C, Tc=33 °C, Tg=78.7 °C)*

The heat duty of the evaporator and the COP increases for both cycles as the evaporator temperature rises. The range of the heat duty of the evaporator is several kWs and the range of the COP is 0.01 for each concentration for both cycles.

# Chapter 5. Sodium-based working pairs

The next working pairs examined are aqueous sodium-based: $H_2O$/NaOH and $H_2O$/HCOONa. The same assumptions were made in simulating all of the components in the model to allow for a meaningful comparison and inputs such as high and low pressures and temperatures were equal.

## 5.1. Mass balance verification of sodium-based working pairs

As in the lithium-based working pairs, the mass balance verification is examined. As seen in Table 5.1 below, the streams 1 and 1A have equal mass flow rates for both the sodium-based working pairs. This demonstrates that the mass flow is conserved in the model for these working pairs.

*Table 5.1. Single effect sodium-based working pairs mass balance verification*

| Mass Flow (kg/s) | Stream 1 | Stream 1A |
|---|---|---|
| Total | 0.7839 | 0.7839 |
| $H_2O$ | 0.3810 | 0.3810 |
| NaOH | 0.4029 | 0.4029 |
| HCOONa | 0.4029 | 0.4029 |

## 5.2. Energy conservation verification of sodium-based working pairs

In addition, the energy conservation verification is examined. As seen in Table 5.2 below, the sums of the four heat streams equal zero for all working pairs, therefore the models are successful.

*Table 5.2. Single effect sodium-based working pairs energy conservation verification*

| | $H_2O$/NaOH | $H_2O$/HCOONa |
|---|---|---|
| Qcondenser (kW) | 323.791 | 849.629 |
| Qabsorber (kW) | 425.846 | 825.878 |
| Qevaporator (kW) | 311.868 | 810.641 |
| Qdesorber (kW) | 437.895 | 865.94 |
| Sum | 0 | 0 |

## 5.3. Parameter results comparison of sodium-based working pairs

A set of important and easy to compare results for the single-effect cycle for the selected working fluids is presented below. The results showed that among the two working fluids being assessed and $H_2O$/LiBr, $H_2O$/HCOONa has the highest COP value of 0.9361, followed by $H_2O$/LiBr and $H_2O$/NaOH with COP values of 0.8448 and 0.7122 respectively. $H_2O$/HCOONa has the highest weak solution concentration. Table 5.3 shows the cycle parameter results for $H_2O$/LiBr, $H_2O$/NaOH and $H_2O$/HCOONa.

*Table 5.3. Single-effect sodium-based working pairs parameter results*

| Parameter | $H_2O$/LiBr | $H_2O$/NaOH | $H_2O$/HCOONa |
|---|---|---|---|
| P low (kPa) | 1.228 | 1.228 | 1.228 |
| P high (kPa) | 5.033 | 5.033 | 5.033 |
| Conc. strong sol. (-) | 0.514 | 0.514 | 0.514 |
| Conc. Weak sol. (-) | 0.61538 | 0.61713 | 0.90873 |
| COP (-) | 0.84479 | 0.71219 | 0.93613 |

## 5.4. State point results of sodium-based working pairs

The state point results for the sodium-based working pairs are presented in Table 5.4 and Table 5.5.

*Table 5.4. State point results for the single effect $H_2O$/NaOH cycle*

| State Point | $XH_2O$ (-) | XNaOH (-) | Temperature (°C) | Pressure (kPa) | Mass Flow (kg/s) | Vapor Fraction (-) |
|---|---|---|---|---|---|---|
| 1 | 0.486 | 0.514 | 33 | 1.228 | 0.7839 | 0 |
| 2 | 0.486 | 0.514 | 33 | 5.033 | 0.7839 | 0 |
| 3 | 0.486 | 0.514 | 40.52 | 5.033 | 0.7839 | 0 |
| 4 | 0.383 | 0.617 | 78.7 | 5.033 | 0.6529 | 0 |
| 5 | 0.383 | 0.617 | 69.58 | 5.033 | 0.6529 | 0 |

| | | | | | | |
|---|---|---|---|---|---|---|
| 6 | 0.383 | 0.617 | 52.27 | 1.228 | 0.6529 | 0.023 |
| 7 | 1 | 0 | 58.97 | 5.033 | 0.131 | 1 |
| 8 | 1 | 0 | 33 | 5.033 | 0.131 | 0 |
| 9 | 1 | 0 | 10 | 1.228 | 0.131 | 0.039 |
| 10 | 1 | 0 | 10 | 1.228 | 0.131 | 1 |

*Table 5.5. State point results for the single effect $H_2O$/HCOONa cycle*

| State Point | $XH_2O$ (-) | XHCOONa (-) | Temperature (°C) | Pressure (kPa) | Mass Flow (kg/s) | Vapor Fraction (-) |
|---|---|---|---|---|---|---|
| 1 | 0.486 | 0.514 | 33 | 1.228 | 0.7839 | 0 |
| 2 | 0.486 | 0.514 | 33 | 5.033 | 0.7839 | 0 |
| 3 | 0.486 | 0.514 | 42.63 | 5.033 | 0.7839 | 0 |
| 4 | 0.0913 | 0.9087 | 78.7 | 5.033 | 0.4434 | 0 |
| 5 | 0.0913 | 0.9087 | 52.36 | 5.033 | 0.4434 | 0 |
| 6 | 0.0913 | 0.9087 | 48.13 | 1.228 | 0.4434 | 0.003 |
| 7 | 1 | 0 | 71.4 | 5.033 | 0.3405 | 1 |
| 8 | 1 | 0 | 33 | 5.033 | 0.3405 | 0 |
| 9 | 1 | 0 | 10 | 1.228 | 0.3405 | 0.039 |
| 10 | 1 | 0 | 10 | 1.228 | 0.3405 | 1 |

## 5.5. Sensitivity analysis for sodium-based working pairs

The sensitivity analysis for the sodium-based working pairs follows. It will be run for the same values of the concentrations of the strong solution and for the same values of generator and evaporator temperatures as in the sensitivity analysis of the previous working pairs.

The results of the sensitivity analysis while varying the generator temperature for the sodium-based working pairs are presented below.

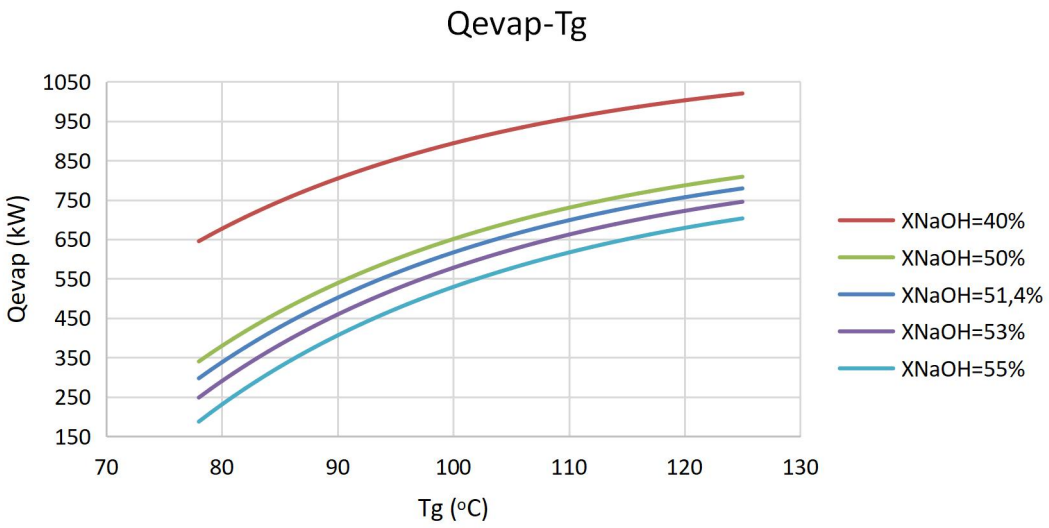


*Figure 5.1. Qevap-Tg diagram for various XNaOH values (Ta=33 °C, Tc=33 °C, Te=10 °C)*

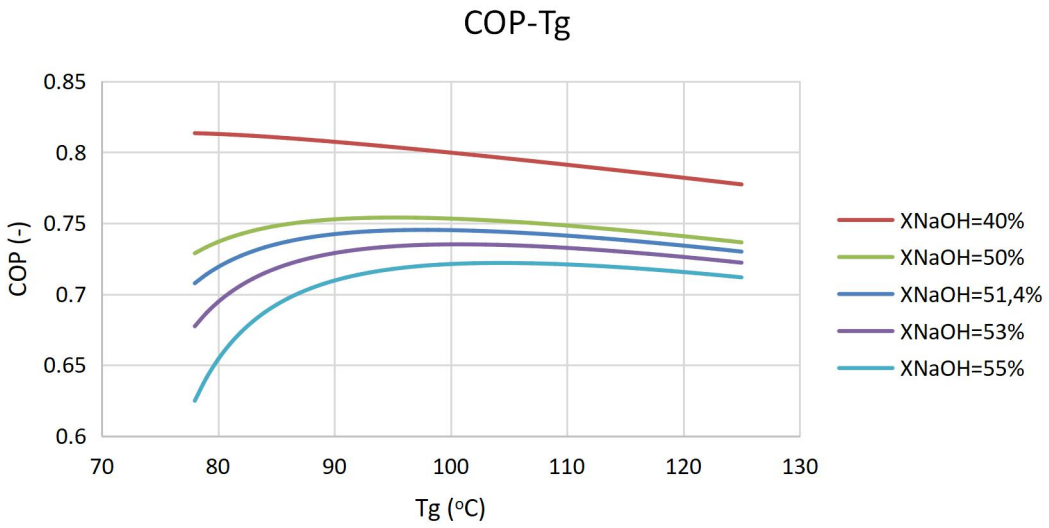


*Figure 5.2. COP-Tg diagram for various XNaOH values (Ta=33 °C, Tc=33 °C, Te=10 °C)*

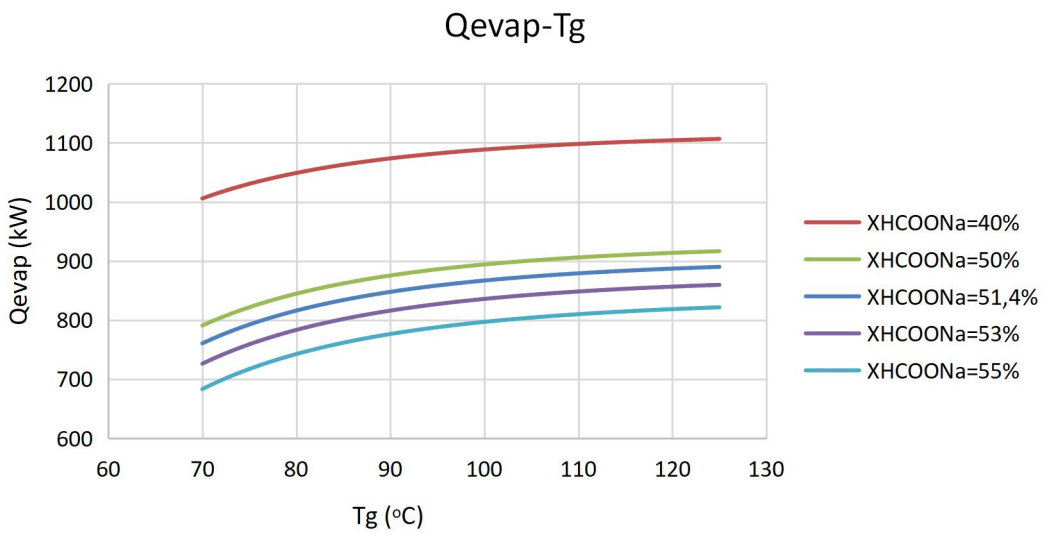


*Figure 5.3. Qevap-Tg diagram for various XHCOONa values (Ta=33 °C, Tc=33 °C, Te=10 °C)*

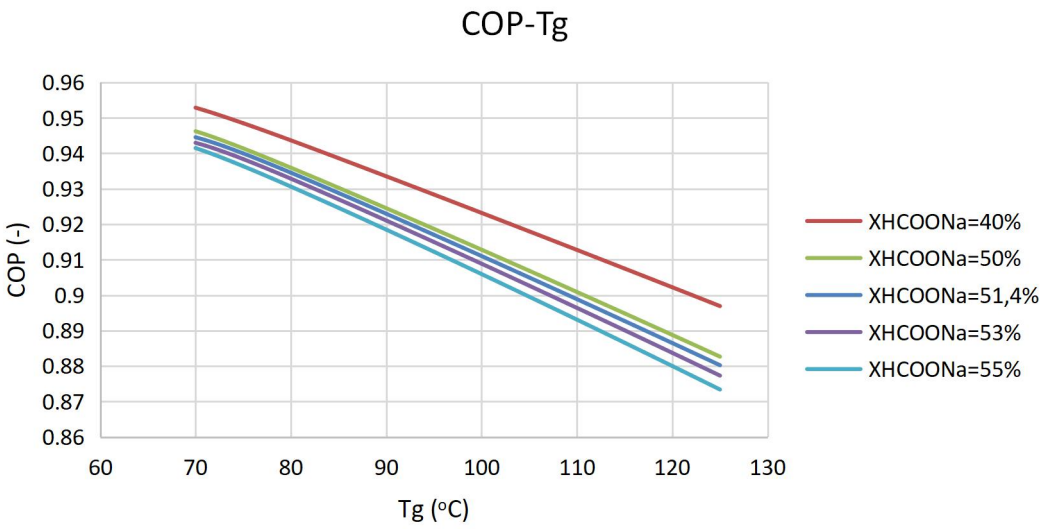


*Figure 5.4. COP-Tg diagram for various XHCOONa values (Ta=33 °C, Tc=33 °C, Te=10 °C)*

The heat duty of the evaporator increases for both working pairs as the generator temperature rises. The increase in the $H_2O$/NaOH cycle is steeper than that of the $H_2O$/HCOONa cycle. The COP for the $H_2O$/HCOONa cycle decreases and for the $H_2O$/NaOH increases until 90-100 °C, depending on the concentration, and then decreases as the generator temperature rises. The curves of the COP for the $H_2O$/HCOONa cycle have a straight form, while the curves of the COP for the $H_2O$/NaOH cycle have a curvy form.

The results of the sensitivity analysis while varying the evaporator temperature for the sodium-based working pairs are presented below.

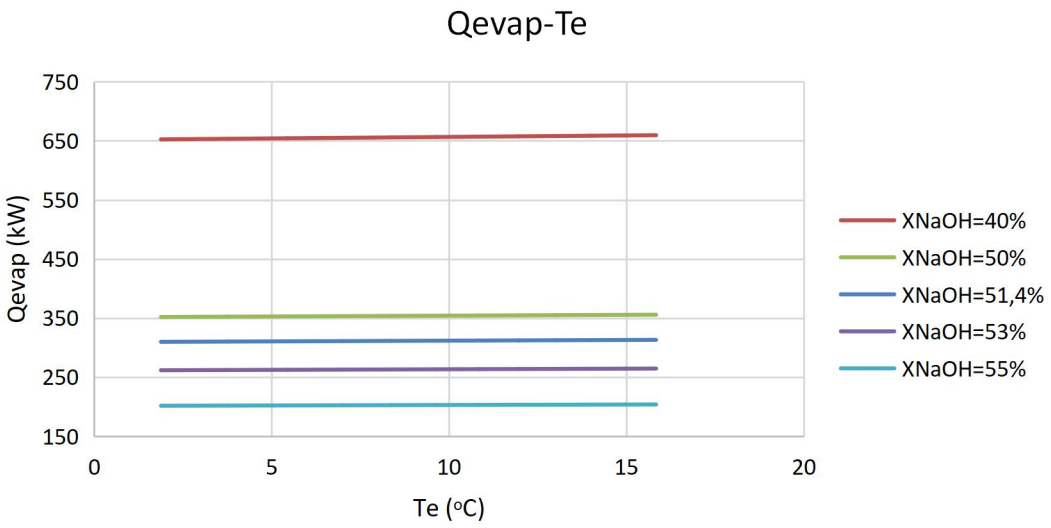


*Figure 5.5. Qevap-Te diagram for various XNaOH values (Ta=33 °C, Tc=33 °C, Tg=78.7 °C)*

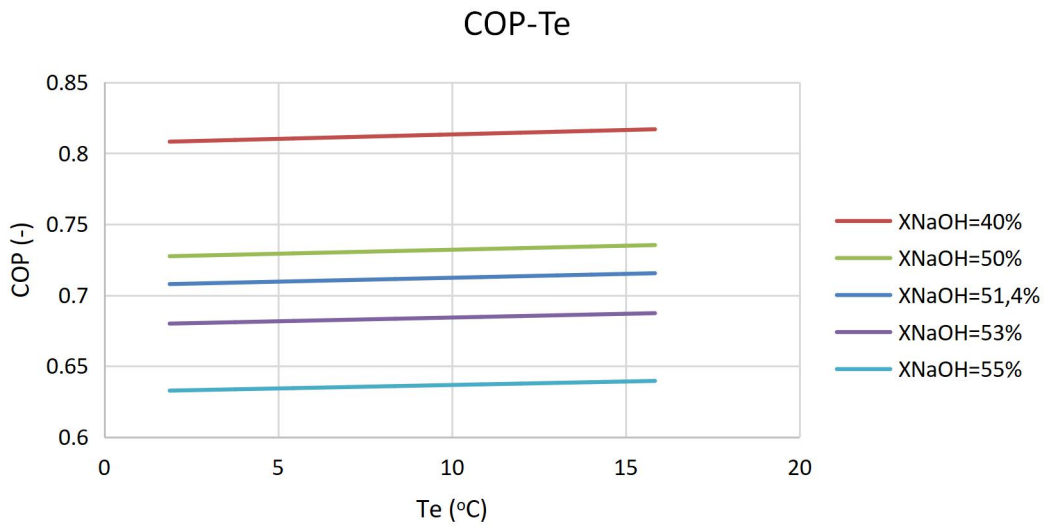


*Figure 5.6. COP-Te diagram for various XNaOH values (Ta=33 °C, Tc=33 °C, Tg=78.7 °C)*

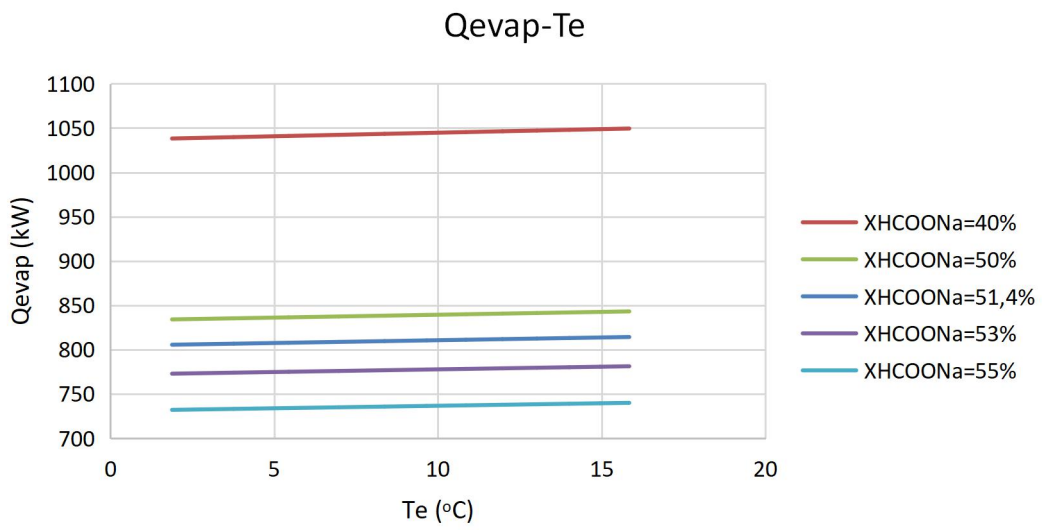


*Figure 5.7. Qevap-Te diagram for various XHCOONa values (Ta=33 °C, Tc=33 °C, Tg=78.7 °C)*

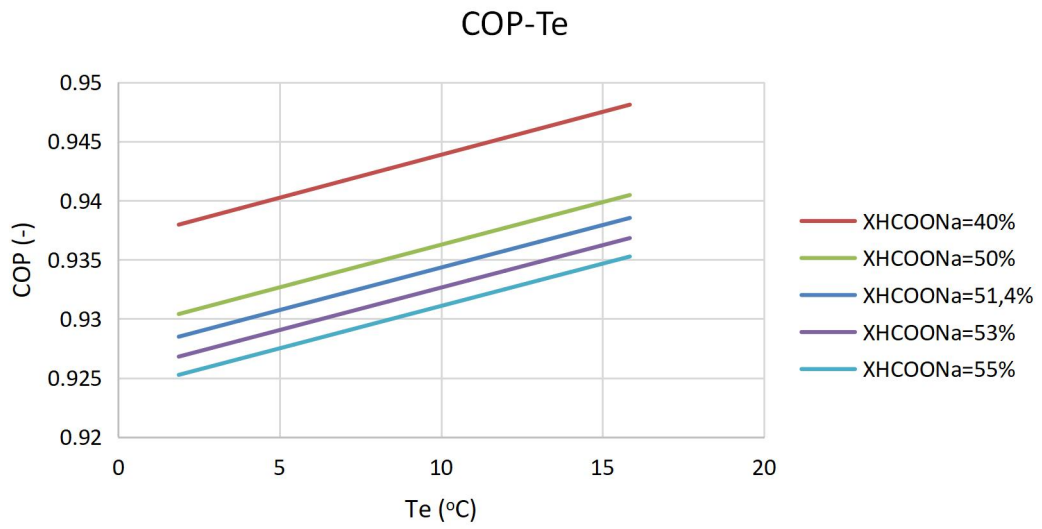


*Figure 5.8. COP-Te diagram for various XHCOONa values (Ta=33 °C, Tc=33 °C, Tg=78.7 °C)*

The heat duty of the evaporator and the COP increase for both cycles as the evaporator temperature rises. It is clear that both the heat duty of the evaporator and the COP of the $H_2O$/HCOONa cycle have higher values for each concentration than those of the $H_2O$/NaOH cycle.

# Chapter 6. Ternary mixtures

The next working fluids examined are ternary mixtures: $H_2O$/LiBr+$LiNO_3$ (salt mole ratio 4:1), $H_2O$/LiBr+$ZnBr_2$ (2:1), $H_2O$/LiCl+$LiNO_3$ (2.8:1), $H_2O$/LiCl+$ZnCl_2$ (2:1) and $H_2O$/LiBr+LiI (4:1) [27]. The same assumptions were made in simulating all of the components in the model to allow for a meaningful comparison and inputs such as high and low pressures and temperatures were equal.

## 6.1. Mass balance verification of ternary mixtures

As in the previous working pairs, the mass balance verification is examined. As seen in Table 6.1 below, the streams 1 and 1A have equal mass flow rates for all the ternary mixtures. This demonstrates that the mass flow is conserved in the model for these ternary mixtures.

*Table 6.1. Single effect ternary mixtures mass balance verification*

| Mass Flow (kg/s) | Stream 1 | Stream 1A |
|---|---|---|
| Total | 0.7839 | 0.7839 |
| $H_2O$ | 0.3810 | 0.3810 |
| LiBr+$LiNO_3$ | 0.4029 | 0.4029 |
| LiBr+$ZnBr_2$ | 0.4029 | 0.4029 |
| LiCl+$LiNO_3$ | 0.4029 | 0.4029 |
| LiCl+$ZnCl_2$ | 0.4029 | 0.4029 |
| LiBr+LiI | 0.4029 | 0.4029 |

## 6.2. Energy conservation verification of ternary mixtures

Once again, the energy conservation verification is examined. As seen in Table 6.2 below, the sums of the four heat streams equal zero for all working pairs, therefore the models are successful.

*Table 6.2. Single effect ternary mixtures energy conservation verification*

| | $H_2O$/LiBr+$LiNO_3$ | $H_2O$/LiBr+$ZnBr_2$ | $H_2O$/LiCl+$LiNO_3$ | $H_2O$/LiCl+$ZnCl_2$ | $H_2O$/LiBr+LiI |
|---|---|---|---|---|---|
| Qcondenser (kW) | 450.194 | 568.676 | 517.744 | 586.806 | 444.066 |
| Qabsorber (kW) | 484.349 | 588.127 | 556.206 | 612.341 | 477.447 |

| | | | | | |
|---|---|---|---|---|---|
| Qevaporator (kW) | 431.765 | 544.149 | 495.838 | 561.346 | 425.952 |
| Qdesorber (kW) | 502.836 | 612.612 | 578.212 | 637.867 | 495.593 |
| Sum | 0 | 0 | 0 | 0 | 0 |

## 6.3. Parameter results comparison of ternary mixtures

A set of important and easy to compare results for the single-effect cycle for the selected working fluids is presented below. The results showed that among the ternary working fluids being assessed and $H_2O$/LiBr, $H_2O$/LiBr+$ZnBr_2$ has the highest COP value of 0.88824, followed by $H_2O$/LiCl+$ZnCl_2$, $H_2O$/LiBr+LiI, $H_2O$/LiBr+LiNO3, $H_2O$/LiCl+LiNO3 and $H_2O$/LiBr with COP values of 0.88824, 0.88003, 0.85947, 0.85865, 0.85753 and 0.84479 respectively. $H_2O$/LiCl+$ZnCl_2$ has the highest weak solution concentration.

Table 6.3 shows the cycle parameter results for $H_2O$/LiBr, $H_2O$/LiBr+$LiNO_3$, $H_2O$/LiBr+$ZnBr_2$, $H_2O$/LiCl+$LiNO_3$, $H_2O$/LiCl+$ZnCl_2$ and $H_2O$/LiBr+LiI.

*Table 6.3. Single-effect ternary mixtures parameter results*

| Parameter | $H_2O$/ LiBr | $H_2O$/ LiBr+$LiNO_3$ | $H_2O$/ LiBr+$ZnBr_2$ | $H_2O$/ LiCl+$LiNO_3$ | $H_2O$/ LiCl+$ZnCl_2$ | $H_2O$/ LiBr+LiI |
|---|---|---|---|---|---|---|
| P low (kPa) | 1.228 | 1.228 | 1.228 | 1.228 | 1.228 | 1.228 |
| P high (kPa) | 5.033 | 5.033 | 5.033 | 5.033 | 5.033 | 5.033 |
| Conc. strong sol. (-) | 0.514 | 0.514 | 0.514 | 0.514 | 0.514 | 0.514 |
| Conc. weak sol. (-) | 0.61538 | 0.66871 | 0.72556 | 0.69998 | 0.73512 | 0.66601 |
| COP (-) | 0.84479 | 0.85865 | 0.88824 | 0.85753 | 0.88003 | 0.85947 |

## 6.4. State point results of ternary mixtures

The state point results for the ternary mixtures are presented in Table 6.4, Table 6.5, Table 6.6, Table 6.7 and Table 6.8.

*Table 6.4. State point results for the single effect $H_2O$/LiBr+$LiNO_3$ cycle*

| State Point | $XH_2O$ (-) | XLiBr+$LiNO_3$ (-) | Temperature (°C) | Pressure (kPa) | Mass Flow (kg/s) | Vapor Fraction (-) |
|---|---|---|---|---|---|---|
| 1 | 0.486 | 0.514 | 33 | 1.228 | 0.7839 | 0 |
| 2 | 0.486 | 0.514 | 33 | 5.033 | 0.7839 | 0 |
| 3 | 0.486 | 0.5148 | 45.36 | 5.033 | 0.7839 | 0 |
| 4 | 0.3313 | 0.6687 | 78.7 | 5.033 | 0.6025 | 0 |
| 5 | 0.3313 | 0.6687 | 59.2 | 5.033 | 0.6025 | 0 |
| 6 | 0.3313 | 0.6687 | 50.74 | 1.228 | 0.6025 | 0.009 |
| 7 | 1 | 0 | 64.58 | 5.033 | 0.1814 | 1 |
| 8 | 1 | 0 | 33 | 5.033 | 0.1814 | 0 |
| 9 | 1 | 0 | 10 | 1.228 | 0.1814 | 0.039 |
| 10 | 1 | 0 | 10 | 1.228 | 0.1814 | 1 |

*Table 6.5. State point results for the single effect $H_2O$/LiBr+$ZnBr_2$ cycle*

| State Point | $XH_2O$ (-) | XLiBr+$ZnBr_2$ (-) | Temperature (°C) | Pressure (kPa) | Mass Flow (kg/s) | Vapor Fraction (-) |
|---|---|---|---|---|---|---|
| 1 | 0.486 | 0.514 | 33 | 1.228 | 0.7839 | 0 |
| 2 | 0.486 | 0.514 | 33 | 5.033 | 0.7839 | 0 |
| 3 | 0.486 | 0.514 | 46.49 | 5.033 | 0.7839 | 0 |
| 4 | 0.274 | 0.726 | 78.7 | 5.033 | 0.5553 | 0 |
| 5 | 0.274 | 0.726 | 51.28 | 5.033 | 0.5553 | 0 |
| 6 | 0.274 | 0.726 | 50.35 | 1.228 | 0.5553 | 0.0009 |
| 7 | 1 | 0 | 67.6 | 5.033 | 0.2286 | 1 |
| 8 | 1 | 0 | 33 | 5.033 | 0.2286 | 0 |
| 9 | 1 | 0 | 10 | 1.228 | 0.2286 | 0.039 |

| | | | | | | |
|---|---|---|---|---|---|---|
| 10 | 1 | 0 | 10 | 1.228 | 0.2286 | 1 |

*Table 6.6. State point results for the single effect $H_2O$/LiCl+$LiNO_3$ cycle*

| State Point | $XH_2O$ (-) | XLiCl+$LiNO_3$ (-) | Temperature (°C) | Pressure (kPa) | Mass Flow (kg/s) | Vapor Fraction (-) |
|---|---|---|---|---|---|---|
| 1 | 0.486 | 0.514 | 33 | 1.228 | 0.7839 | 0 |
| 2 | 0.486 | 0.514 | 33 | 5.033 | 0.7839 | 0 |
| 3 | 0.486 | 0.514 | 43 | 5.033 | 0.7839 | 0 |
| 4 | 0.3 | 0.7 | 78.7 | 5.033 | 0.5756 | 0 |
| 5 | 0.3 | 0.7 | 63.48 | 5.033 | 0.5756 | 0 |
| 6 | 0.3 | 0.7 | 50.13 | 1.228 | 0.5756 | 0.014 |
| 7 | 1 | 0 | 66.47 | 5.033 | 0.2083 | 1 |
| 8 | 1 | 0 | 33 | 5.033 | 0.2083 | 0 |
| 9 | 1 | 0 | 10 | 1.228 | 0.2083 | 0.039 |
| 10 | 1 | 0 | 10 | 1.228 | 0.2083 | 1 |

*Table 6.7. State point results for the single effect $H_2O$/LiCl+$ZnCl_2$ cycle*

| State Point | $XH_2O$ (-) | XLiCl+$ZnCl_2$ (-) | Temperature (°C) | Pressure (kPa) | Mass Flow (kg/s) | Vapor Fraction (-) |
|---|---|---|---|---|---|---|
| 1 | 0.486 | 0.514 | 33 | 1.228 | 0.7839 | 0 |
| 2 | 0.486 | 0.514 | 33 | 5.033 | 0.7839 | 0 |
| 3 | 0.486 | 0.514 | 43.98 | 5.033 | 0.7839 | 0 |
| 4 | 0.265 | 0.735 | 78.7 | 5.033 | 0.5481 | 0 |
| 5 | 0.265 | 0.735 | 59.79 | 5.033 | 0.5481 | 0 |
| 6 | 0.265 | 0.735 | 49.87 | 1.228 | 0.5481 | 0.009 |
| 7 | 1 | 0 | 67.95 | 5.033 | 0.2358 | 1 |

| | | | | | | |
|---|---|---|---|---|---|---|
| 8 | 1 | 0 | 33 | 5.033 | 0.2358 | 0 |
| 9 | 1 | 0 | 10 | 1.228 | 0.2358 | 0.039 |
| 10 | 1 | 0 | 10 | 1.228 | 0.2358 | 1 |

*Table 6.8. State point results for the single effect $H_2O$/LiBr+LiI cycle*

| State Point | $XH_2O$ (-) | XLiBr+LiI (-) | Temperature (°C) | Pressure (kPa) | Mass Flow (kg/s) | Vapor Fraction (-) |
|---|---|---|---|---|---|---|
| 1 | 0.486 | 0.514 | 33 | 1.228 | 0.7839 | 0 |
| 2 | 0.486 | 0.514 | 33 | 5.033 | 0.7839 | 0 |
| 3 | 0.486 | 0.514 | 45.76 | 5.033 | 0.7839 | 0 |
| 4 | 0.334 | 0.666 | 78.7 | 5.033 | 0.6049 | 0 |
| 5 | 0.334 | 0.666 | 58.26 | 5.033 | 0.6049 | 0 |
| 6 | 0.334 | 0.666 | 50.83 | 1.228 | 0.6049 | 0.007 |
| 7 | 1 | 0 | 64.38 | 5.033 | 0.1789 | 1 |
| 8 | 1 | 0 | 33 | 5.033 | 0.1789 | 0 |
| 9 | 1 | 0 | 10 | 1.228 | 0.1789 | 0.039 |
| 10 | 1 | 0 | 10 | 1.228 | 0.1789 | 1 |

## 6.5. Sensitivity analysis for ternary mixtures

The sensitivity analysis for the ternary mixtures follows. It will be run for the same values of the concentrations of the strong solution and for the same values of generator and evaporator temperatures as in the sensitivity analysis of the previous working pairs.

The results of the sensitivity analysis while varying the generator temperature for the ternary mixtures are presented below.

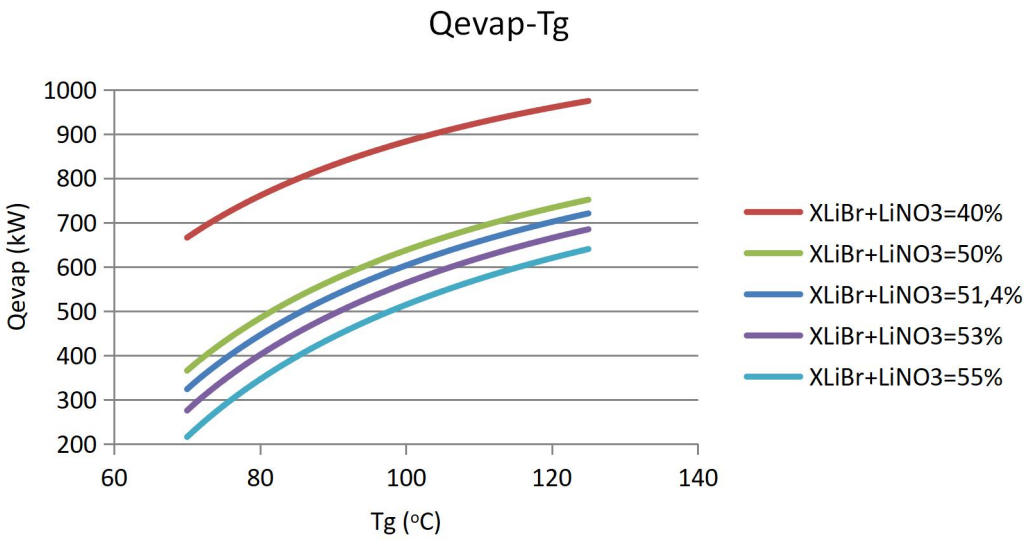


*Figure 6.1. Qevap-Tg diagram for various XLiBr+LiNO3 (4:1) values (Ta=33 °C, Tc=33 °C, Te=10 °C)*

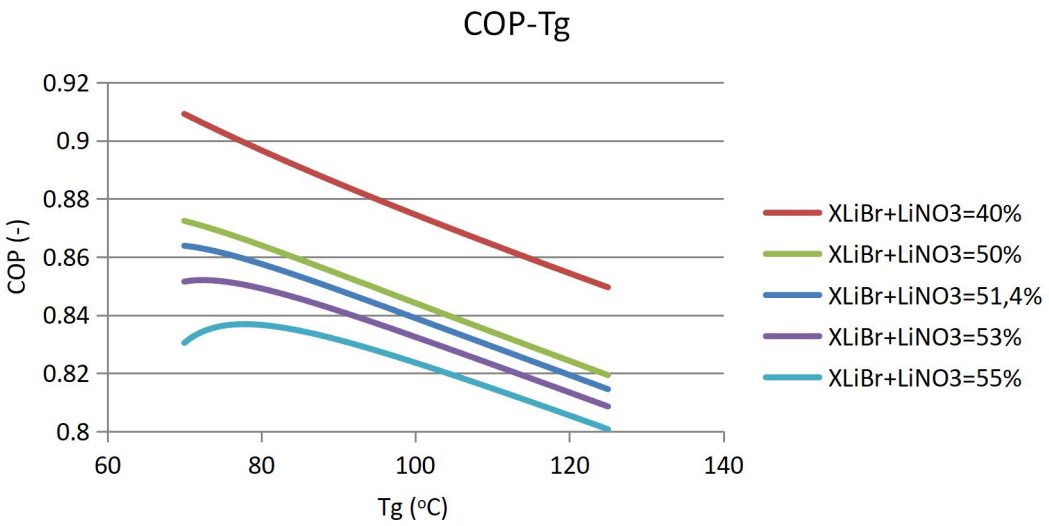


*Figure 6.2. COP-Tg diagram for various XLiBr+LiNO$_3$ (4:1) values (Ta=33 °C, Tc=33 °C, Te=10 °C)*

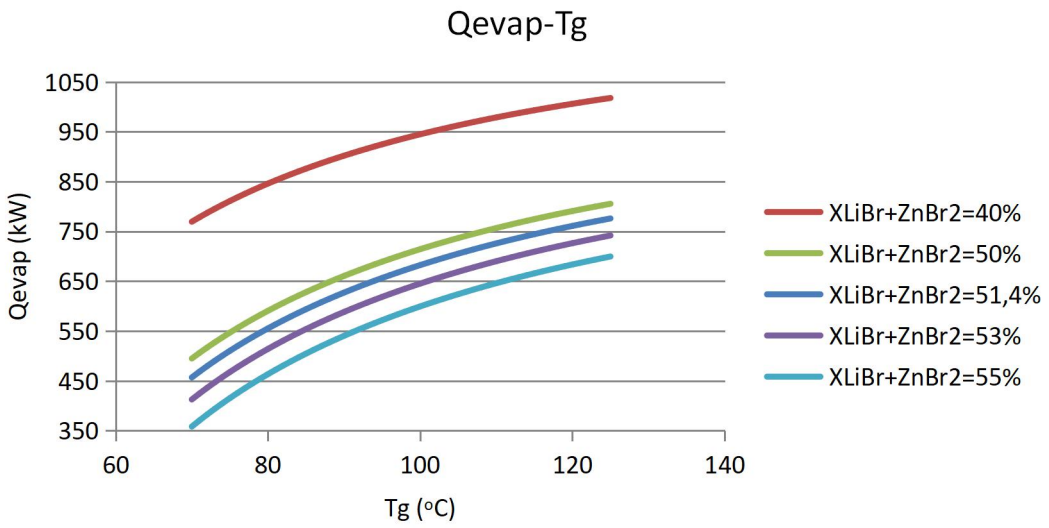


*Figure 6.3. Qevap-Tg diagram for various XLiBr+$ZnBr_2$ (2:1) values (Ta=33 °C, Tc=33 °C, Te=10 °C)*

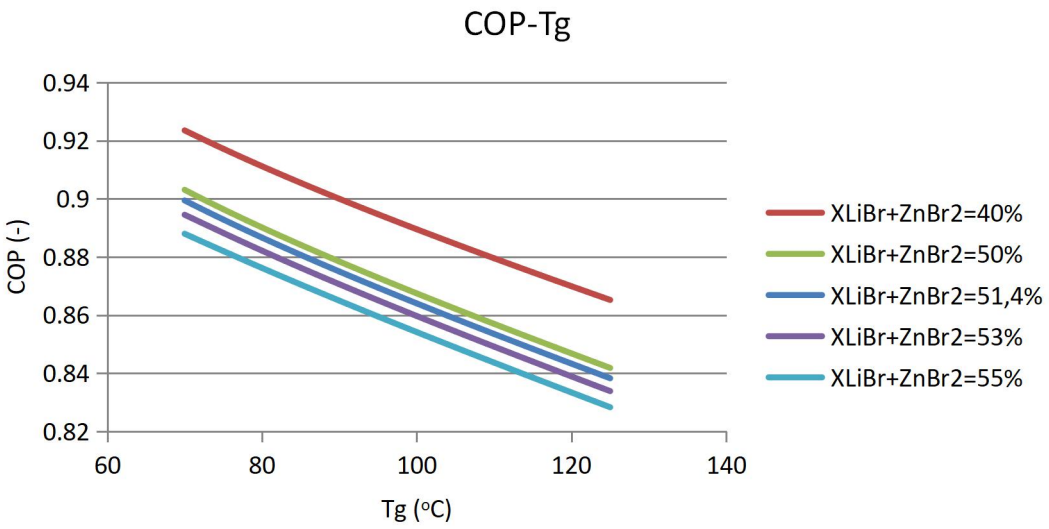


*Figure 6.4. COP-Tg diagram for various XLiBr+$ZnBr_2$ (2:1) values (Ta=33 °C, Tc=33 °C, Te=10 °C)*

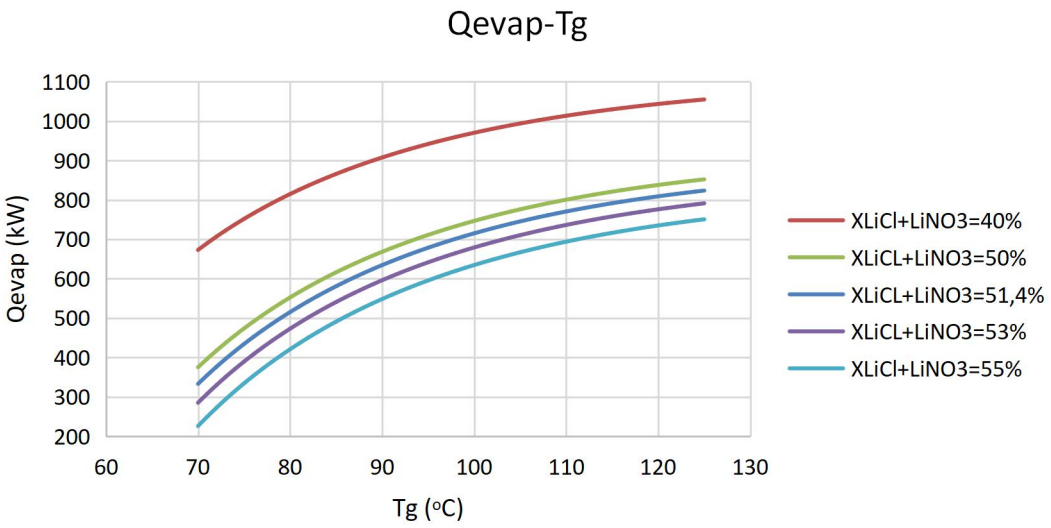


*Figure 6.5. Qevap-Tg diagram for various XLiCl+LiNO₃ (2.8:1) values (Ta=33 °C, Tc=33 °C, Te=10 °C)*

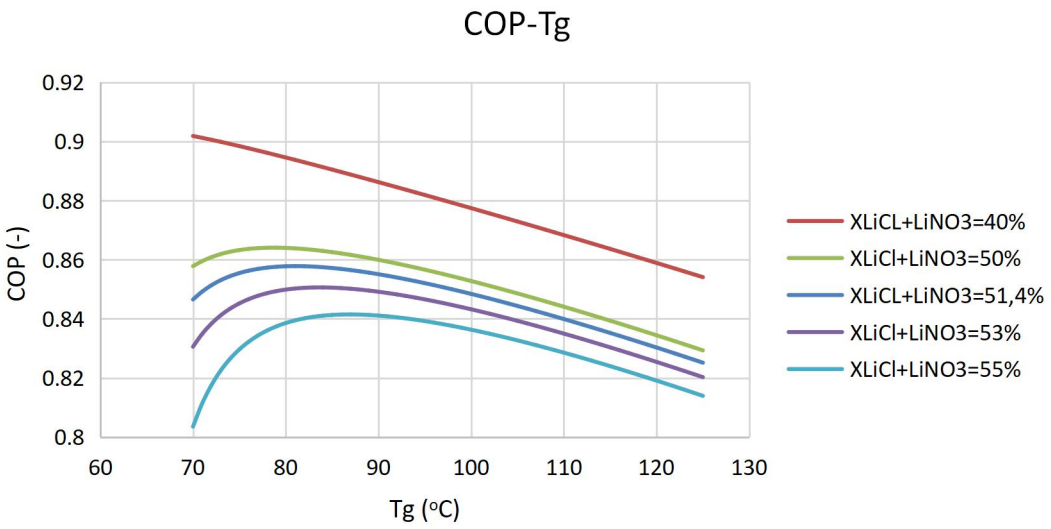


*Figure 6.6. COP-Tg diagram for various XLiCl+LiNO₃ (2.8:1) values (Ta=33 °C, Tc=33 °C, Te=10 °C)*

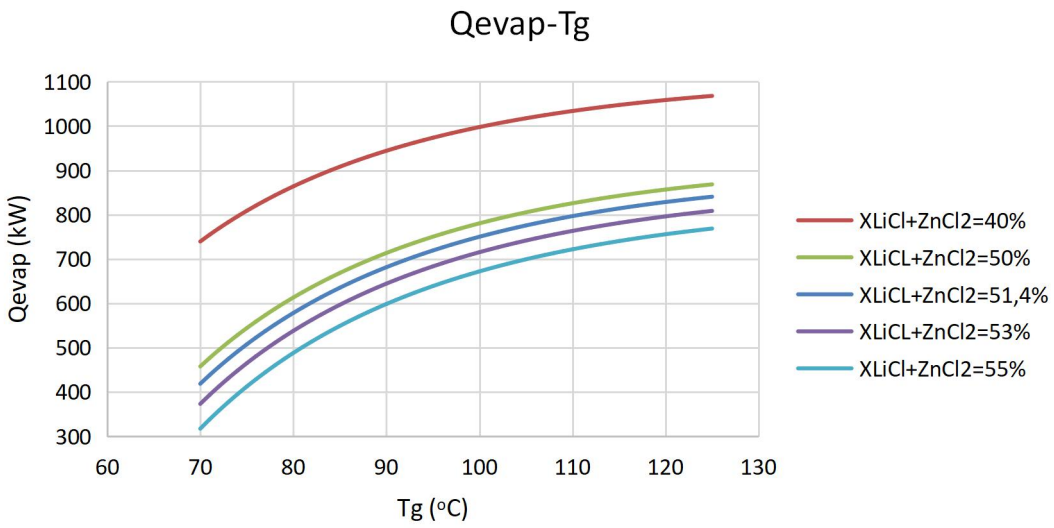


*Figure 6.7. Qevap-Tg diagram for various XLiCl+$ZnCl_2$ (2:1) values (Ta=33 °C, Tc=33 °C, Te=10 °C)*

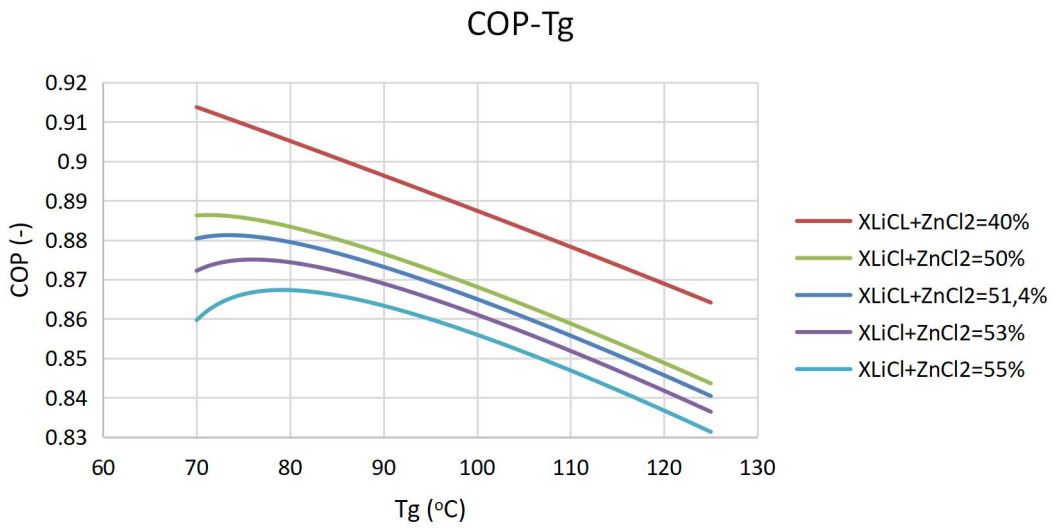


*Figure 6.8. COP-Tg diagram for various XLiCl+$ZnCl_2$ (2:1) values (Ta=33 °C, Tc=33 °C, Te=10 °C)*

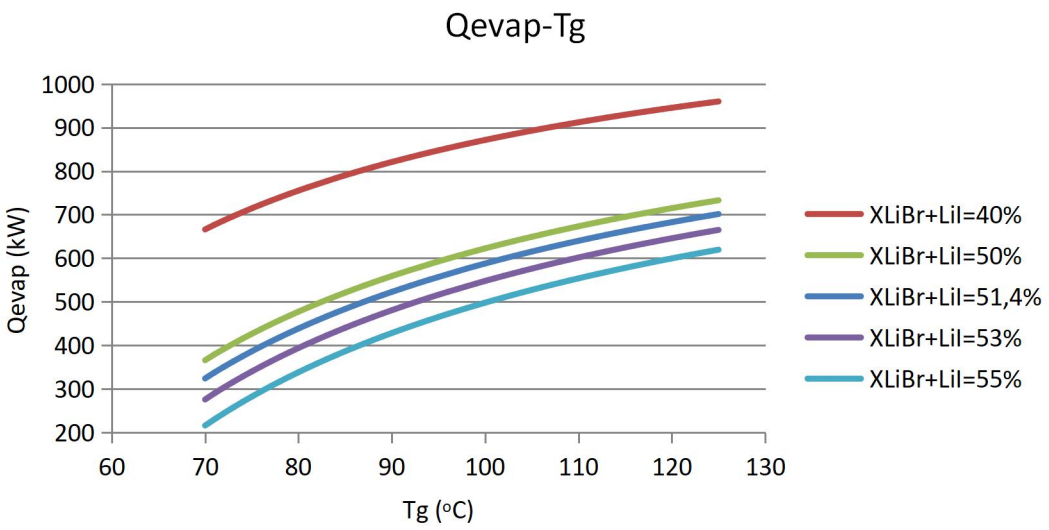


*Figure 6.9. Qevap-Tg diagram for various XLiBr+LiI (4:1) values (Ta=33 °C, Tc=33 °C, Te=10 °C)*

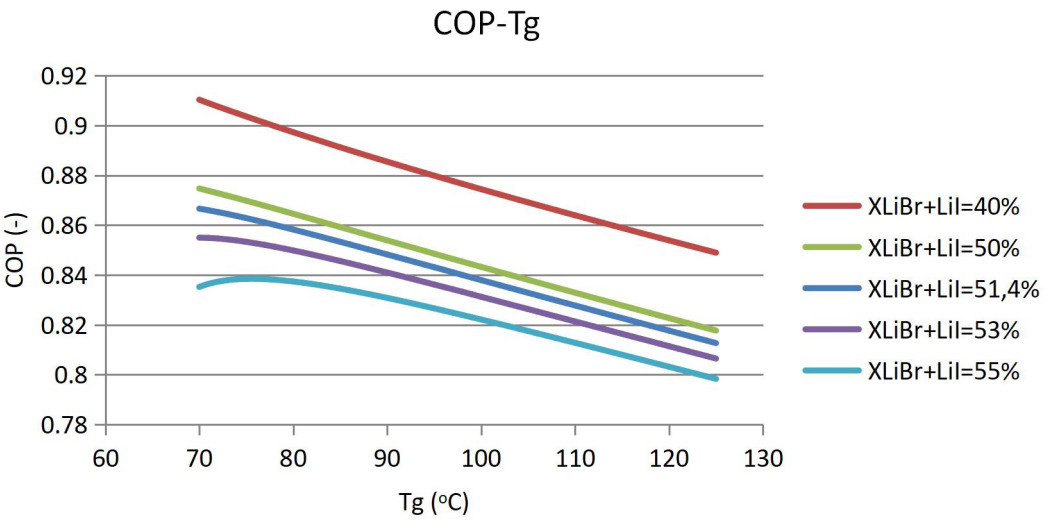


*Figure 6.10. COP-Tg diagram for various XLiBr+LiI (4:1) values (Ta=33 °C, Tc=33 °C, Te=10 °C)*

The heat duty of the evaporator increases for every ternary mixture as the generator temperature rises. The range of the Qevap for each ternary mixture and concentration is mainly 300-400 kW. The COP generally decreases as the generator temperature rises, except for the lower generator temperatures and the higher concentrations where there is an increase until a certain temperature. The range of the COP for each ternary mixture and concentration is approximately 0.07.

The results of the sensitivity analysis while varying the evaporator temperature for the ternary mixtures are presented below.

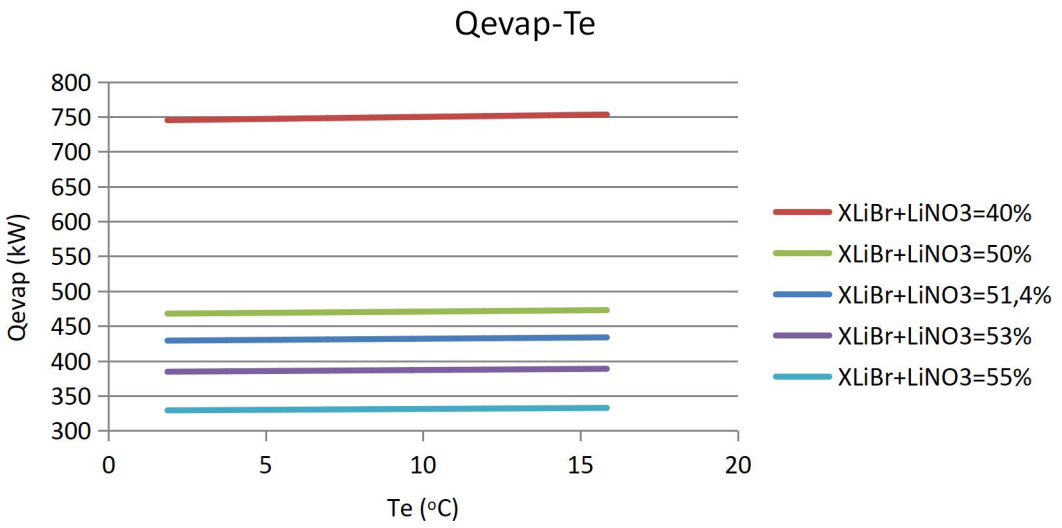


*Figure 6.11. Qevap-Te diagram for various XLiBr+LiNO$_3$ (4:1) values (Ta=33 °C, Tc=33 °C, Tg=78.7 °C)*

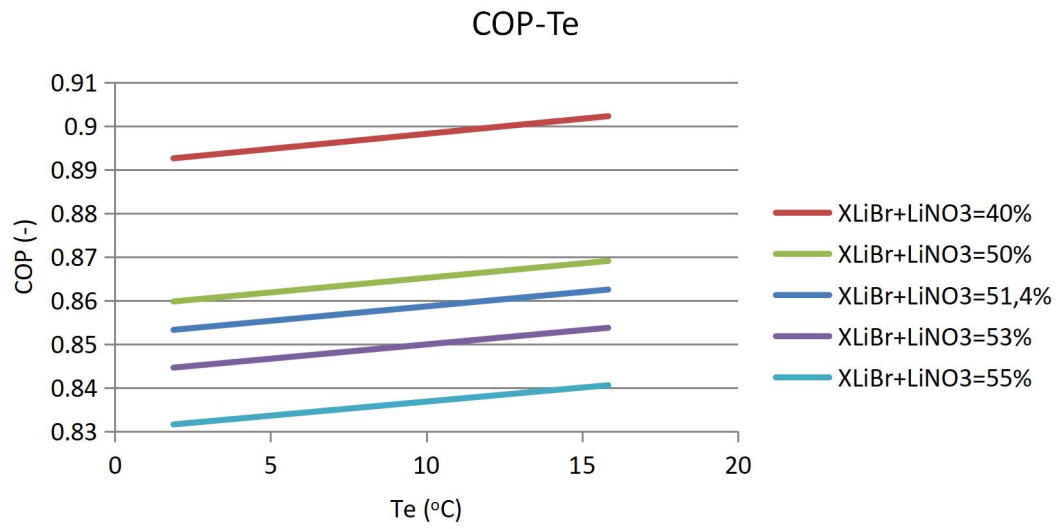


*Figure 6.12. COP-Te diagram for various XLiBr+LiNO$_3$ (4:1) values (Ta=33 °C, Tc=33 °C, Tg=78.7 °C)*

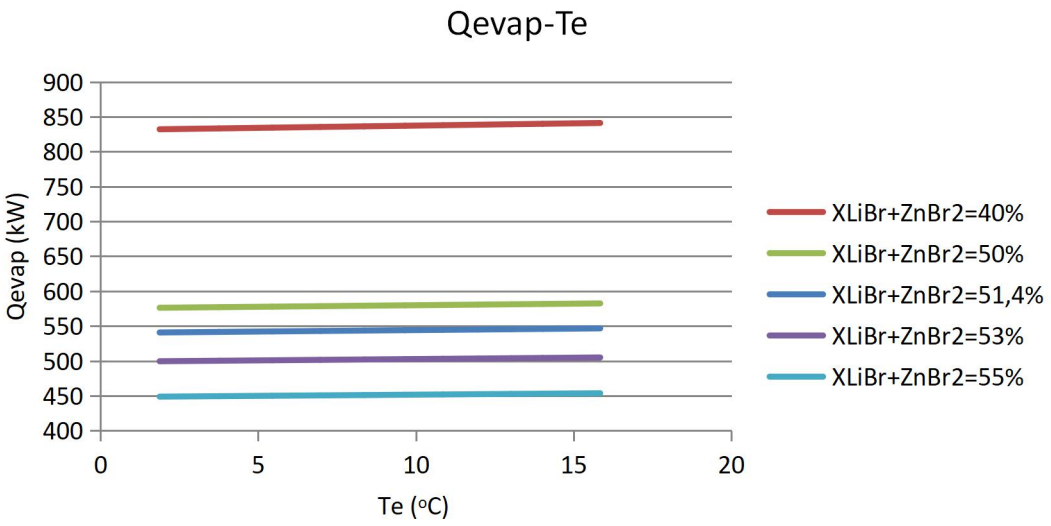


*Figure 6.13. Qevap-Te diagram for various XLiBr+$ZnBr_2$ (2:1) values (Ta=33 °C, Tc=33 °C, Tg=78.7 °C)*

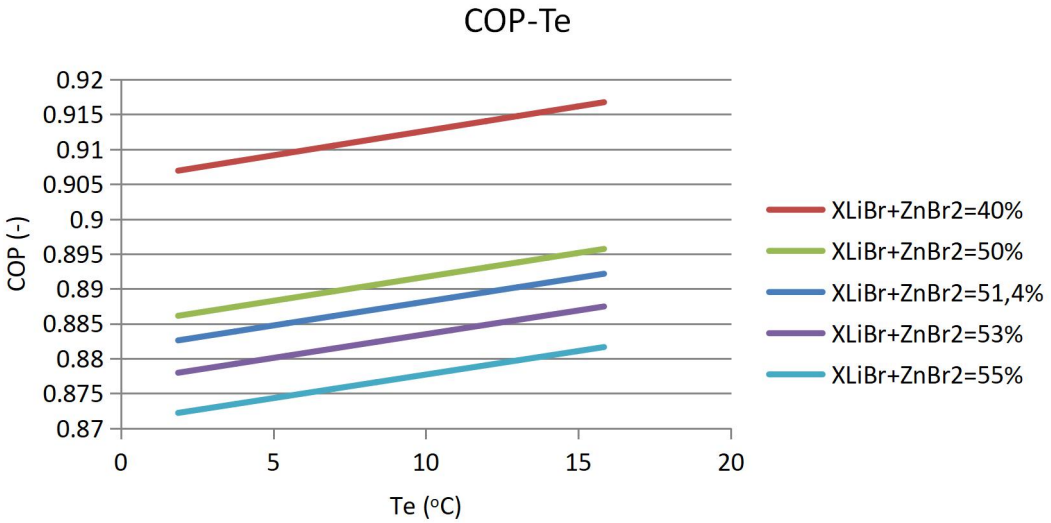


*Figure 6.14. COP-Te diagram for various XLiBr+$ZnBr_2$ (2:1) values (Ta=33 °C, Tc=33 °C, Tg=78.7 °C)*

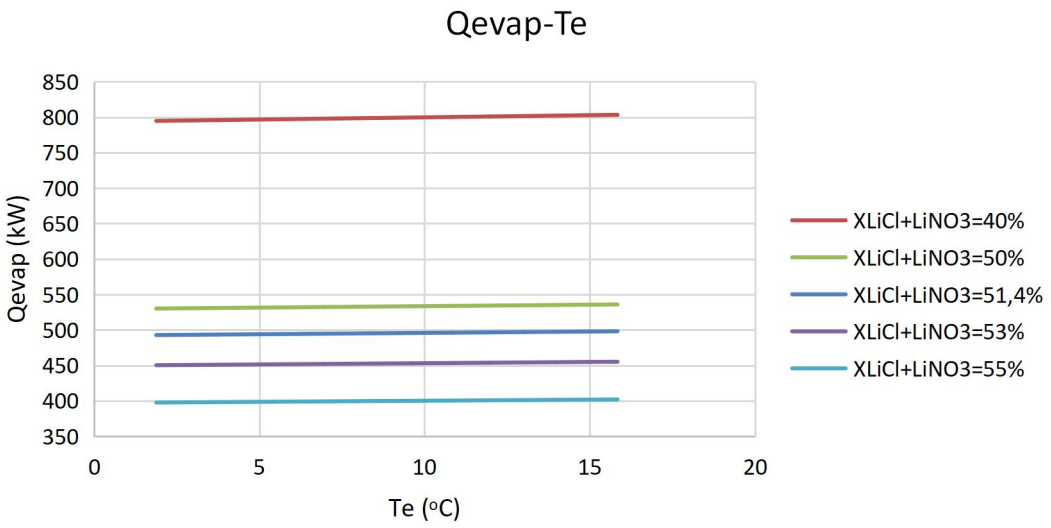


*Figure 6.15. Qevap-Te diagram for various XLiCl+LiNO$_3$ (2.8:1) values (Ta=33 °C, Tc=33 °C, Tg=78.7 °C)*

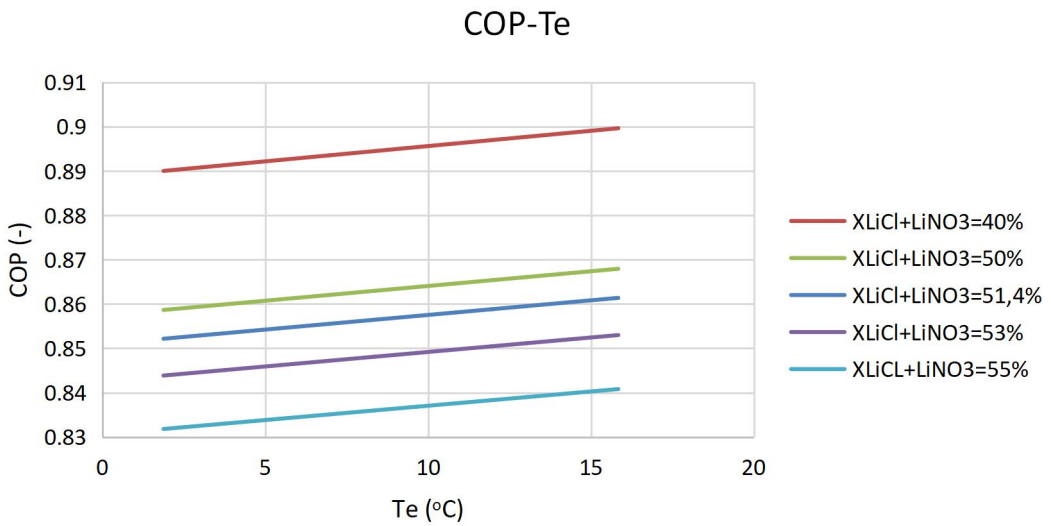


*Figure 6.16. COP-Te diagram for various XLiCl+LiNO$_3$ (2.8:1) values (Ta=33 °C, Tc=33 °C, Tg=78.7 °C)*

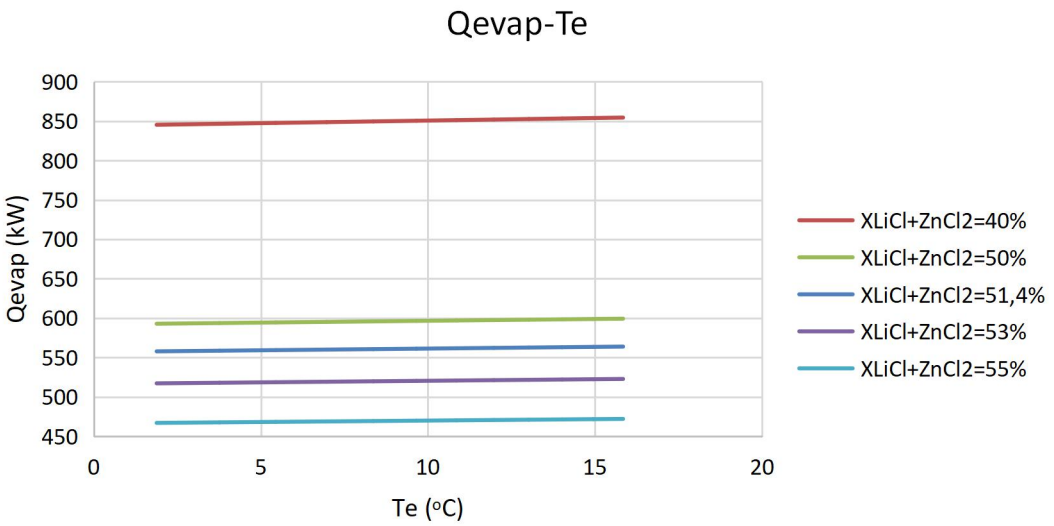


*Figure 6.17. Qevap-Te diagram for various XLiCl+$ZnCl_2$ (2:1) values (Ta=33 °C, Tc=33 °C, Tg=78.7 °C)*

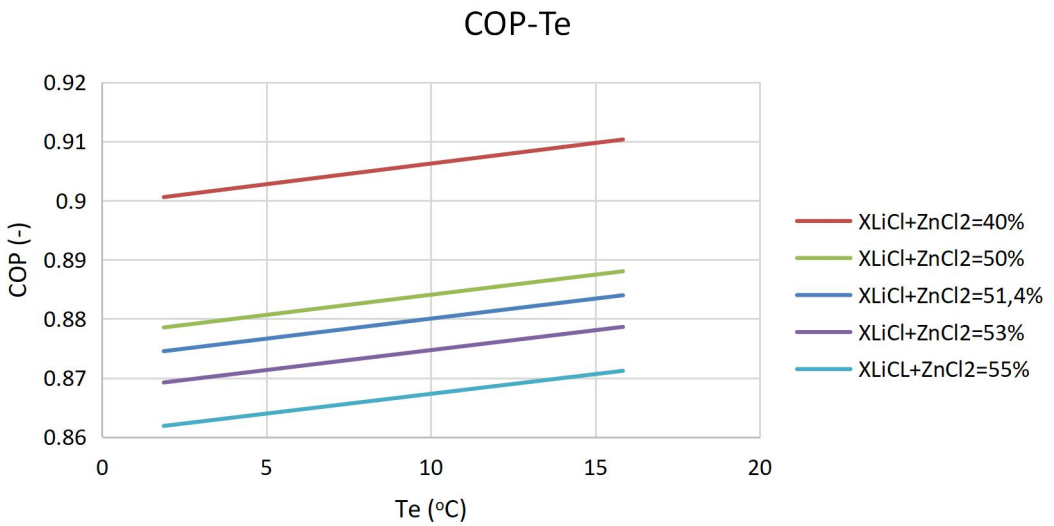


*Figure 6.18. COP-Te diagram for various XLiCl+$ZnCl_2$ (2:1) values (Ta=33 °C, Tc=33 °C, Tg=78.7 °C)*

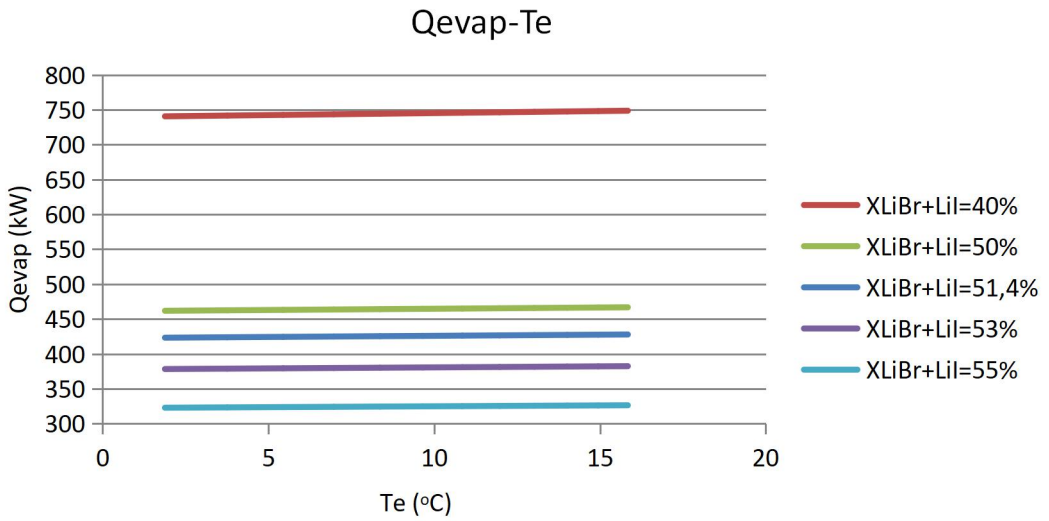


*Figure 6.19. Qevap-Te diagram for various XLiBr+LiI (4:1) values (Ta=33 °C, Tc=33 °C, Tg=78.7 °C)*

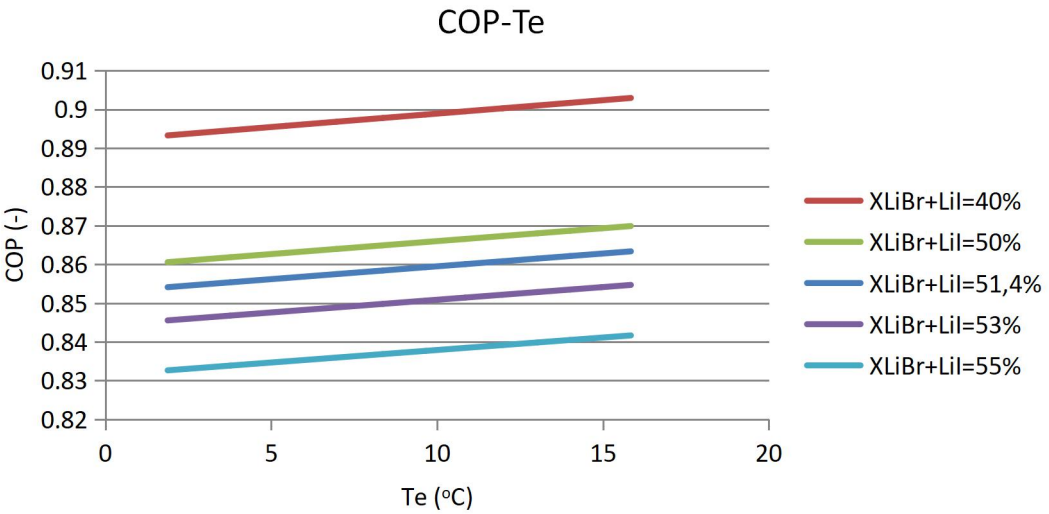


*Figure 6.20. COP-Te diagram for various XLiBr+LiI (4:1) values (Ta=33 °C, Tc=33 °C, Tg=78.7 °C)*

The heat duty of the evaporator and the COP increase for every cycle as the evaporator temperature rises. The higher values of Qevap and COP for a concentraion of 40% are observed for $H_2O$/LiBr+$ZnBr_2$ and $H_2O$/LiCl+$ZnCl_2$.

# Chapter 7. Ammonia/Water Cycle Modeling with Aspen Plus

The results and, especially, the COP of the $NH_3/H_2O$ cycle are needed as a reference for the results of the other cycles and for comparison. In this chapter, the way that the $NH_3/H_2O$ cycle is modeled is shown.

## 7.1. Property method

A property method specific to these working fluids was not available. Therefore, a more general method had to be used. The property method used for the $NH_3/H_2O$ solution was the Peng-Robinson method and its selection is presented in Figure 7.1.

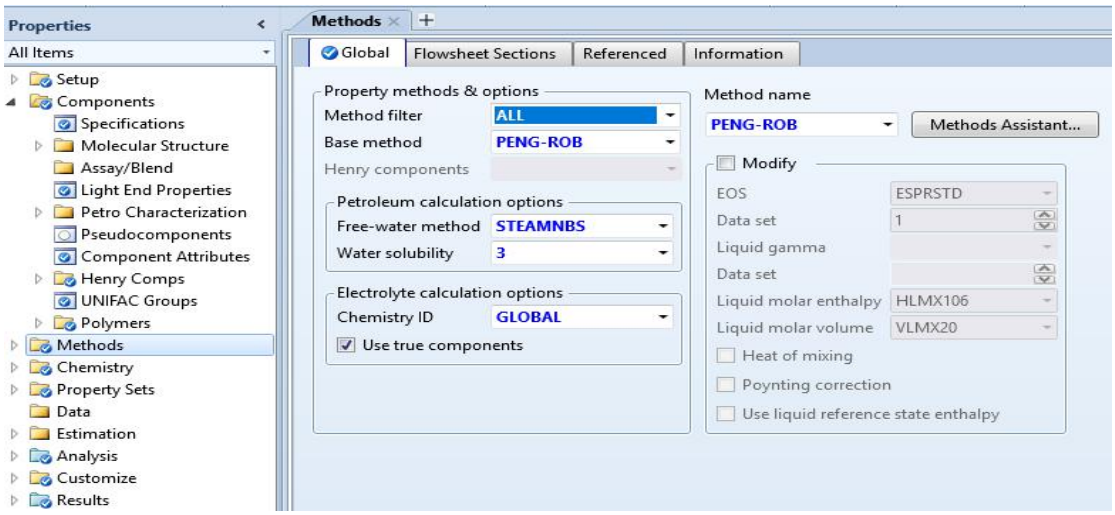


*Figure 7.1. Property method selection in Aspen Plus*

## 7.2. State points

It is more difficult to separate $NH_3/H_2O$ than $H_2O$/LiBr in the desorber due to the quite different vapor pressures of the two components. The vapor exit of the desorber is only 90-95% refrigerant in $NH_3/H_2O$, compared to virtually 100% steam for the $H_2O$/LiBr cycle. The issue is that a two component refrigerant will have a large temperature glide in the evaporator if evaporated completely. The working fluid can't be fully evaporated because a temperature glide greater than a few degrees Kelvin is undesirable and this leads to a reduced cooling capacity.

A rectifier is placed after the vapor exit of the desorber to condense some of the non-refrigerant. Hence, a much higher percentage refrigerant goes to the condenser.

A vapor/liquid heat exchanger (VLHX) is placed in the cycle with one side after the evaporator and before the absorber and the other after the condenser and before the refrigerant valve. The inclusion of this heat exchanger enhances the COP of the cycle.

After running the cycle, it was concluded that a solution heat exchanger (SHX) with one side after the pump and before the desorber and the other after the desorber and before the

solution valve was unnecessary because the enhancement of the cycle was minimal compared to its cost. State points 3 and 5 are omitted.

The state points will be defined in the following way and will be referred as such throughout this chapter to avoid confusion. For the single effect cycle of $NH_3/H_2O$, the absorber exit is state 1, the pump exit is state 2, the liquid exit of the desorber is state 4, the solution valve exit is state 6, the gas exit of the desorber leading to the rectifier is state 7, the exit of the rectifier leading back to the desorber is state 8, the gas exit of the desorber is state 9, the condenser exit is state 10, the vapor/liquid heat exchanger exit leading to the refrigerant valve is state 11, the refrigerant valve exit is state 12, the evaporator exit is state 13, and the vapor/liquid heat exchanger exit leading to the absorber is state 14.

Some assumptions need to be made for the cycle in order to help the modeling process. States 1, 4 and 10 are saturated liquid, state 9 is saturated vapor, state 13 vapor quality is calculated by the evaporator, state 2 is calculated by the solution pump model, states 11 and 14 are calculated by the VLHX model, state 6 is calculated by the solution valve model and state 12 is calculated by the refrigerant valve model.

## 7.3. Components modeling

At this point, it will be shown how the various parts of the cycle in Aspen Plus are modeled. As in the $H_2O$/LiBr cycle, some parts are very simple and consist of a single block. Many basic components (pumps, valves etc) might be modeled simply by selecting the equivalent block in Aspen Plus. Other components, like the desorber, are more complex and need a number of blocks to be adequately represented. The complexity depends on the process and how it is programmed in Aspen Plus.

### 7.3.1 State Point 1

Since Aspen Plus uses a sequential solver, a “break” in closed cycles is needed to give the model inputs, inserted in this case at state point 1. Therefore, the exit of the absorber (stream 1A) and the inlet of the pump (stream 1) are not connected and if the two streams conclude giving the same results, it is an indication that the model is well designed and has converged. The inputs for state 1 are the temperature, a vapor quality of zero, the mass flow rate, and the concentration of ammonia and water. The “break” is presented in Figure 7.2.

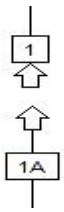


*Figure 7.2. The “break” between stream 1 and stream 1A*

### 7.3.2 Valves

The valves are modeled simply by selecting VALVE2 in valve/pressure changers in the simulation window. As in the $H_2O$/LiBr cycle, there are two valves that need to be modeled,

one solution valve and one refrigerant valve. The only input needed for both valves is the outlet pressure. In “Calculation type”, “Adiabatic flash for specified outlet pressure (pressure changer)” is selected. To increase the possibility of convergence, one may raise the number of iterations. The valve model is presented in Figure 7.3.

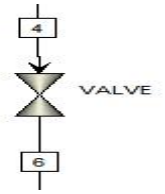


*Figure 7.3. $NH_3/H_2O$ valve model in Aspen Plus*

### 7.3.3 Pump

A pump is used after state point 1 and increases its pressure to a value determined as an input in discharge pressure. ICON1 is selected in pump/pressure changers in the simulation window. The efficiency in both pump and driver is considered 1, as the effect of the pump on the total energy balance is negligible (the pump work is less than 0.1% of the heat duties of the other components). The pump model is presented in Figure 7.4.

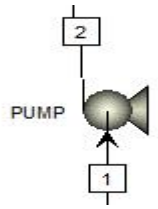


*Figure 7.4. $NH_3/H_2O$ pump model in Aspen Plus*

### 7.3.4 Evaporator

The evaporator is modeled as a heater. Modeling the evaporator, or the succeeding components, as heat exchangers with two heaters was unnecessary as it only complicated the cycle and led to warnings and errors in Aspen Plus. The inputs for the evaporator were zero pressure drop and the outlet temperature. Zero degrees of superheating was not given as an input because the temperature glide is very big for a vapor quality near 1, as it is clear from the T-x-y diagram (green line) for Vapor-Liquid-Equilibrium (VLE) of ammonia, generated in the Aspen Plus Properties tab. The diagram is shown in Figure 7.5. Heat is added in the evaporator.

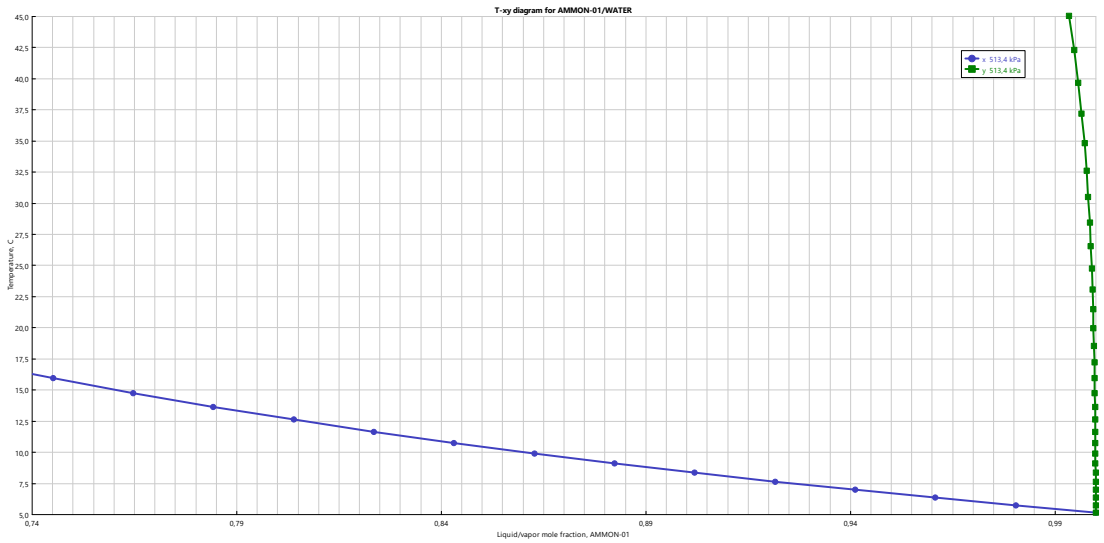


*Figure 7.5. T-x-y diagram for VLE of ammonia*

The evaporator model is presented in Figure 7.6.

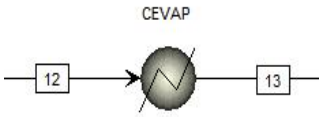


*Figure 7.6. $NH_3/H_2O$ evaporator model in Aspen Plus*

### 7.3.5 Condenser

The condenser is also modeled as a heater. The inputs for the condenser were zero pressure drop and zero vapor fraction, as the water exits the condenser as saturated liquid. Heat is rejected from the condenser. The condenser model is presented in Figure 7.6.

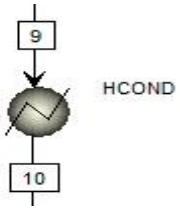


*Figure 7.7. $NH_3/H_2O$ condenser model in Aspen Plus*

### 7.3.6 Absorber

The absorber is modeled as a heater with a solution inlet (stream 6), a refrigerant inlet (stream 14) and a solution exit (stream 1A). The inputs are zero pressure drop and the outlet temperature. Heat is rejected from the absorber. The absorber model is presented in Figure 7.7.

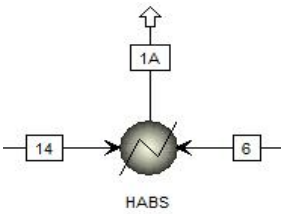


*Figure 7.8. $NH_3/H_2O$ absorber model in Aspen Plus*

### 7.3.7 Desorber

A distillation column was used to model the desorber, which is shown in Figure 7.8. The desorber model in the $NH_3/H_2O$ model is not the same as in the $H_2O$/LiBr model because the working fluids interact in a more complex manner. The inputs are the split fraction in the stream spec and the mass fractions. In the outlet flash, temperature is given as an input for stream 7.

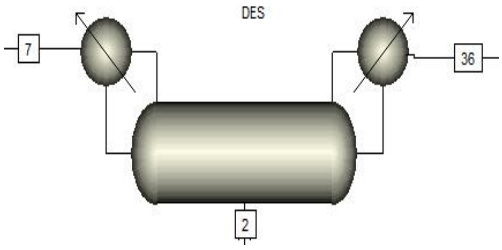


*Figure 7.9. $NH_3/H_2O$ desorber model in Aspen Plus*

### 7.3.8 Rectifier

The rectifier is placed after the desorber and its function is to condense out some of the solution, leaving higher percentage ammonia. This is accomplished using a flash block, with inputs of zero pressure drop and heat duty. The liquid exit of the rectifier (state point 8) combines with the liquid exit of the desorber to form state 4 and the gaseous exit of the rectifier goes to the condenser as state point 9. The rectifier model and its surrounding components are shown in Figure 7.9.

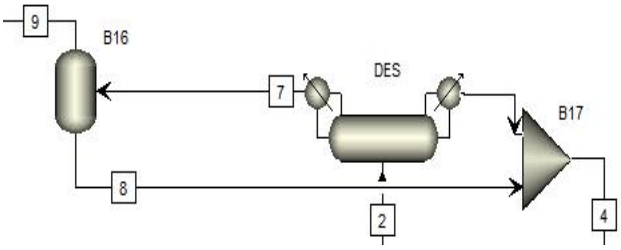


*Figure 7.10. $NH_3/H_2O$ rectifier model in Aspen Plus*

### 7.3.9 Vapor/liquid heat exchanger

The vapor/liquid heat exchanger (VLHX) enhances the COP and increases the cooling capacity. Although it adds complexity and initial cost to the design, it is worth including in the cycle. One side of the heat exchanger is placed between the condenser and the refrigerant valve and the other side is placed between the evaporator and the absorber. The inputs of the VLHX are zero pressure drop and the heat duty. The VLHX model is shown in Figure 7.10.

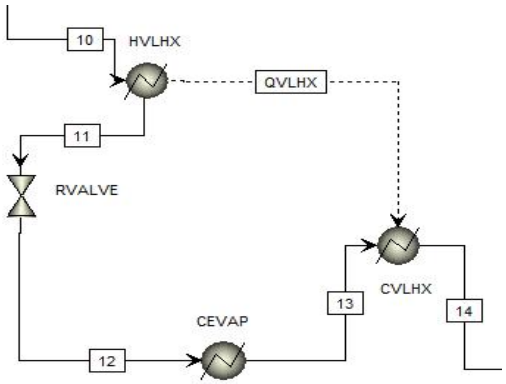


*Figure 7.11. $NH_3/H_2O$ VLHX model in Aspen Plus*

## 7.4. Complete model

The complete model of the $NH_3/H_2O$ absorption cycle is shown in Figure 7.11.

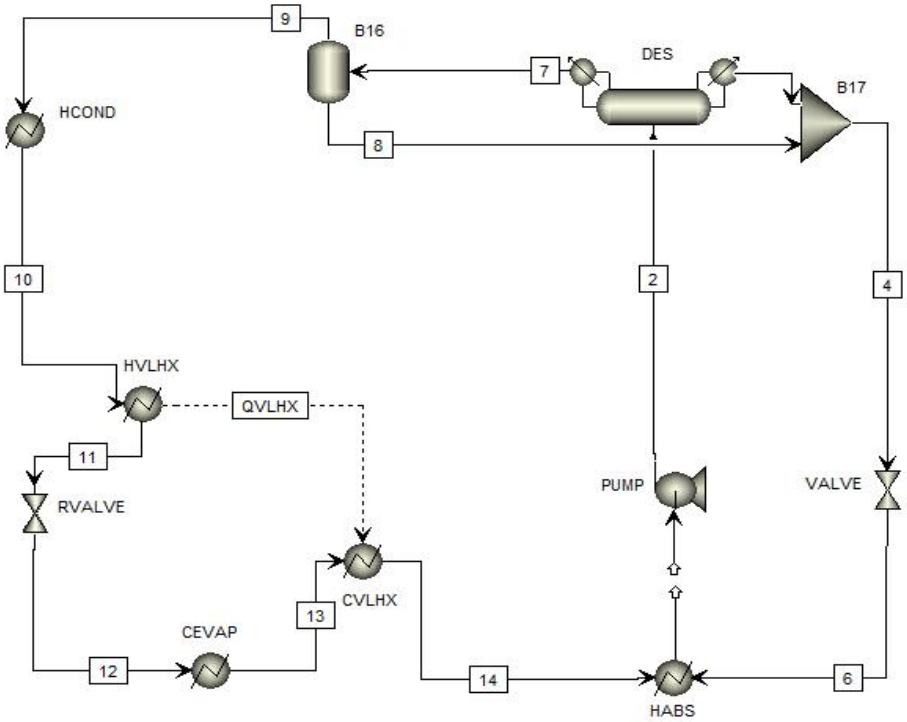


*Figure 7.12. Complete model of the single effect $NH_3/H_2O$ cycle in Aspen Plus*

# Chapter 8. Ammonia/Water model validation

In order to assess the validity of the model, the results must be checked in two ways. Firstly, a mass balance verification has to be performed to ensure that the system is correctly modeled. Then, an energy conservation verification is necessary to check for inconsistencies in the various blocks which add or reject heat.

## 8.1. Mass balance verification

After the absorber exit and before the pump inlet a "break" was modeled to provide inputs. The purpose of this "break" is to demonstrate if the model is well formulated by means of identical results, especially component and mass flow rates, between the streams before and after it.

As seen in Table 8.1 below, the streams 1 and 1A have equal mass flow rates. This demonstrates that the mass flow is conserved in the model.

*Table 8.1. Single effect $NH_3/H_2O$ mass balance verification*

| Mass Flow (kg/s) | Stream 1 | Stream 1A |
|---|---|---|
| Total | 0.7839 | 0.7839 |
| $NH_3$ | 0.4703 | 0.4703 |
| $H_2O$ | 0.3136 | 0.3136 |

## 8.2. Energy conservation verification

Moreover, an energy conservation verification is achieved in this model as the net amount of energy into and out of the cycle equals to zero. There are five components exchanging energy in the form of heat, while four are taken into consideration as the pump's contribution is negligible. The absorber and the condenser reject heat from the cycle, while the evaporator and the desorber add heat. Internal energy transfer, such as in the vapor/liquid heat exchanger, is not regarded in the energy conservation verification. The energy equilibrium is presented in the following equation:

$$\left|Q_{des}+Q_{evap}\right|-\left|Q_{abs}+Q_{cond}\right|=111.192+84.729-100.874-95.122=0 \qquad (2.1)$$

As a result, the model is successful as far as energy conservation is concerned.

## 8.3. State point results

After running the model of the single effect $NH_3/H_2O$ cycle in Aspen Plus the following results were provided. They are presented in Table 8.2.

*Table 8.2. State point results for the single effect $NH_3/H_2O$ cycle*

| State Point | $XNH_3$ (-) | $XH_2O$ (-) | Temperature (°C) | Pressure (kPa) | Mass Flow (kg/s) | Vapor Fraction (-) |
|---|---|---|---|---|---|---|
| 1 | 0.6 | 0.4 | 26.1 | 513.4 | 0.7839 | 0 |
| 2 | 0.6 | 0.4 | 26.18 | 1528 | 0.7839 | 0 |
| 4 | 0.559 | 0.441 | 27 | 1528 | 0.7084 | 0 |
| 6 | 0.559 | 0.441 | 27.2 | 513.4 | 0.7084 | 0 |
| 7 | 0.927 | 0.073 | 78.7 | 1528 | 0.0862 | 0.878 |
| 8 | 0.497 | 0.503 | 78.7 | 1528 | 0.0108 | 0 |
| 9 | 0.988 | 0.012 | 78.7 | 1528 | 0.0754 | 1 |
| 10 | 0.988 | 0.012 | 40.06 | 1528 | 0.0754 | 0 |
| 11 | 0.988 | 0.012 | 8.08 | 1528 | 0.0754 | 0 |
| 12 | 0.988 | 0.012 | 5.5 | 513.4 | 0.0754 | 0.01 |
| 13 | 0.988 | 0.012 | 8.2 | 513.4 | 0.0754 | 0.883 |
| 14 | 0.988 | 0.012 | 25.75 | 513.4 | 0.0754 | 0.974 |

As shown by the results above, the low pressure is 513.4 kPa and the high pressure is 1528 kPa. The concentration of $H_2O$ in the strong solution side is 40% and in the weak solution side is 44.14%. The vapor fraction is either 0 or 1, namely saturated liquid and saturated vapor, except for state point 7 where it equals to 0.878, which is why the rectifier is used, state point 12 where it equals 0.01, which is an acceptable value, state point 13 where it equals 0.883, due to the form of the VLE diagram as explained above and state point 14 where it equals 0.974, which is an acceptable value. As far as the mass flow rates are concerned, 90.37% of the total mass flow is led to the weak solution side, which is a typical value. Finally, the evaporation temperature is 8.2 °C (due to the temperature glide, the temperature in state point 12 and 13 is not the same), the desorber temperature is 78.7 °C, the condenser temperature is 40 °C and the absorber temperature is 26.1 °C. Overall, the results are normal for a typical single-effect $NH_3/H_2O$ cycle.

The heat duties and the COP of the cycle are presented in Table 8.3. The COP value is very satisfying as it is a bit above the typical COP value of a standard single-effect $NH_3/H_2O$ cycle.

*Table 8.3. Heat duties and COP of the single-effect $NH_3/H_2O$ cycle*

| | |
|---|---|
| Qcondenser (kW) | 95.122 |
| Qabsorber (kW) | 100.874 |
| Qevaporator (kW) | 84.729 |
| Qdesorber (kW) | 111.192 |
| COP (-) | 0.762 |

## 8.4. Sensitivity analysis

The next step in this study is to run a sensitivity analysis in order to examine the model's behaviour to the changing variables. More specifically, the change of the value of Qevap (kW) and COP for different temperatures of the generator will be examined.

The generator temperature Tg is varied from 50 °C to 100 °C with an increment of 1°C, because it is observed that the $NH_3/H_2O$ cycle has a better performance for lower temperatures. Then, the heat duties of the evaporator and the generator are defined and tabulated. The COP is also tabulated and its mathematical formula is written in the Fortran window. This sensitivity analysis is run for an $H_2O$ concentration of 40% only, because this is the concentration where the previous cycles had the best performance.

The sensitivity analysis while varying the evaporator temperature was not done because the outlet temperature of the evaporator was given as an input in Aspen Plus instead of zero degrees of superheating as mentioned in the previous chapter.

The results of the sensitivity analysis while varying the generator temperature are presented below.

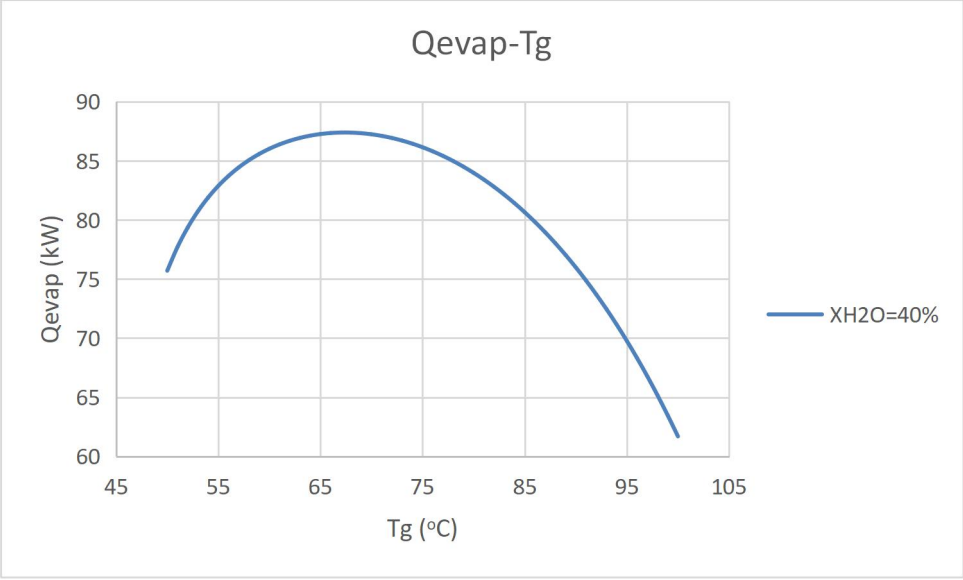

*Figure 8.1. Qevap-Tg diagram for $XH_2O$=40% (Ta=26.1 °C, Tc=40 °C, Te=8.2 °C)*

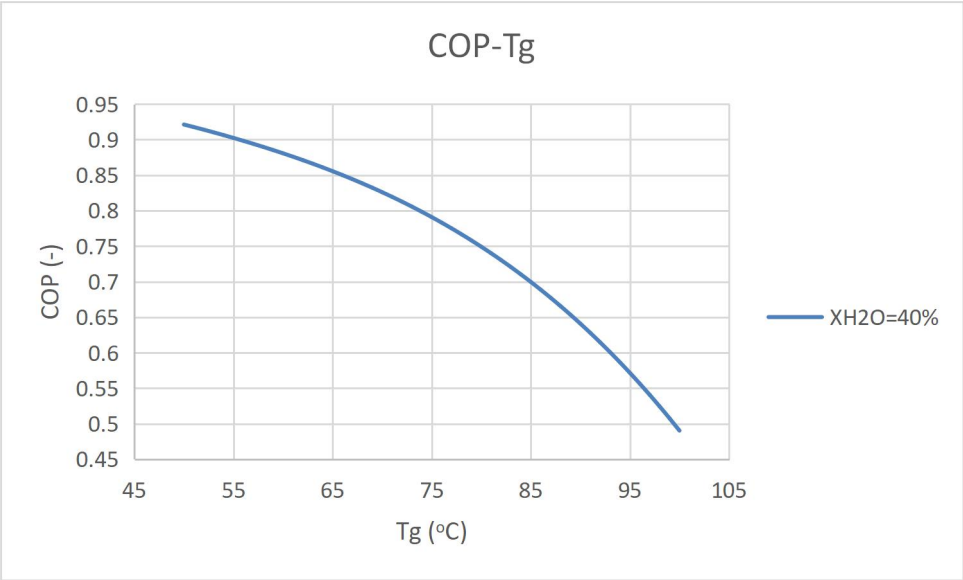


*Figure 8.2. COP-Tg diagram for $XH_2O$=40% (Ta=26.1 °C, Tc=40 °C, Te=8.2 °C)*

The heat duty of the evaporator is under 90 kW for every generator temperature which sets the $NH_3/H_2O$ cycle below every other cycle examined as far as Qevap is concerned. The heat duty of the evaporator increases as the generator temperature rises until 68.5 °C and then decreases. The COP of the cycle decreases as the generator temperature rises.

# Chapter 9. Cost calculation

## 9.1. Introduction

Most engineering design projects are conducted to provide data from which capital and operating cost estimates can be produced. Each plant is constructed to create a profit, and an estimate of the necessary investment and manufacturing costs are required before a project's profitability can be evaluated [28].

The Fixed capital investment is the total cost of designing, constructing and installing a plant and the associated modifications necessary to prepare the site of the plant. The fixed capital investment consists of [28]:

- The inside battery limits (ISBL) investment – the cost of the plant itself.
- The changes and improvements to the infrastructure of the site, known as off-site or OSBL investment.
- Engineering and construction costs.
- Contingency charges.

### 9.1.1 ISBL

The cost of the ISBL involves the cost of procurement and installation of all the process machinery making up the new plant.

The direct field costs include [28]:

- All the major process equipment, such as vessels, reactors, columns, furnaces, heat exchangers, coolers, pumps, etc.
- Bulk items, such as piping and valves.
- Civil works such as roads, foundations, buildings, etc.
- Installation labour and supervision.

In addition to the direct field costs there will be indirect field costs including:

- Construction costs such as construction equipment rental, construction workshops, etc.
- Field expenses and services such as field canteens, specialists' costs, etc.
- Construction insurance.
- Labour benefits and burdens (social security, workers compensation, etc.).
- Miscellaneous overhead items such as agent's fees, legal costs, import duties, special freight costs, local taxes, etc.

### 9.1.2 OSBL

Off-site cost or OSBL investment includes the costs of the additions that must be made to the site infrastructure to accommodate adding a new plant or increasing the capacity of an existing plant.

Off-site investments may include [28]:

- Electric main substations, transformers, switchgear and power lines
- Power generation plants, turbine engines, standby generators.
- Boilers, steam mains, condensate lines, boiler feed water treatment plant, supply pumps.
- Cooling towers, circulation pumps, cooling water mains, cooling water treatment.
- Workshops and maintenance facilities.
- Emergency services, fire fighting equipment, fire hydrants, medical facilities, etc.
- Site security, fencing, gatehouses, landscaping.

Off-site costs are typically estimated as a percentage of ISBL costs in the early stages of design. For typical petrochemical projects, off-site costs are usually between 20% and 50% of ISBL cost. A value of 30% will be used.

An example of this is sites that have undergone contraction, where some plants have closed, leaving underutilized infrastructure ('brown-field' sites). On the other hand, if the site infrastructure has to be repaired or upgraded to comply with new laws, or if the plant is built on a completely new site (a 'green-field' site), then off-site costs will increase.

### 9.1.3 Engineering costs

The engineering costs include the costs of detailed design and other engineering services required to carry out the project [28]:

- Detailed design engineering of process equipment, piping systems, control systems and off-sites, plant layout, drafting, cost engineering, scale models and civil engineering.
- Procurement of main plant items and bulks.
- Construction supervision and services.
- Administrative charges, including engineering supervision, project management, expediting, inspection, travel and living expenses and home office overheads.
- Bonding.
- Contractor's profit.

Very few working businesses, except for very tiny projects, maintain a big enough engineering staff to carry out all these operations internally. In most instances, one or more significant contracting companies in engineering will be introduced.

A rule of thumb for engineering costs is 30% of ISBL plus OSBL cost for smaller projects and 10% of ISBL plus OSBL cost for larger projects. The absorption chiller is considered a small project.

### 9.1.4 Contingency Charges

Contingency charges are additional expenses added to the project budget to allow the cost estimate to vary. All cost estimates are uncertain and the final installed cost of many items is unknown until successful installation has been accomplished.

Apart from errors in the cost estimate, contingency costs also help cover [28]:

- Changes in project scope,
- Changes in prices (e.g., prices of steel, copper, catalyst, etc.),
- Currency fluctuations,
- Labour disputes,
- Subcontractor problems, and
- Other unexpected problems.

A minimum contingency charge of 10% of ISBL plus OSBL cost should be used on all projects. If the technology is uncertain then higher contingency charges (up to 50%) are used.

## 9.2. Calculations

### 9.2.1 ISBL calculation

To estimate the installed ISBL capital cost of the absorption chiller the costs of the following parts need to be calculated and added: generator, absorber, trays, condenser, evaporator, heat exchanger, pump, driver and working fluid.

Each part's cost is calculated using the Table 9.1 and Table 9.2 [28] and the correlation below:

$$C_e = a + b \cdot S^n \tag{9.1}$$

where

- $C_e$=purchased equipment cost ($) on a US Gulf Coast basis, Jan. 2007 (CE index

(CEPCI)=509.7, NF refinery inflation index=2059.1),

- a, b=cost constants,
- S=size parameter,

- n=exponent for that type of equipment.

A summary of the values used for the calculations is presented in Table 9.1 and Table 9.2 below:

*Table 9.1. Purchased equipment descriptions and units*

| | Equipment | Description | S, Units for size |
|---|---|---|---|
| Generator | Pressure vessels | Vertical, 304 ss | shell mass, kg |
| Absorber | Pressure vessels | Vertical, 304 ss | shell mass, kg |
| Trays | Trays | Sieve trays | diameter, m |
| Condenser | Exchangers | U-tube shell and tube | area, $m^2$ |
| Evaporator | Exchangers | U-tube shell and tube | area, $m^2$ |
| HEX | Exchangers | U-tube shell and tube | area, $m^2$ |
| Pump | Pumps and drivers | Single-stage centrifugal | flow, L/s |

*Table 9.2. Purchased equipment cost constants and exponent*

| | a | b | n |
|---|---|---|---|
| Generator | 15000 | 68 | 0.85 |
| Absorber | 15000 | 68 | 0.85 |
| Trays | 110 | 380 | 1.8 |
| Condenser | 24000 | 46 | 1.2 |
| Evaporator | 24000 | 46 | 1.2 |
| HEX | 24000 | 46 | 1.2 |
| Pump | 6900 | 206 | 0.9 |

It is important to note that the calculations are done for a mass concentration of 40%, as this is the concentration with the highest COP results.

The generator and the absorber are calculated as pressure vessels (vertical, 304 ss). Therefore, their shell mass (kg) needs to be calculated:

$$shell\_mass = \pi \cdot D_c \cdot L_c \cdot t_w \cdot \rho \quad (9.2)$$

where

- $D_c$=vessel diameter (m),

$D_c=D_i+2 \cdot t_w$,

- $L_c$=vessel length (m),

$L_c=30 \cdot x$ approximately, where x is the volume flow in L/s,

- ρ=metal density (kg/m$^3$),

304 stainless steel: ρ=8000 kg/m$^3$,

- $t_w$=wall thickness (m).

The wall thickness $t_w$ is calculated by the following formula [28]:

$$t_w = \frac{P_i \cdot D_i}{2 \cdot S \cdot E - 1.2 \cdot P_i} \quad (9.3)$$

where

- $D_i$=internal diameter (m),

which is considered as:

$$D_i = \frac{L_c}{10} \quad (9.4)$$

- S=maximum allowable stress (N/mm$^2$),

for type 304 stainless steel at 500 °F (260 °C) it is 12.9 ksi or roughly 89 N/mm$^2$,

- Pi=internal pressure (Pa),

the design pressure of the vessels should be 10% above the operating pressure,

- E=welded-joint efficiency,

E=1.

The calculated cost $C_e$ ($) is converted in € (when this thesis was written, 1$ was equal to 0.89696 €) and then increased by a factor of 4, according to Hand's method [28].

The results for the costs (€) of the generator and the absorber are presented in Table 9.3 (water is omitted from the tables below for simplistic reasons):

*Table 9.3. Generator and absorber costs for each working pair*

| | LiBr | LiF | LiCl | NaOH | HCOONa | $LiBr+LiNO_3$ |
|---|---|---|---|---|---|---|
| Generator | 59570.2 | 58243.5 | 60730.5 | 58841.6 | 72818.6 | 59826.5 |
| Absorber | 55551.8 | 55151.9 | 55901.6 | 55332.2 | 59545.8 | 55629.1 |
| | $LiBr+ZnBr_2$ | $LiCl+LiNO_3$ | $LiCl+ZnCl_2$ | LiBr+LiI | $NH_3$ | |
| Generator | 58998.3 | 60825.1 | 59826.5 | 59486.3 | 3591822 | |
| Absorber | 55379.4 | 55930.1 | 55629.1 | 55526.5 | 1430080 | |

According to the results above, the cost of the generator is the highest for the $NH_3/H_2O$ cycle, followed by the $H_2O$/HCOONa cycle, while it is the lowest for the $H_2O$/LiF cycle. The cost of the generator for the $NH_3/H_2O$ cycle is so much higher due to the very high pressures compared to the other working pairs and the bigger volume flow which results to a bigger vessel length. The results follow the same pattern for the cost of the absorber.

The cost per tray for both the generator and the absorber is calculated as sieve tray based on the internal diameter $D_i$. It is then multiplied by the number of trays which is:

$$No.\_of\_trays = 1.667 \cdot L_c \tag{9.5}$$

The calculated cost $C_e$ ($) is converted in € and then increased by a factor of 1.3, according to Hand's method. The result is multiplied by 2 to take into consideration both the generator and the absorber.

The results for the costs (€) of the total trays are presented in Table 9.4:

*Table 9.4. Trays costs for each working pair*

| | LiBr | LiF | LiCl | NaOH | HCOONa | $LiBr+LiNO_3$ |
|---|---|---|---|---|---|---|
| Trays | 77088.7 | 58564.5 | 92715.5 | 68299.5 | 268584.7 | 81998.4 |
| | $LiBr+ZnBr_2$ | $LiCl+LiNO_3$ | $LiCl+ZnCl_2$ | LiBr+LiI | $NH_3$ | |
| Trays | 69639.4 | 93533.1 | 81998.4 | 76369.8 | 390451.5 | |

The results for the costs of the trays follow the same pattern as the results for the costs of the generator and the absorber, as there is also a dependence of the cost on the vessel length.

The condenser, the evaporator and the HEX (or VLHX in the case of $NH_3/H_2O$) are calculated as exchangers (U-tube shell and tube). Therefore, their area ($m^2$) needs to be calculated:

$$A = \frac{Q}{U \cdot LMTD} \tag{9.6}$$

where

- Q=heat duty (W),
- U=overall heat transfer coefficient ($W/m^{2\cdot}K$),

according to the tables in [29],

Condenser: U=550 $Btu/hr{\cdot}ft^{2\cdot}F$=3123 $W/m^{2\cdot}K$,

Evaporator: U=150 $Btu/hr{\cdot}ft^{2\cdot}F$=851 $W/m^{2\cdot}K$,

HEX: U=250 $Btu/hr{\cdot}ft^{2\cdot}F$=1420 $W/m^{2\cdot}K$,

- LMTD=logarithmic mean temperature difference,

$$LMTD = \frac{\Delta T_A - \Delta T_B}{\ln(\frac{\Delta T_A}{\Delta T_B})} \tag{9.7}$$

where

$\Delta T_A$ is the temperature difference between the two streams at end A, and $\Delta T_B$ is the temperature difference between the two streams at end B. It is assumed that a generic heat exchanger has two ends (which are called "A" and "B") at which the hot and cold streams enter or exit on either side.

The calculated cost $C_e$ ($) is converted in € and then increased by a factor of 3.5, according to Hand's method.

The results for the costs (€) of the condenser, the evaporator and the HEX are presented in Table 9.5:

*Table 9.5. Condenser, evaporator and HEX costs for each working pair*

| | LiBr | LiF | LiCl | NaOH | HCOONa | LiBr+$LiNO_3$ |
|---|---|---|---|---|---|---|
| Condenser | 77602.2 | 78531.7 | 77933.8 | 77614.5 | 79085.2 | 77954.2 |
| Evaporator | 197492.3 | 255489.8 | 218208.4 | 198260.1 | 289964.5 | 219479.7 |
| HEX or VLHX | 75622.8 | 75523.1 | 75549.2 | 75391.3 | 75427 | 75410 |

| | $LiBr+ZnBr_2$ | $LiCl+LiNO_3$ | $LiCl+ZnCl_2$ | LiBr+LiI | $NH_3$ | |
|---|---|---|---|---|---|---|
| Condenser | 78281.6 | 78139.6 | 78332.3 | 77937.1 | 75486.5 | |
| Evaporator | 239897.3 | 231084 | 243064.7 | 218442.2 | 79104.7 | |
| HEX or VLHX | 75432.3 | 75400.6 | 75408 | 75411.6 | 75874.3 | |

The results show that the cost of the evaporator is the biggest among the heat exchangers for every working pair due to the relatively high heat duty and the quite low overall heat transfer coefficient and LMTD.

The cost of the condenser and the evaporator is the highest for the $H_2O$/HCOONa cycle and the lowest for the $NH_3/H_2O$ cycle. The cost of the HEX or VLHX is the highest for the $NH_3/H_2O$ cycle and the lowest for the $H_2O$/NaOH cycle.

The pump is calculated as single-stage centrifugal. Therefore, their volume flow (L/s) in state point 1 is required.

The calculated cost $C_e$ ($) is converted in € and then increased by a factor of 4 and a factor of 1.3 , according to Hand's method.

The results for the cost (€) of the pump are presented in Table 9.6:

*Table 9.6. Pump costs for each working pair*

| | LiBr | LiF | LiCl | NaOH | HCOONa | $LiBr+LiNO_3$ |
|---|---|---|---|---|---|---|
| Pump | 32769.9 | 32718.6 | 32811.4 | 32744.3 | 33080.6 | 32778.9 |
| | $LiBr+ZnBr_2$ | $LiCl+LiNO_3$ | $LiCl+ZnCl_2$ | LiBr+LiI | $NH_3$ | |
| Pump | 32750.8 | 32813 | 32779.6 | 32767.7 | 33196.3 | |

The highest pump cost is that of the $NH_3/H_2O$ cycle, followed by the pump cost of the $H_2O$/HCOONa cycle, while the lowest is that of the $H_2O$/LiF cycle.

The cost of the driver is considered 400 € for every working pair, which is a typical value.

The cost of the total mass of the working fluids, not including the water used, circulating in the absorption cycle is calculated by multiplying the total mass (kg) with the price in €/kg.

The mass of the working fluid is assumed to be 2 kg/kWevap and by multiplying with the heat duty of the evaporator (Qevap) and the percentage of the working fluid in the working pair (for example, the percentage of LiBr is 40% in the $H_2O$/LiBr cycle, the percentage of

$LiNO_3$ is 10.5% and the percentage of LiCl is 29.5% in the $H_2O$/LiCl+$LiNO_3$ cycle) the total mass (kg) is calculated.

The prices (€/kg) of the various working fluids found in the internet are presented in Table 9.7:

*Table 9.7. Prices of the various working fluids*

| | LiBr | LiF | LiCl | LiI | NaOH |
|---|---|---|---|---|---|
| Price (€/kg) | 139.2 | 176.5 | 75.2 | 1410 | 40.4 |
| | HCOONa | $LiNO_3$ | $ZnBr_2$ | $ZnCl_2$ | NH3 |
| Price (€/kg) | 58.8 | 204.9 | 171.5 | 113.6 | 4.5 |

The NH3 price is very low as it is a very commonly used substance in the market, in contrast with LiI.

The results for the cost (€) of the total mass circulating in the cycle are presented in Table 9.8:

*Table 9.8. Total mass costs for each working pair*

| | LiBr | LiF | LiCl | NaOH | HCOONa | LiBr+$LiNO_3$ |
|---|---|---|---|---|---|---|
| Total mass cost | 72742 | 127503.9 | 44756.6 | 21199.9 | 49103.3 | 91376.1 |
| | LiBr+$ZnBr_2$ | LiCl+$LiNO_3$ | LiCl+$ZnCl_2$ | LiBr+LiI | $NH_3$ | |
| Total mass cost | 100438.7 | 69874.6 | 59855.9 | 234535 | 455.5 | |

As it was expected, the total mass costs of the $H_2O$/LiBr+LiI cycle is the highest and the total mass cost of the $NH_3$/$H_2O$ cycle is the lowest.

The cost of the ISBL investment (€) is calculated by adding all the costs above. The results are shown in Table 9.9:

*Table 9.9. ISBL costs for each working pair*

| | LiBr | LiF | LiCl | NaOH | HCOONa | LiBr+$LiNO_3$ |
|---|---|---|---|---|---|---|
| ISBL | 648839.8 | 742127.1 | 659006.8 | 588083 | 928009.6 | 694852.8 |
| | LiBr+$ZnBr_2$ | LiCl+$LiNO_3$ | LiCl+$ZnCl_2$ | LiBr+LiI | $NH_3$ | |
| ISBL | 711217.8 | 698000.1 | 687294.5 | 830876 | 5676871.4 | |

It is clear that the most expensive working pair in terms of the ISBL investment is the $NH_3/H_2O$. The main reason is that the components of this cycle are more demanding and complicated due to the more extreme conditions of the cycle in comparison to the $H_2O$/LiBr model. Moreover, there is a factor of uncertainty for this working pair as far as the model in Aspen Plus is concerned, which could explain the unreasonably high cost of the pair. The second most expensive cycle is that of $H_2O$/HCOONa, followed by that of $H_2O$/LiBr+LiI, mainly due to the high market price of LiI. The rest of the working pairs are very close as far as the ISBL cost is concerned.

### 9.2.2 OSBL calculation

The cost of the OSBL investment (€) is assumed as 30% of the ISBL cost. The results are shown in Table 9.10:

*Table 9.10. OSBL costs for each working pair*

| | LiBr | LiF | LiCl | NaOH | HCOONa | LiBr+$LiNO_3$ |
|---|---|---|---|---|---|---|
| OSBL | 194652 | 194652 | 197702.1 | 176425 | 278402.9 | 208455.8 |
| | LiBr+$ZnBr_2$ | LiCl+$LiNO_3$ | LiCl+$ZnCl_2$ | LiBr+LiI | $NH_3$ | |
| OSBL | 213365.3 | 209400 | 206188.3 | 249262.9 | 1703061.4 | |

The same conclusions (as for the ISBL costs) can be drawn for the OSBL costs as they are a percentage of the ISBL costs.

### 9.2.3 Engineering costs calculation

The Engineering costs (€) are assumed as 30% of the sum of ISBL and OSBL costs. The results are shown in Table 9.11:

*Table 9.11. Engineering costs for each working pair*

| | LiBr | LiF | LiCl | NaOH | HCOONa | LiBr+$LiNO_3$ |
|---|---|---|---|---|---|---|
| Engineering costs | 253047.5 | 281033.7 | 257012.7 | 229352.5 | 361923.7 | 270992.6 |
| | LiBr+$ZnBr_2$ | LiCl+$LiNO_3$ | LiCl+$ZnCl_2$ | LiBr+LiI | $NH_3$ | |
| Engineering costs | 277374.9 | 272220 | 268044.8 | 324041.7 | 2213979.8 | |

The Engineering costs of the various working pairs follow the same pattern as the ISBL and OSBL costs.

### 9.2.4 Contingency charges calculation

The Contingency charges (€) are assumed as 10% of the sum of ISBL and OSBL costs. The results are shown in Table 9.12:

*Table 9.12. Contingency charges for each working pair*

| | LiBr | LiF | LiCl | NaOH | HCOONa | $LiBr+LiNO_3$ |
|---|---|---|---|---|---|---|
| Contingency | 84349.2 | 93677.9 | 85670.9 | 76450.8 | 120641.2 | 90330.9 |
| | $LiBr+ZnBr_2$ | $LiCl+LiNO_3$ | $LiCl+ZnCl_2$ | LiBr+LiI | $NH_3$ | |
| Contingency | 92458.3 | 90740 | 89348.3 | 108013.9 | 737993.3 | |

The Contingency charges are the least expensive costs but add significantly to the total cost of the project. The pattern of the costs of the working pairs is the same.

### 9.2.5 Fixed capital investment calculation

The Fixed capital investment costs (€) are the sum of the ISBL costs, OSBL costs, Engineering costs and Contingency charges. The results are shown in Table 9.13:

*Table 9.13. Fixed capital investment costs for each working pair*

| | LiBr | LiF | LiCl | NaOH | HCOONa | $LiBr+LiNO_3$ |
|---|---|---|---|---|---|---|
| Fixed capital | 1180888.5 | 1350671.3 | 1199392.5 | 1070311.6 | 1688977 | 1264632 |
| | $LiBr+ZnBr_2$ | $LiCl+LiNO_3$ | $LiCl+ZnCl_2$ | LiBr+LiI | $NH_3$ | |
| Fixed capital | 1294416.4 | 1270360.2 | 1250876 | 1512194.8 | 10331906 | |

It is clear that after all the calculations the most expensive pairs are $NH_3/H_2O$, $H_2O$/HCOONa and $H_2O$/LiBr+LiI, whereas the least expensive pairs are $H_2O$/NaOH, $H_2O$/LiBr and $H_2O$/LiCl. It is worth noting again that the cost of the $NH_3/H_2O$ pair is unreasonably high due to a level of uncertainty of the results of the model of this pair because of the peculiarity of $NH_3$. Below is an example of the distribution of the various costs of the $H_2O$/HCOONa pair.

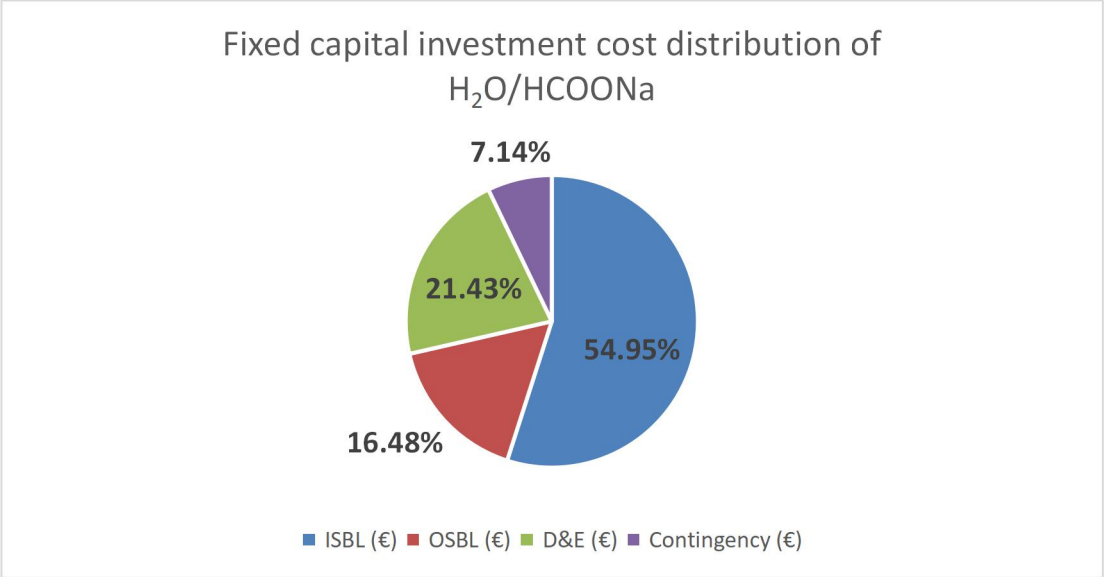


*Figure 9.1. Fixed capital investment cost distribution of H2O/HCOONa*

It is clear that the ISBL costs are the highest followed by the Engineering costs.

# Chapter 10. Conclusions-Propositions

On the basis of the preceding analysis, the conclusions drawn regarding the behavior of the single-stage absorption refrigeration cycle models for the various alternative pairs are considered to be expected. On Aspen Plus Modeling:

- The various parts of the cycle were modeled either with a single block or a combination of blocks, as in the case of the Solution Heat Exchanger (SHX) which consisted of two heater blocks and of the desorber which had increased complexity due to the separation process. The heat exchangers (except SHX and desorber) were chosen to be modeled with one heater block (instead of two) in order to avoid undesirable errors.

- The models as a whole are functional and show no errors or warnings. The process of selecting the right inputs to avoid errors (and warnings) was time consuming and laborious.

- Mass balance verification and energy conservation verification confirmed the validity of the models.

- The results of the $H_2O$/LiBr cycle compared to previous study results have negligible differences. This means that the model is suitable for use.

- In the $NH_3/H_2O$ cycle there were some differences in modeling due to the special properties of ammonia. In particular, it was considered necessary to use a rectifier to better separate ammonia from water, the Solution heat exchanger (SHX) was omitted due to negligible enhancement of the cycle efficiency over its high cost and the Vapor/liquid heat exchanger (VLHX) was added, which increased the complexity and cost of the cycle but it greatly improved the performance. Moreover, the sensitivity analysis for various temperatures of the evaporator was not possible because the evaporator temperature was given as an input instead of zero degrees of superheating due to the very steep curve of the VLE diagram for a vapor quality near 1.

Figure 10.1 and Figure 10.2 show (in descending order) the results for every pair (including ternary mixtures) of the cooling capacity Qevap and the coefficient of performance COP for a mass concentration of the absorbent in the rich solution equal to 40% (for Xabsorbent=40% the values of Qevap and COP are the highest) and for the following conditions: Ta=33 °C, Tc=33 °C, Tg=78.7 °C και Te=10 °C, except for $NH_3/H_2O$ where: Ta=26.1 °C, Tc=40 °C, Tg=78.7 °C and Te=8.2 °C.

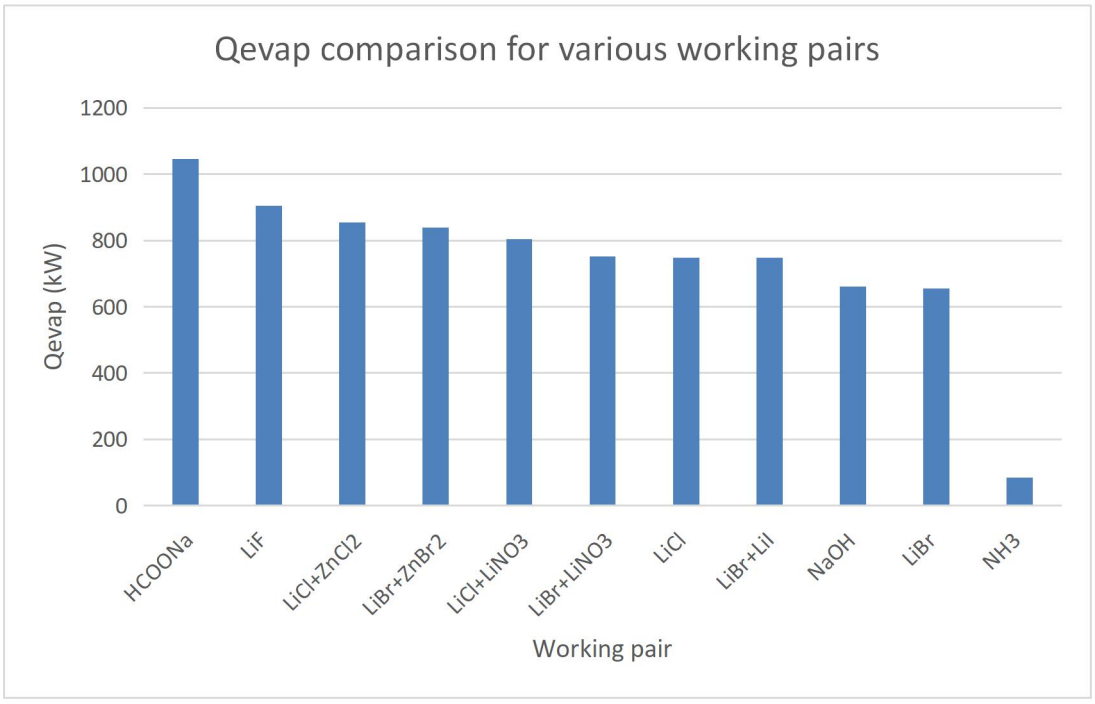


*Figure 10.1. Qevap comparison diagram for Xabsorbent=40% (Ta=33 °C, Tc=33 °C, Tg=78.7 °C, Te=10 °C, except for $NH_3/H_2O$ where: Ta=26.1 °C, Tc=40 °C, Tg=78.7 °C, Te=8.2 °C)*

From the diagram above it is clear that $H_2O$/HCOONa has the highest cooling capacity, exceeding 1000 kW. It is followed by $H_2O$/LiF which is slightly above 900 kW and $H_2O$/LiCl+$ZnCl_2$, $H_2O$/LiBr+$ZnBr_2$ and $H_2O$/LiCl+$LiNO_3$ which exceed 800 kW. Below the 800 kW limit are $H_2O$/LiBr+$LiNO_3$, $H_2O$/LiCl and $H_2O$/LiBr+LiI, while $H_2O$/NaOH and $H_2O$/LiBr do not exceed 700 kW. $NH_3/H_2O$ does not exceed 100 kW of cooling capacity and the major difference with the other pairs lies in the special properties of ammonia and its separate cycle model.

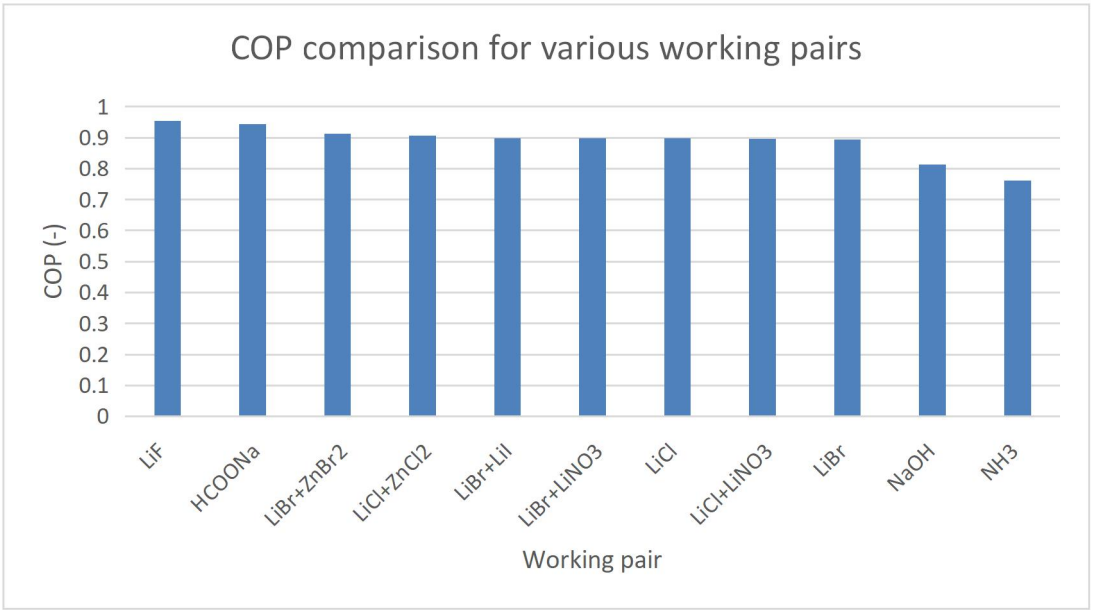

*Figure 10.2. COP comparison diagram for Xabsorbent=40% (Ta=33 °C, Tc=33 °C, Tg=78.7 °C, Te=10 °C, except for $NH_3/H_2O$ where: Ta=26.1 °C, Tc=40 °C, Tg=78.7 °C, Te=8.2 °C)*

As far as COP is concerned, $H_2O$/LiF has the highest value exceeding 0.95, followed by $H_2O$/HCOONa, $H_2O$/LiBr+$ZnBr_2$ and $H_2O$/LiCl+$ZnCl_2$ which exceed 0.9. $H_2O$/LiBr+LiI, $H_2O$/LiBr+$LiNO_3$, $H_2O$/LiCl, $H_2O$/LiCl+$LiNO_3$ and $H_2O$/LiBr follow with values above 0.89, whereas the lowest values belong to the $H_2O$/NaOH and $NH_3/H_2O$ pairs.

Figure 10.3, Figure 10.4, Figure 10.5 and Figure 10.6 depict the sensitivity analysis of the cooling capacity Qevap and the coefficient of performance COP for every pair for a mass concentration of the absorbent in the rich solution equal to 40% for various temperatures of the generator and the evaporator.

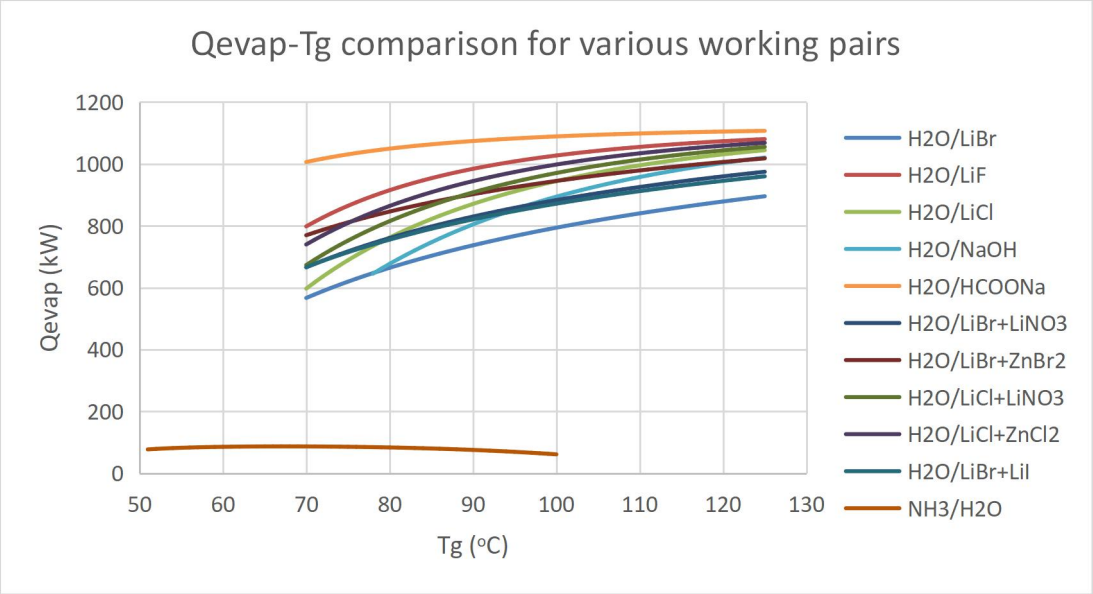


*Figure 10.3. Qevap-Tg comparison diagram for Xabsorbent=40% (Ta=33 °C, Tc=33 °C, Te=10 °C, except for $NH_3/H_2O$ where: Ta=26.1 °C, Tc=40 °C, Te=8.2 °C)*

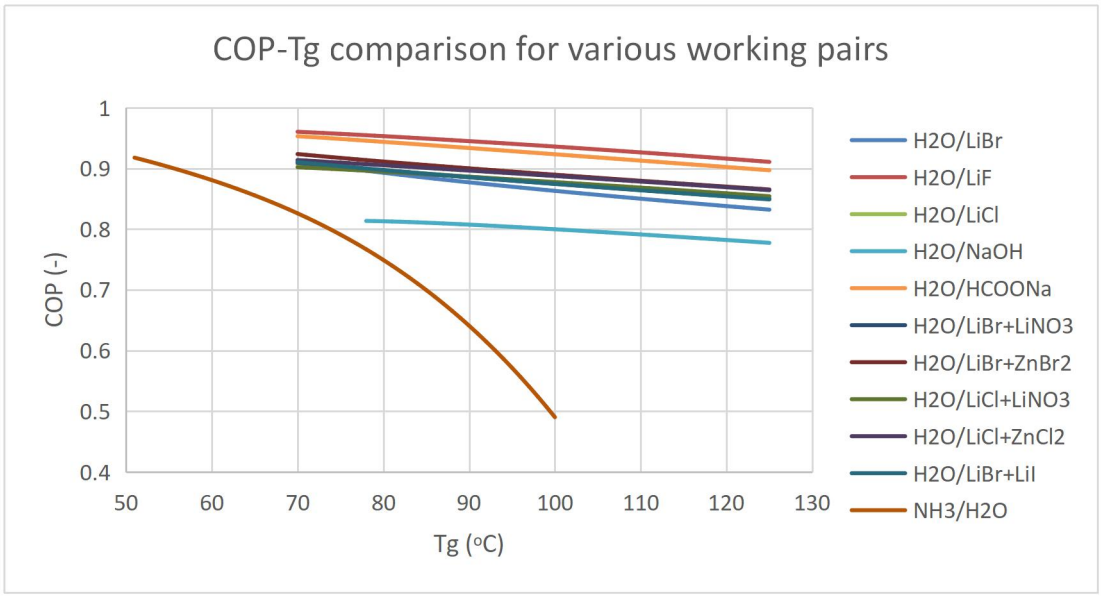


*Figure 10.4. COP-Tg comparison diagram for Xabsorbent=40% (Ta=33 °C, Tc=33 °C, Te=10 °C, except for $NH_3/H_2O$ where: Ta=26.1 °C, Tc=40 °C, Te=8.2 °C)*

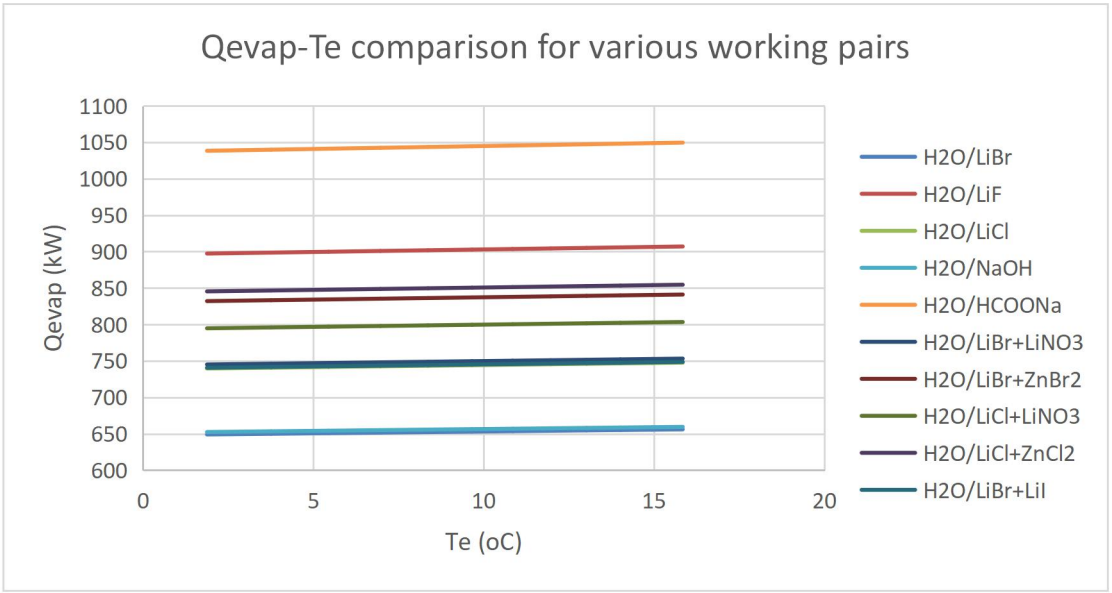


*Figure 10.5. Qevap-Te comparison diagram for Xabsorbent=40% (Ta=33 °C, Tc=33 °C, Tg=78.7 °C)*

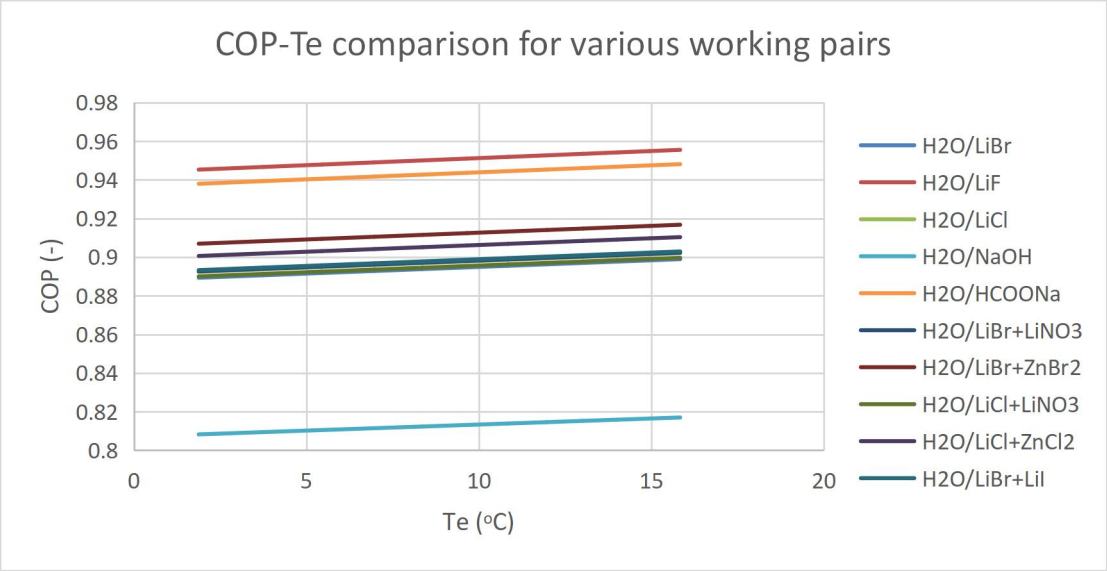


*Figure 10.6. COP-Te comparison diagram for Xabsorbent=40% (Ta=33 °C, Tc=33 °C, Tg=78.7 °C)*

The following can easily be deduced:

- Higher cooling capacity and COP are obtained for a mass concentration of the absorbent in the rich solution of 40% for all working pairs and the curves of the sensitivity analysis are similar to previous studies.
- Based on the diagrams above, the $H_2O$/HCOONa, $H_2O$/LiF, $H_2O$/LiCl+$ZnCl_2$, $H_2O$/LiCl+$LiNO_3$, and $H_2O$/LiBr+$ZnBr_2$ working pairs have the highest cooling capacity over the entire range of the generator and evaporator temperatures, while the conventional $NH_3/H_2O$ and $H_2O$/LiBr working pairs have the lowest values.
- Correspondingly, as far as COP is concerned, the $H_2O$/LiF, $H_2O$/HCOONa, $H_2O$/LiBr+$ZnBr_2$, $H_2O$/LiCl+$ZnCl_2$ and $H_2O$/LiBr+LiI working pairs have the highest values, whereas the $NH_3/H_2O$ and $H_2O$/NaOH working pairs have the lowest values.
- The $H_2O$/NaOH working pair shows errors for generator temperatures below 78 °C.
- The $NH_3/H_2O$ working pair has a range of lower generator temperatures because its COP receives higher values as the generator temperature drops.

The values of the Total Fixed Capital Investment cost for all the working pairs are presented in Figure 10.7 (in ascending order). In Figure 10.8 the $NH_3/H_2O$ working pair is omitted in order to allow for a better perspective of the costs of the other working pairs. Inside the parenthesis are the cooling capacities (kW).

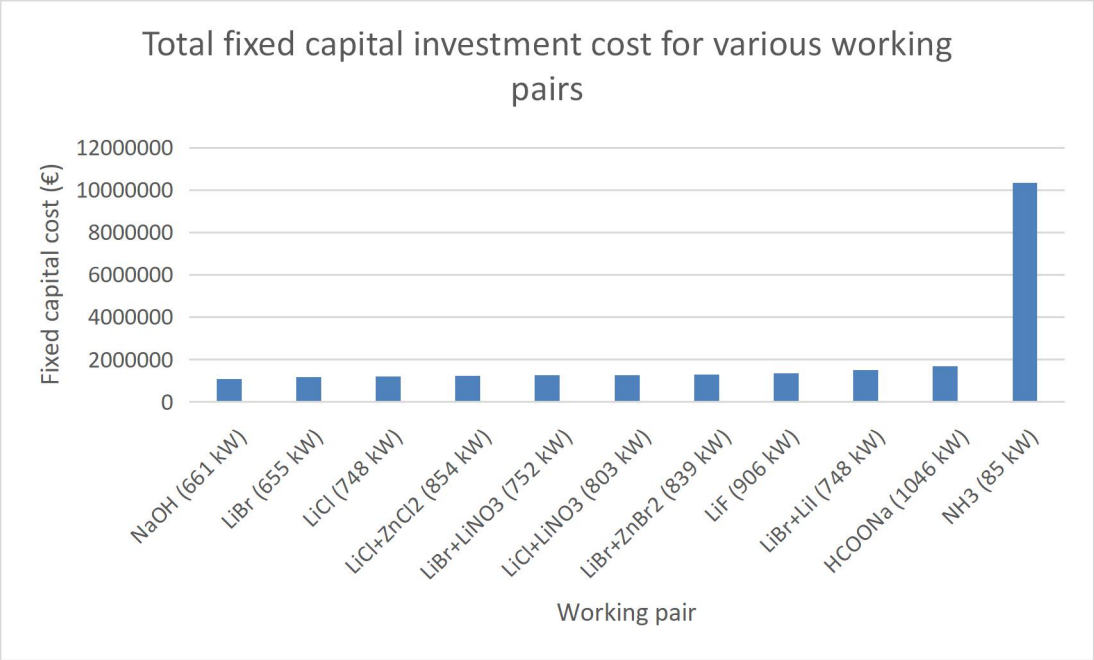


*Figure 10.7. Total Fixed Capital Investment cost for various working pairs for Xabsorbent=40% (Ta=33 °C, Tc=33 °C, Tg=78.7 °C, Te=10 °C, except for $NH_3/H_2O$ where: Ta=26.1 °C, Tc=40 °C, Tg=78.7 °C, Te=8.2 °C)*

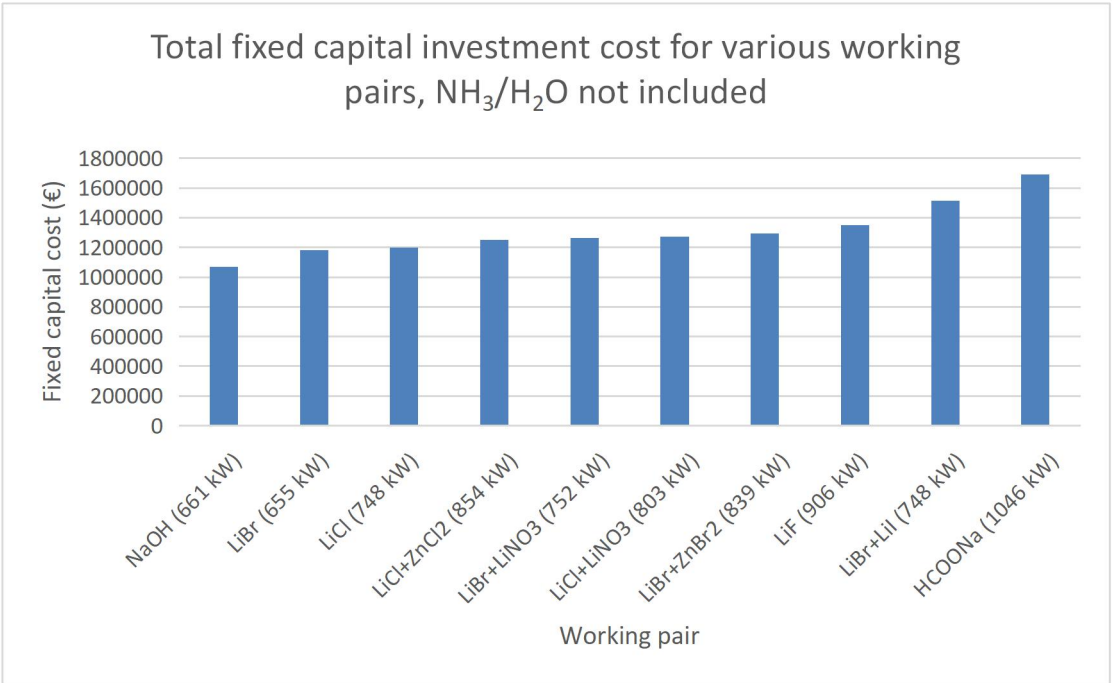


*Figure 10.8. Total Fixed Capital Investment cost for various working pairs for Xabsorbent=40% (Ta=33 °C, Tc=33 °C, Tg=78.7 °C, Te=10 °C), $NH_3/H_2O$ not included*

The highest cost by far is that of the $NH_3/H_2O$ pair due to the much higher pressures on which its cycle operates and exceeds € 10.3 million. The peculiarity of $NH_3$ which affects its model might be the reason of such an unreasonably high cost. The lowest cost at just over € 1 million is presented by the $H_2O$/NaOH pair followed by $H_2O$/LiBr, $H_2O$/LiCl, $H_2O$/LiCl+$ZnCl_2$,

$H_2O$/LiBr+$LiNO_3$, $H_2O$/LiCl+$LiNO_3$ and $H_2O$/LiBr+$ZnBr_2$ the costs of which lie between € 1.1 million and € 1.3 million. Finally, the $H_2O$/LiF, $H_2O$/LiBr+LiI and $H_2O$/HCOONa pairs cost between € 1.3 million and € 1.7 million.

The values of the Total Fixed Capital Investment cost per kW of cooling capacity for all the working pairs, except $NH_3/H_2O$, are presented in Figure 10.9 (in ascending order). Inside the parenthesis are the cooling capacities (kW).

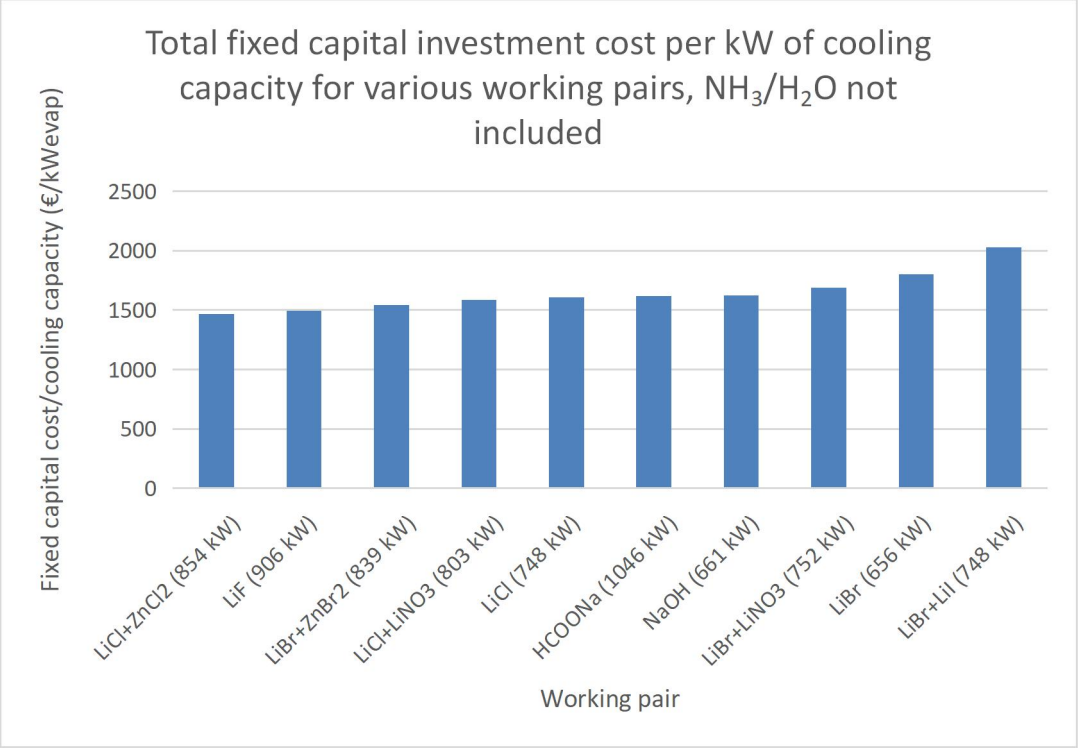


*Figure 10.9. Total Fixed Capital Investment cost per cooling capacity for various working pairs for Xabsorbent=40% (Ta=33 °C, Tc=33 °C, Tg=78.7 °C, Te=10 °C), $NH_3/H_2O$ not included*

The highest cost per kW of cooling capacity by far is that of the $NH_3/H_2O$ pair due to the much higher pressures on which its cycle operates and its value is 122271.1 €/kWevap, approximately 60 times the second highest value and, as mentioned earlier, might be due to a degree of uncertainty of the results of the model of this pair. The lowest cost per kW of cooling capacity close to 1500 €/kWevap is presented by the $H_2O$/LiCl+$ZnCl_2$ pair followed by $H_2O$/LiF, $H_2O$/LiBr+$ZnBr_2$, $H_2O$/LiCl+$LiNO_3$, $H_2O$/LiCl, $H_2O$/HCOONa, $H_2O$/NaOH and $H_2O$/LiBr+$LiNO_3$ the costs per kW of which lie under 1700 €/kWevap. Finally, the $H_2O$/LiBr and $H_2O$/LiBr+LiI pairs have values above 1800 €/kWevap and 2000 €/kWevap respectively.

Taking into account the COP and the Total Fixed Capital Investment cost per kW of cooling capacity the worst working pairs appear to be $NH_3/H_2O$, $H_2O$/LiBr and $H_2O$/NaOH, whereas the best appear to be $H_2O$/LiF, $H_2O$/LiCl+$ZnCl_2$, $H_2O$/LiBr+$ZnBr_2$ and $H_2O$/HCOONa.

In order to extend the present work it is suggested to further study and deepen the following topics:

- Investigation of the same pairs for Double-effect, Triple-effect, Half-effect and Generator-Absorber heat eXchange (GAX) absorption cycles.
- Connection of the absorption cycle models with various heat sources in the generator, such as geothermal heat, waste heat from gas turbines etc.
- Deepening of the economic analysis with even more indicators (IRR, NPV, LCOE etc.).

# References


1.American Society of Heating, R., and Inc Air-Conditioning Engineers, *2014 ASHRAE Handbook - Refrigeration (SI Edition).* American Society of Heating, Refrigerating and Air-Conditioning Engineers, Inc, 2014.

2.Stoecker, W.F., *Industrial Refrigeration handbook* New York: McGraw-Hill, 1998.

3. https://en.wikipedia.org/wiki/Iceman_(occupation)#/media/File:Bundesarchiv_Bild_183-47890-0001,_Berlin,_Kinder_mit_dem_Eismann.jpg.

4.www.wikipedia.org/refrigeration.

5.Sarbu, I., Sebachiervici C., *Solar Heating and Cooling Systems.* 2017. **Chapter 7**.

6.http://ffden-2.phys.uaf.edu/212_spring2007.web.dir/sedona_price/phys_212_webproj_refrigerators.html.

7.Roumpedakis, T., *Techno-economic investigations of a solar driven ORC-sorption system for combined cooling, heating and power.* 2018.

8.Karellas, S., Roumpedakis T., Tzouganatos N., Braimakis K., *Solar Cooling Technologies.* 2018.

9.www.sciencedirect.com/topics/chemical-engineering/absorption-refrigeration.

10.https://en.wikipedia.org/wiki/Absorption_refrigerator.

11.Sarbu, I., Sebachiervici C., *Solar Heating and Cooling Systems.* 2017. **Chapter 7** p. 261-270.

12.Gordon, J.M., and Kim Choon Ng., *Cool Thermodynamics: The Engineering and Physics of Predictive, Diagnostic and Optimization Methods for Cooling Systems* Cambridge: Cambridge International Science Publishing, 2000.

13.Granryd, E., et, al, *Refrigerating Engineering.* Stockholm: Royal Institute of Technology, KTH, Department of Energy Technology, Division of Applied Thermodynamics and Refrigeration, 2009.

14.Cho, S.-H., and Jong-Nam Kim *Modeling of a Silica Gel/Water Adsorption-Cooling System.* 1992.

15.Suzuki, M., *Heat Recovery Systems and CHP.* 1993.

16.Zhang, L.Z., and Ling Wang, *Applied Thermal Engineering* 1997.

17.Wade, L., E. Ryba, C. Weston, and J. Alvarez, *Test performance of a 2 W, 137 K Sorption Refrigerator.* 1992.

18.Wang, L.W., and R.G. Oliveira, *Progress in Energy and Combustion Science.* 2006.

19.Richardson , J.F., J.H. Harker, and J.R. Backhurst, *Coulson and Richardson's Chemical Engineering, Vol 2, Particle Technology and Separation Processes.* 5th ed. Elsevier, 2007.

20.Loh, W.S., El-Sharkawy, I.I., Ng, K.C., and Saha, B.B., *Adsorption cooling cycles for alternative adsorbent/adsorbate pairs working at partial vacuum and pressurized conditions.* Applied Thermal Engineering, 2009.

21.Fahrenheit©, *Fahrenheit: eZea.* 2018.

22.Kim, D.-S., *Solar Absorption Cooling.* 2007.

23.Boudéhenn, F., Sylvain Bonnot, Hélène Demasles, Florent Lefrançois, Maxime Perier-Muzet, and Delphine Triché, *Development and Performances Overview of Ammonia-Water Absorption Chillers with Cooling Capacities from 5 to 100 kW.* Energy Procedia 2016.

24.Henning, H.-M., *Solar Assisted Air Conditioning of Buildings—An Overview.* Applied Thermal Engineering 2007.

25. Somers, C., *Simulation of Absorption Cycles for Integration into Refining Processes.* 2009.
26.R. Maryami, A.A.D., *An exergy based comparative study between LiBr/water absorption refrigeration systems from half effect to triple effect.* Applied Thermal Engineering, 2017.
27.Saravanan, R., Maiya M.P., *Thermodynamic Comparison of Water-based Working Fluid Combinations for a Vapour Absorption Refrigeration System.* Applied Thermal Engineering, 1998.
28.Towler, G., and Sinnott R., *Chemical Engineering Design, Principles, Practice and Economics of Plant and Process Design, Second Edition.* 2012.
29.*https://www.engineersedge.com/*.